The Thesis Committee for Maggie Elizabeth Becker
Certifies that this is the approved version of the following Thesis:

Investigation of Bond in Unreinforced Concrete Interfaces for Partial Depth Repairs and New Construction

APPROVED BY
SUPERVISING COMMITTEE:

Juan Murcia-Delso, Supervisor

Oguzhan Bayrak

Investigation of Bond in Unreinforced Concrete Interfaces for Partial Depth Repairs and New Construction

by

Maggie Elizabeth Becker

Thesis

Presented to the Faculty of the Graduate School of

The University of Texas at Austin

in Partial Fulfillment

of the Requirements

for the Degree of

Master of Science in Engineering

The University of Texas at Austin

December 2020

Dedication

To my mother and father,

for being the greatest parents and role models.

To Aaron,

for your encouragement through it all.

Acknowledgements

Looking back at the past two years, this project has surrounded me with experts in their profession. These acknowledgements attempt to summarize how thankful I am to everyone who helped along the way.

I would like to begin by thanking my advisors: Dr. Jeff West and Dr. Juan Murcia-Delso. Dr. West, thank you for your guidance and confidence in me along the way. You always made time to meet and discuss the project and I will always be grateful for that. Your enthusiasm for structural engineering is inspiring. Dr. Murcia, you have taught nearly every course I have taken on concrete and have shaped the engineer I am today. Your relentless dedication to this project was encouraging to me during the stressful times. Also, thank you to Dr. Bayrak for being a reader for this thesis. Your laboratory experience is remarkable, and I am grateful to have you involved.

I would like to extend my appreciation the American Concrete Institute (ACI), the Precast/prestressed Concrete Institute (PCI), and Wiss, Janney, Elstner Associates, Inc. (WJE) for providing financial support for this project.

Thank you to Chuck Larosche (WJE), Lee Lawrence (WJE), and the ACI and PCI advisory committees for offering their vast industry experience.

To the employees at Wiss, Janney, Elstner Associates, Inc. in Austin, Texas namely Lane Thompson, Hunter Starr, Katy Aughenbaugh, Jason Sentz, and Kevin Copeland. Thank you for welcoming me into the office. I am so appreciative of the time you all have taken to help with this research. I am even more appreciative of the close friendships I have made with each of you.

I would like to thank James Prewitt at Lauren Concrete for his generosity donating concrete, and Tim Badilla at Restek, Inc. for his help with the concrete surface roughening.

A special thank you to the FSEL staff members: Abdullah Hamid, David Braley, and Dennis Fillip. This project is a result of their dedication to students and faculty, especially in the time of a pandemic.

I would not have made it without my fellow graduate students at FSEL. First and foremost, Ghassan Fawaz. Ghassan, you were a great friend and mentor to me. You helped me through each step of my project and were always there to talk about engineering or anything else going on in life. In addition, I would like to thank Xiaoyi Chen, Nidhi Khare, Yibin Shao, and Jarrod Zaborac for their help.

This project has provided me with knowledge, experience, and opportunity. I am so honored to have been a part of the graduate program at the University of Texas at Austin.

Maggie Becker
December 4, 2020

Abstract

Investigation of Bond in Unreinforced Concrete Interfaces for Partial Depth Repairs and New Construction

Maggie Elizabeth Becker, M.S.E.

The University of Texas at Austin, 2020

Supervisor: Juan Murcia-Delso

This thesis presents an experimental study on the horizontal shear strength of reinforced concrete slabs and beams with unreinforced concrete-to-concrete interfaces. Current design provisions for new construction and repair applications in ACI 318-19 and ACI 562-19 codes attribute a low capacity for concrete-to-concrete interfaces that are unreinforced. Specifically, the nominal strength of an intentionally roughened, unreinforced interface is 80 psi, and an unreinforced interface without intentional roughening is assumed to have no shear strength.

The goal of this research is to provide recommendations for redefining horizontal shear provisions for unreinforced interfaces in partial depth repairs and precast construction. To quantify interface strength, experimental tests were performed in two discrete phases: direct shear and direct tensile pull-off tests on slabs, then flexural tests on beams, each of which having differing surface roughnesses and topping slab workability.

The roughnesses used for this experimental program was representative of both partial depth repair and new construction.

Direct shear strengths from guillotine testing ranged from 400 psi to 1000 psi, with float (smooth) conditions providing the lowest strength and hydrodemolition roughening providing the highest strength. Direct tensile pull-off strengths ranged from 190 psi to 420 psi for toppings made of concrete with moderate workability and different roughnesses, while bond of toppings made of concrete with low workability was so weak that it failed during pull-off test preparations. The average horizontal shear strength along the unreinforced interface of beams subjected to flexure ranged from 530 psi to 550 psi for broom, tine and hydrodemolition roughening conditions. The maximum horizontal shear stress towards the topping ends of these beams were estimated in between 800 psi and 900 psi. However, beam specimens with smoother interfaces (floated and sandblasted) presented signs of debonding prior to flexural testing.

The research results indicate that a sound (i.e., not bruised or microcracked by concrete removal), laitance and defect free interface with uniform and sufficiently rough surface texture in combination with well consolidated the repair or topping material are keys to high shear and tensile bond strengths. The results show that unreinforced interfaces with these characteristics can achieve interface shear strengths significantly higher than the ACI nominal shear strength of 80 psi.

Table of Contents

List of Tables xiv
List of Figures xvi
Chapter 1 : Introduction 1
1.1 Background 1
1.2 Research Goal and Scope 2
1.3 Structure of the Thesis 2
Chapter 2 : Literature Review 4
2.1 Determining Horizontal Shear Demand 4
2.1.1 Segment Method 4
2.1.2 Sectional Method (or Classical Elastic Method) 6
2.1.3 Simplified Elastic Behavior 7
2.2 Experimental Studies on Horizontal Shear Capacity of Unreinforced Interfaces - Beam Testing 8
2.2.1 Revesz (1953) 9
2.2.2 Hanson (1960) 10
2.2.3 Saemann and Washa (1964) 13
2.2.4 Seibel and Latham (1988) 15
2.2.5 Kovach and Naito (2008) 17
2.2.6 Swan (2011) 24
2.2.7 Summary of previous beam tests on unreinforced interfaces 26
2.3 Experimental Studies on Horizontal Shear Capacity of Unreinforced Interfaces - Bond Tests 29
2.3.1 Comparison between bond test methods 31
2.3.2 Variability of different bond test methods 32
2.4 Other Shear Tests on Unreinforced Interfaces 33
2.4.1 Hanson (1960) 34
2.4.2 Seibel and Latham (1988) 36

2.4.3 Swan (2011) 38
2.5 Code Provisions for Calculating Horizontal Shear Capacity 39
2.5.1 American Concrete Institute 318- Building Code Requirements for Structural Concrete (ACI 318-19) 40
2.5.2 American Concrete Institute 562- Code Requirements for Assessment, Repair, and Rehabilitation of Existing Concrete Structures and Commentary (ACI 562-19) 41
Chapter 3 : Phase 1 - Experimental Program 43
3.1 Overview 43
3.2 Specimen Design and Test Variables 43
3.3 Concrete Mixtures and Placement Procedures 46
3.4 Interface Conditions 48
3.5 Concrete placement Sequence 51
3.6 Surface Roughness Characterization 52
3.6.1 CSP by Visual Comparison 53
3.6.2 Mean Texture Depth by Sand Patch Test 53
3.6.3 Mean Texture Depth by Analysis of 3D Data from Line Laser Scanner 55
3.7 Bond Strength Testing Methods 56
3.7.1 Direct Shear (Guillotine) Testing 56
3.7.2 Direct Tensile Pull-off Testing 58
Chapter 4 : Phase 1 - Experimental Results and Discussion 60
4.1 Material Testing Data 60
4.1.1 Slump 60
4.1.2 Compressive Strength 61
4.1.3 Splitting Tensile Strength 61
4.2 Surface Roughness Characterization Results 62
4.2.1 CSP by Visual Comparison Results 62
4.2.2 Mean Texture Depth by Sand Patch Test and Line Laser Scanner 63

4.3 Direct Shear (Guillotine) Results 64
4.4 Direct Tensile Pull-off Results 71
4.5 Phase 1 - Discussion 74
4.5.1 Effectiveness of Surface Preparation Techniques Investigated 75
Repair Interfaces 75
Precast Interfaces 76
4.5.2 Correlation Between Strength Test Results and Mean Texture Depth 77
4.5.3 Comparison of Shear and Tensile Strength Results 83
4.5.4 Comparison of Shear Strength Results to Design Values 87
Chapter 5 : Phase 2 - Test Program 91
5.1 Overview 91
5.2 Experimental Variables 91
5.3 Specimen Design 93
5.4 Specimen Fabrication 96
5.4.1 Substrate Fabrication 96
5.4.2 Method for interface debonding 99
5.4.3 Topping Fabrication 100
5.5 Beam Test Setup and loading protocol 102
5.6 Beam Instrumentation 105
5.7 Core testing of slabs 108
Chapter 6 : Phase 2 - Experimental Results and Discussion 109
6.1 Material Test Results 109
6.1.1 Concrete Slump 109
6.1.2 Compressive and Splitting Tensile Strengths 110
6.2 Surface Roughness Characterization by Mean Texture Depth from Line Laser Scanner Results 110
6.3 Beam Test Results 114
6.3.1 Observed damage 114

6.3.2 Load vs. Midspan Deflection Response 119
6.3.3 Load vs. Slip Response 120
6.3.4 Moment vs. strain response 123
6.3.5 Estimated interface shear stresses at failure 127
Material stress-strain models 128
Method A: stress distribution based on linear strain profile 128
Method B: Linear strain profile for compression region only and enforcing equilibrium 130
Method C: Strain profile from applied moment and moment-curvature analysis 131
Comparing Strain Profile Methods 133
Horizontal Shear Stress Demands 135
6.4 Direct Tensile and Shear tests - Phase 2 138
6.5 Phase 2-Discussion 140
6.5.1 Comparison of interface roughness and bond strength results from Phase 1 versus Phase 2 140
Repair specimens 141
Precast specimens 142
6.5.2 Direct shear and direct tensile pull-off results from Phase 2 versus beam test results 143
6.5.3 Mean texture depth versus beam test results 144
6.5.4 Effectiveness of beam test to assess horizontal shear capacity 145
6.5.5 ACI 318 horizontal shear code provisions versus beam test results 146
Chapter 7 : Summary and Conclusions 148
7.1 Phase 1 148
7.1.1 Effect of Interface preparation - Repair Series 148
7.1.2 Effect of Interface Preparation - Precast Series 149
7.1.3 Effect of Consolidation Method 150

7.1.4 Effect of Interface Surface Roughness on Shear and Tensile Bond Strength 150
Correlation Between Direct Shear Strength and Tensile Pull-off Strength..... 150
Core Size for Tensile Bond Pull-off Test 151
Interface Shear Bond Strength for Design 152
Guillotine Shear Test Method 152
7.2 Phase 2 152
7.2.1 Effect of Interface Conditions on Beam Interface Bond Capacity..... 153
7.2.2 Correlation of Horizontal Shear Capacity from Beam Strengths to Direct Shear Strengths and Direct Tensile Pull-off Strengths..... 154
7.2.3 Effectiveness of the Beam Test to Study Interface Shear 155
7.2.4 Methods of Calculating Horizontal Shear Demand Permitted by ACI 318-19 155
7.2.5 Horizontal Shear Capacity from Beam Tests Compared to Limit in ACI 318-19 and ACI 562-19 Code 155
7.3 Application of Research Findings 156
References 158

List of Tables

Table 2-1: Results from specimens with unreinforced interfaces from Revesz (1953). ..10

Table 2-2: Results from specimens with unreinforced interfaces from Hanson (1960). .12

Table 2-3: Results from specimens with unreinforced interfaces from Saemann and Washa (1964).....14

Table 2-4: Results from specimens with unreinforced interfaces from Seibel and Latham (1988). 17

Table 2-5: Horizontal shear stress from phase 1 beams tested by Kovach and Naito (2008). 20

Table 2-6: Results from Phase 2 beams specimens tested by Kovach and Naito (2008).22

Table 2-7: Results from beams specimens tested by Swan (2011). 25

Table 2-8: Summary of horizontal shear tests on beams with unreinforced interfaces. ..26

Table 2-9: Push-off specimen results from tests by Hanson (1960). 35

Table 2-10: Push-off test results from Seibel and Latham (1988). 37

Table 2-11: Average shear stresses from Iosipescu specimens tested by Swan (2011)...39

Table 2-12: Evolution of the ACI 318 horizontal shear capacity (psi). 40

Table 3-1. Phase 1 testing program matrix.....45

Table 3-2. Concrete workability and placement techniques 47

Table 3-3: Slab specimen parameters.....52

Table 4-1. Measured concrete slump. 60

Table 4-2. Concrete compressive strength results.....61

Table 4-3: Splitting Tensile Strength Results.....62

Table 4-4: ICRI CSP Values for repair interface conditions.....62

Table 4-5: Comparison of MTD from line laser scanner and sand patch test.....63

Table 4-6: Average mean texture depth for each interface condition based on LLS measurements. 64

Table 4-7. Phase 1 Direct shear strength results. 65

Table 4-8: Phase 1 Direct tensile pull-off strength results. 72

Table 4-9. Ratio of average interface direct shear strength to direct tensile pull-off strength 84

Table 4-10. Estimated characteristic design interface shear strengths based on Tolerance Factor Method (10% Fractile). 89

Table 5-1: Phase 2 Beam Specimen Test Matrix 92

Table 5-2: Phase 2 Slab Specimen Test Matrix 92

Table 6-1. Phase 2 measured concrete slump.....109

Table 6-2. Phase 2 concrete compressive strength results. 110

Table 6-3: Phase 2 concrete splitting tensile strength results.....110

Table 6-4: Phase 2 Mean Texture Depth obtained from LLS. 111

Table 6-5: Percent difference between compression strains in center of topping compared to outer edge of topping. 124

Table 6-6: Tension and compressive forces using linear strain profile along beam depth. 130

Table 6-7: Comparison of strains for test data and strains from strain compatibility analysis. 132

Table 6-8: Moments at each cross section for different strain profiles. 135

Table 6-9: Summary of horizontal shear stress at interface failure.....137

Table 6-10: Phase 2 direct shear (guillotine) results. 139

Table 6-11: Phase 2 direct tensile pull-off results.....139

Table 6-12: Phase 2 results summary.....144

Table 6-13: Summary of horizontal shear stress from beam tests. 146

List of Figures

Figure 2-1: Horizontal shear demand - Segment method (global force equilibrium). 5

Figure 2-2: Horizontal shear demand - Sectional method. 7

Figure 2-3: Cross-section of T-beam tested by Revesz (1953). 9

Figure 2-4: Girder specimens tested by Hanson (1960) 11

Figure 2-5: Girder loading and elevation by Hanson (1960). 11

Figure 2-6: Beam cross-section in Saemann and Washa (1964). 13

Figure 2-7: Elevation of reinforcement layout for slab panel tests by Seibel and Latham (1988). 16

Figure 2-8: Load application for slab panel tests by Seibel and Latham (1988). 16

Figure 2-9: Cross-section and elevation of T-beam specimens in Phase 1 tested by Kovach and Naito (2008). 18

Figure 2-10: Cross-section of T-beam in Phase 2 tested by Kovach and Naito (2008). ..21

Figure 2-11: Cross-section of beams tested by Swan (2011). 24

Figure 2-12: Beam loading conditions tested in Swan (2011). 25

Figure 2-13: Shear test methods. 30

Figure 2-14: Push-off specimens tested by Hanson (1960). 34

Figure 2-15: Load application of shear block tests by Seibel and Latham (1988). 37

Figure 2-16: Iosipescu test setup in Swan (2011). 38

Figure 3-1: Slab specimen general layout. 45

Figure 3-2. Tining rake. 48

Figure 3-3. Substrate roughened with tining rake. 48

Figure 3-4. Stiff-bristle broom. 48

Figure 3-5. Substrate roughened with broom. 48

Figure 3-6. Typical repair surface prepared by hydrodemolition (CSP 9-10). 49

Figure 3-7. Hydrodemolition procedure.....49

Figure 3-8. Typical repair surface condition prepared by mechanical abrasion (bush hammer followed by sand blasting – CSP 6-7).....50

Figure 3-9. Bush hammer bit.....50

Figure 3-10. Typical repair surface prepared by sandblast only. (CSP 3). 50

Figure 3-11. Sandblast procedure.....50

Figure 3-12. ICRI CSP Comparators. 53

Figure 3-13. Measuring volume of sand for ASTM E965 Sand Patch Test. 55

Figure 3-14. Measuring diameter of sand circle after spreading onto concrete surface per ASTM E965.....55

Figure 3-15. Line Laser Scanner on the tined substrate specimen. 56

Figure 3-16. Sample LLS 3D scan data for tined substrate specimen. 56

Figure 3-17. Guillotine shear jig – side view. 57

Figure 3-18. Guillotine shear jig – top view. 57

Figure 3-19. Core sample inside guillotine jog placed within concrete compression testing machine.....57

Figure 3-20. Core sample shear failure interface after testing (loading head removed). .57

Figure 3-21. Direct tensile pull-off testing device. 59

Figure 3-22. Direct tensile pull-off testing sample.....59

Figure 4-1. Average direct shear (guillotine) strength results (psi). Note current ACI interface nominal shear strength for design is 80 psi. 66

Figure 4-2. Direct shear failure plane at interface bond line (whole specimen). 66

Figure 4-3. Direct shear failure plane at interface bond line (only substrate portion of core shown). 66

Figure 4-4. Direct shear failure plane propagating into topping layer (whole specimen). 67

Figure 4-5. Direct shear failure plane propagating into topping layer (only substrate portion of core shown).....67

Figure 4-6. Visual comparison of interface conditions for precast specimens with topping concrete placed under different conditions. 69

Figure 4-7. Direct shear test orientation for precast specimen loaded perpendicular to the roughening direction.....71

Figure 4-8. Direct shear test orientation for precast specimen loaded parallel to the roughening direction.....71

Figure 4-9: Average direct tensile pull-off results (psi). 73

Figure 4-10. Measured mean texture depths and bond strengths for difference surface preparation techniques.....80

Figure 4-11: Mean texture depth vs. direct tensile pull-off strength. 81

Figure 4-12: Mean texture depth vs. direct shear strength. 82

Figure 4-13. Precast Series Tine Interface: Close up view of topping consolidation in substrate groove created by tining rake. 83

Figure 4-14: Correlation between interface direct shear strength and direct tensile pull-off strength.....85

Figure 4-15. Variation of ratio of shear-to-tensile bond strength with respect to mean texture depth. 86

Figure 5-1. Hydrodemolition.....93

Figure 5-2. Sandblast.....93

Figure 5-3. Tine.....93

Figure 5-4. Broom 93

Figure 5-5: Beam specimen cross-section – Failure end.....95

Figure 5-6: Beam specimens cross-section – Non-failure end. 95

Figure 5-7: Beam specimen elevation view. 96

Figure 5-8: Beam substrate rebar cages ready for casting.....97

Figure 5-9: Beam substrate showing stirrups on non-failure end that extend into topping as interface reinforcement. 97

Figure 5-10: Hydrodemolition compared to CSP 10 comparator. 98

Figure 5-11: Sandblast compared to CSP 3 comparator. 99

Figure 5-12: Hydrodemolition substrate with debonding foam tape. 100

Figure 5-13: Beams ready for topping pour. 101

Figure 5-14: Soaking substrates before casting to achieve SSD conditions. 101

Figure 5-15: Beam test setup. 103

Figure 5-16: Pin support 104

Figure 5-17: Roller support 104

Figure 5-18: Loading plates 105

Figure 5-19: Linear potentiometer layout. 106

Figure 5-20: End-slip linear potentiometers. 106

Figure 5-21: Side face linear potentiometer. 107

Figure 5-22: Strain gauge layout. 108

Figure 6-1: MTD results for Phase 2 specimens. 112

Figure 6-2: Phase 2 MTD groups. 113

Figure 6-3: Crack progression of monolithic beam. 115

Figure 6-4: Crack progression of tine beam. 115

Figure 6-5: Crack progression of hydrodemolition beam. 116

Figure 6-6: Failed monolithic beam with estimated location of stirrups. 117

Figure 6-7: Crack pattern after interface slip. 118

Figure 6-8: Interface crack after slip at end of topping slab. 118

Figure 6-9: Top of substrate concrete crushing at midspan when tension steel yielded. Vertical gap seen between topping and substrate on left side of photo.....119

Figure 6-10: Load-vs.-deflection of monolithic, tine, broom, and hydrodemolition specimens. 120

Figure 6-11: Vertical load versus substrate-to-topping slip measured at midspan. 121

Figure 6-12: Vertical load versus substrate-to-topping slip measured 16” from midspan on the failure end: (a) full response, (b) close-up view of slip during interface failure.....121

Figure 6-13: Vertical load versus substrate-to-topping slip measured 32” from midspan on the failure end: (a) full response, (b) close-up view of slip during interface failure.....122

Figure 6-14: Vertical load versus substrate-to-topping slip measured 42” from midspan on the failure end: (a) full response, (b) close-up view of slip during interface failure.....122

Figure 6-15: Slip during interface failure versus distance from midspan. 122

Figure 6-16: Strain in tension steel versus moment: (a) Midspan, (b) 16” from Midspan, and (c) 32” from Midspan. 125

Figure 6-17: Strain in compression steel in center of topping slab versus moment: (a) Midspan, (b) 16” from Midspan, and (c) 32” from Midspan. 126

Figure 6-18: Strain in compression near outer edge of topping slab versus moment: (a) Midspan, (b) 16” from Midspan, and (c) 32” from Midspan. 127

Figure 6-19: Concrete stress-strain model (fib 2010) 128

Figure 6-20: Strain profiles from Method A: linear strain along entire depth using strain gauge data.....129

Figure 6-21: Strain profiles from Method B: linear distribution for compressive region but not for tension region. Equilibrium enforced. 131

Figure 6-22: Strain distributions from strain compatibility analysis.....132

Figure 6-23: Moment distribution along beam length.....134

Figure 6-24: Horizontal shear stress versus distance from midspan on the beam failure end: (a) hydrodemolition beam, (b) tine beam, and c) broom beam. 138

Figure 6-25: MTD results from Phase 1 and Phase 2.....141

Figure 6-26: Direct shear and direct tensile strengths (y-axis) versus beam horizontal shear stress results (x-axis).....144

Figure 6-27: Mean texture depth versus horizontal shear stress from beam tests.....145

Chapter 1 : Introduction

This thesis presents an experimental investigation on the horizontal shear capacity of composite concrete members with unreinforced interfaces.

1.1 BACKGROUND

The design for horizontal shear transfer at an interface between concrete placed at two different times occurs in several scenarios in new construction and repair applications. The ACI 318-19 (ACI 2019) and ACI 562-19 (ACI 2019) design requirements for interface shear transfer limit the nominal strength of an intentionally roughened, unreinforced interface to 80 psi, while an unreinforced interface without intentional roughening is assumed to have no shear strength. These nominal shear strength limits can be punitive for several applications, such as toppings on precast hollow-core slabs and double-T beams, partial depth repairs on slabs and bonded overlays. When interface areas are large, requirements to add interface reinforcement and/or intentional roughening result in considerable time and expense or, in some cases, the decision that some other approach is needed.

Published research findings (e.g., Hanson 1960, Saemann and Washa 1964, Kovach and Naito 2008) suggest that the current 80 psi nominal limit for interface shear stress without interface reinforcement appears to be overly conservative, which may be substantially reducing the cost-effectiveness of topping slab designs and partial depth repair solutions in some situations. This research suggests that ACI standards and related construction practices can benefit from research devoted to redefining nominal interface shear stress limits. In addition, the use of relatively simple testing methods, such as the direct shear or guillotine method, to assess the shear bond strength at interfaces should be

explored as a means to demonstrate adequate interface shear transfer for quality control purposes.

1.2 Research Goal and Scope

This MS thesis presents an experimental study on interface shear transfer in unreinforced concrete interfaces with different roughness conditions. This collaborative research project with Wiss, Janney, Elstner Associates, Inc. (WJE) and the University of Texas at Austin intended to improve design recommendations for unreinforced concrete interfaces in new construction and in partial-depth repair applications. The study comprises two phases of laboratory testing. Phase 1 investigates the (local) interface bond strength of slab specimens through direct shear tests and direct tension pull-off tests. Phase 2 comprises flexural tests on beam specimens to assess interface shear strength under combined bending and shear. The beam tests represent typical interface shear conditions in practical applications and allow correlations to be established with common quality control test methods. The findings from this study are ultimately intended to contribute towards the development of a performance-based design approach for interface bond in topping slab and partial depth repair applications.

1.3 Structure of the Thesis

This thesis is organized in seven chapters. Following this introduction in Chapter 1, Chapter 2 presents a literature review on interface horizontal shear in composite concrete-to-concrete members. Chapter 3 presents the experimental program for Phase 1 testing on composite slabs, including research goals, specimen design and fabrication, and test setup. Chapter 4 presents and discusses the experimental results of Phase 1 testing.

Chapter 5 presents the experimental program for Phase 2 testing on composite beams, including research goals, specimen design and fabrication, test setup, and instrumentation. Chapter 6 presents and discusses the experimental results of Phase 2 testing. Finally, Chapter 7 presents the main findings and conclusions of this study.

Chapter 2 : Literature Review

This chapter presents a literature review on the knowledge related to horizontal shear in unreinforced concrete interfaces. The chapter is organized in the following sections: a review of conventional analytical methods used to calculate horizontal shear demand, a description of previous experimental studies on bond of unreinforced concrete interfaces, and a summary of current design provisions related to horizontal shear in unreinforced interfaces.

2.1 Determining Horizontal Shear Demand

Different analytical methods are available to calculate the horizontal shear demand at a composite interface. The most used are the segment method, the sectional method, and the simplified elastic method. These three methods are described in this section.

2.1.1 Segment Method

The segment method takes a slice of a composite beam and using equilibrium computes the force along the interface by taking the difference between compressive forces in the topping, as shown in Figure 2-1. The resulting force is divided by the area of bonded interface in the chosen segment to find the average interface shear stress. This equation is shown in Equation 2-1.

$$v_h = {(c_1 - c_2)}\Big/{(l * b_v)}$$

Equation 2-1

where,

v_h = Horizontal shear stress (average)

c_1 = Compression force in topping acting on one side of the beam

c_2= Compression force in topping acting on the opposite side of the beam

l = Length of segment taken for free body diagram

b_v = Width of interface resisting horizontal shear transfer

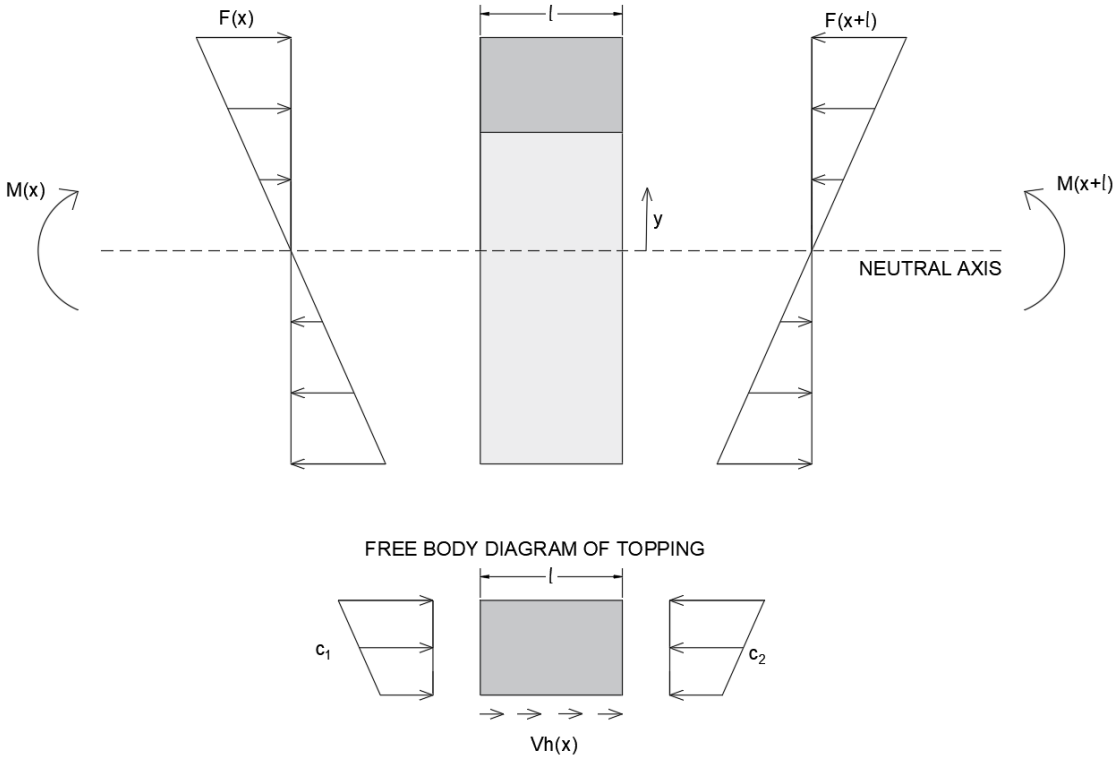

Figure 2-1: Horizontal shear demand - Segment method (global force equilibrium).

The segment method is permitted by ACI 318-19 section §16.4.5.1. It should be noted that the length segment chosen will affect the magnitude of horizontal shear stress. A segment with a high gradient in flexural moment demands will lead to a higher horizontal shear stress. If a segment with a lower gradient in moment demands is chosen, it may result in an unconservative estimate of horizontal shear demand. However, no specific guidelines are provided in ACI 318-19 about the length of the segment.

2.1.2 Sectional Method (or Classical Elastic Method)

The sectional method assumes elastic beam behavior. The method takes a free body diagram of an infinitesimal segment, labeled "dx" in Figure 2-2. Using equilibrium, the horizontal shear force is directly related to the vertical shear at that section. The resulting expression is shown below as Equation 2-2.

$$v_h = {(V * Q)}/{(I * b_v)}$$

Equation 2-2

Where,

v_h = Horizontal shear stress

V = Vertical shear force

Q = First moment of inertia with respect to the neutral axis of the slab

I = Moment of inertia of entire section

b_v = Width of bonded interface

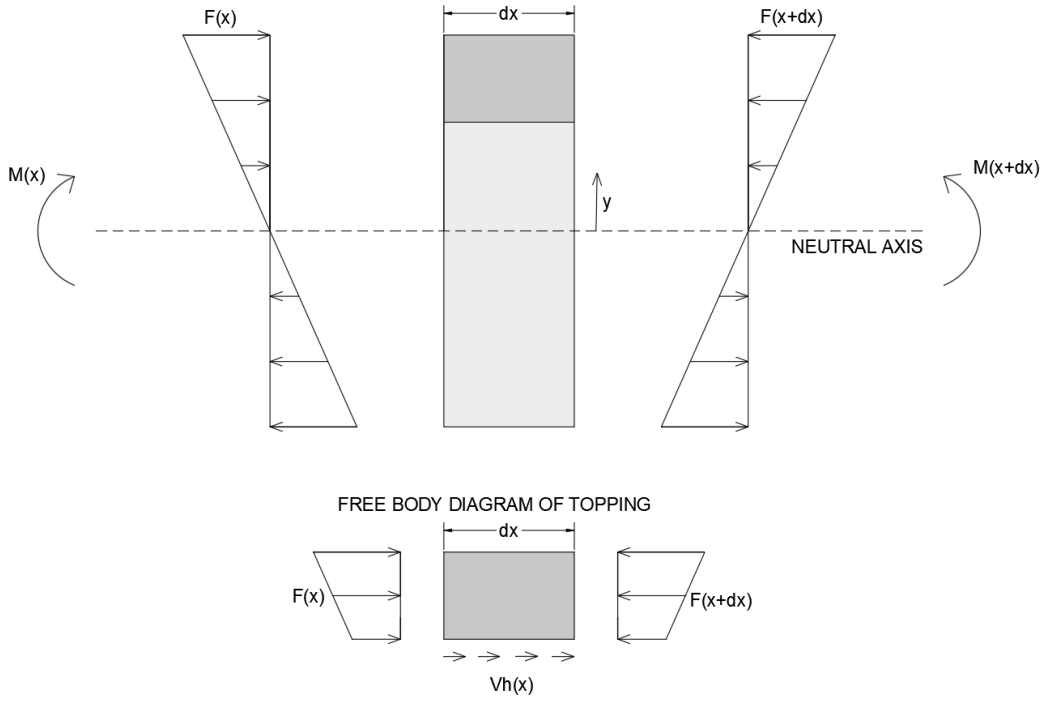

Figure 2-2: Horizontal shear demand - Sectional method.

This method is based on the Euler-Bernoulli theory for elastic beams. While not valid for concrete members at ultimate conditions, and also not a method approved by ACI 318-19, many previous studies (Revesz 1953, Hanson 1960, Saemann and Washa 1964) use the sectional method when determining horizontal shear stress capacity of their specimens.

2.1.3 Simplified Elastic Behavior

The simplified elastic behavior method uses flexural beam theory and analyzes an infinitesimal segment labeled “dx” just as was done in the sectional method. In this method the change in moment (dM) is equated to the shear using Euler-Bernoulli beam

theory (dM=Vdx). The change in moment can also be estimated as the effective depth multiplied by the difference in compressive forces. The resulting equation is shown in Equation 2-3. This derivation uses the same figure as the sectional method previously shown in Figure 2-2.

$$v_u = {V_u}/{(b_v * d)}$$

Equation 2-3

Where,

$v_u =$ Horizontal shear stress

$V_u =$ Vertical shear force

$d =$ Distance from extreme compression fiber for the entire composite section to the centroid of longitudinal tension reinforcement, need not be taken less than 0.80h for prestressed concrete members

$b_v =$ Width of the contact surface

This simplified elastic behavior method is permitted in ACI 318-19 section §16.4.5.1.

2.2 Experimental Studies on Horizontal Shear Capacity of Unreinforced Interfaces - Beam Testing

Several experimental investigations have been conducted to characterize the bond behavior of unreinforced concrete-to-concrete interfaces. The studies presented in this section investigate interface bond strength using beam specimens tested in flexure.

2.2.1 Revesz (1953)

Revesz tested five composite T-beams with unreinforced interfaces to observe behavior in flexure. Four of the beams were prestressed with high tensile strength wire tensioned to various stresses and one specimen was reinforced with mild steel. All specimens had a smooth interface with no reinforcement across the interface. The typical beam cross-section is shown in Figure 2-3. The specimens were loaded at third points of the 14-foot span.

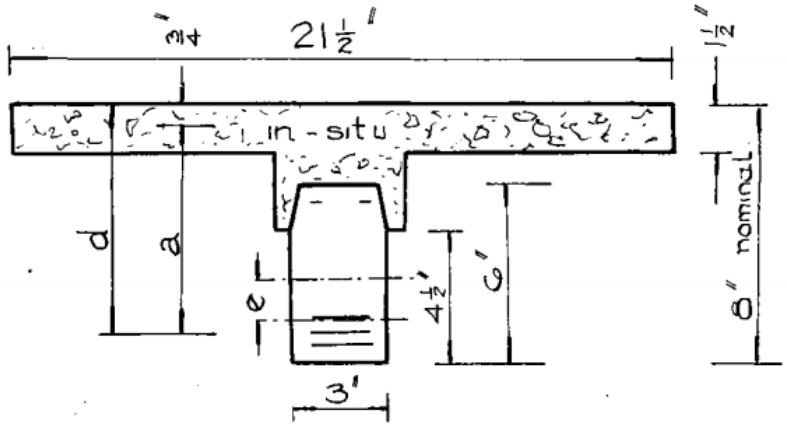

Figure 2-3: Cross-section of T-beam tested by Revesz (1953).

The results of this study are summarized in Table 2-1. Four beams (specimens L, G, F, and N) failed by steel fracture or steel yielding, and one beam (specimen J) failed in horizontal shear. The reported horizontal shear stress at failure for specimen J was 134 psi based on the sectional method. Based on the test observations, Revesz recommended roughening contact surfaces of composite concrete beams to prevent failure by horizontal shear.

Table 2-1: Results from specimens with unreinforced interfaces from Revesz (1953).

Specimen ID	Reinforcement Across the Interface	Interface Roughness Technique	Failure mode	Method for Calculating Horizontal Shear Stress	Reported Horizontal Shear Stress at Horizontal Shear Failure (psi)
L	None	Smooth	Steel Fracture	-	-
G	None	Smooth	Steel Fracture	-	-
F	None	Smooth	Steel Fracture	-	-
N	None	Smooth	Steel Yield	-	-
J	None	Smooth	Horizontal Shear	Sectional	134

2.2.2 Hanson (1960)

Hanson tested sixty-two composite push-off specimens and ten composite T-shaped girders to explore horizontal shear transfer at the concrete interface. Various adhesive bond agents, surface roughnesses, shear keys, stirrups (interfacial ties) and contact lengths were investigated. The push-off tests are discussed in section 2.4.

The composite girders were designed to reach high interface shear stresses before flexural failure. The sectional method was used to find horizontal shear stress, but this method was adapted to consider the cracked transformed cross section. Ten girders were tested, one of which had an unreinforced interface. The specimen with an unreinforced interface, BR1, had a rough[1] and bonded[2] surface. The typical cross-section for the girders is shown in Figure 2-4.

[1] Rough is defined by scraping the surface with steel to approximately ¼ -inch. (Hanson 1960)
[2] Bonded is defined as no attempt to destroy adhesive bond. (Hanson 1960)

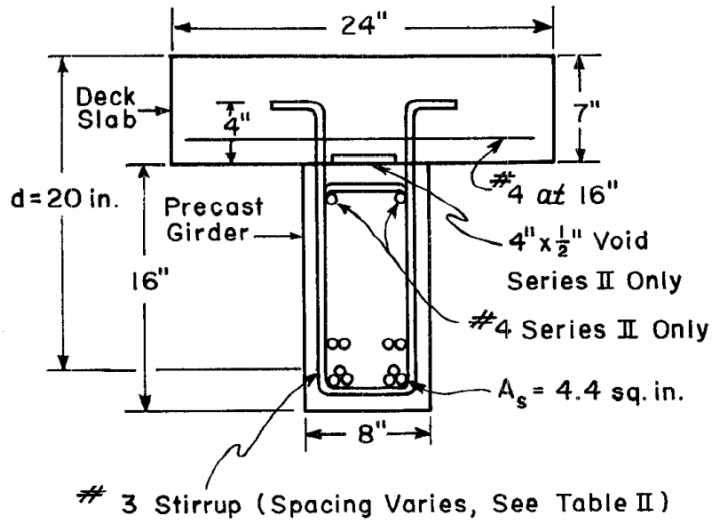

Figure 2-4: Girder specimens tested by Hanson (1960)

The substrate of the girder was cast in plywood forms and consolidated with spud vibrators. The surface conditions were applied and then wet cured for seven days followed by drying for seven days. Then the top deck was poured. This cast was wet cured for seven days and left to dry for seven additional days before testing.

Specimen BR-1 had a 145-inch simple plan with two point loads 25-inches apart in the center of the span. The loading scheme is shown in Figure 2-5.

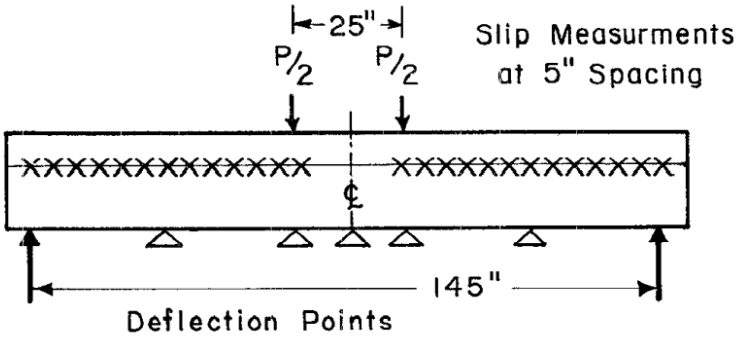

Figure 2-5: Girder loading and elevation by Hanson (1960).

The failure mode of girder BR-1 was noted as a shear-compression failure. Flexural cracks develop and move up toward the point loads. Once the cracks reached the interface they travel along the joint for a short distance. The load or horizontal shear stress at failure was not stated in this study. One conclusion from girder tests was composite action stops when slip between the substrate and topping reach approximately 0.005 inches. The horizontal shear stress of girder BR-1 at a slip of 0.005 inches is approximately 310 psi based on the sectional method. A summary of the results from the beam with an unreinforced interface is provided in Table 2-2.

Table 2-2: Results from specimens with unreinforced interfaces from Hanson (1960).

Specimen ID	**Reinforcement Across the Interface**	**Interface Roughness Technique**	**Failure mode**	**Method for Calculating Horizontal Shear Stress**	**Reported Horizontal Shear Stress at Horizontal Shear Failure (psi)**
BR-1	None	Rough & Bonded	Shear-compression	Sectional	310

Beam and push-off tests results support the conclusion of this study that an unreinforced, rough-bonded interface had a horizontal shear capacity of 500 psi and a smooth-bonded interfaced had a horizontal shear capacity of 300 psi and that 175 psi can be added for each additional percent of reinforcement across the interface. Push-off test results are summarized in section 2.4.1 of this literature review.

2.2.3 Saemann and Washa (1964)

Saemann and Washa tested forty-two composite beams, two of which had no reinforcement across the interface (15C and 16C). The cross-section for these beams is shown in Figure 2-6.

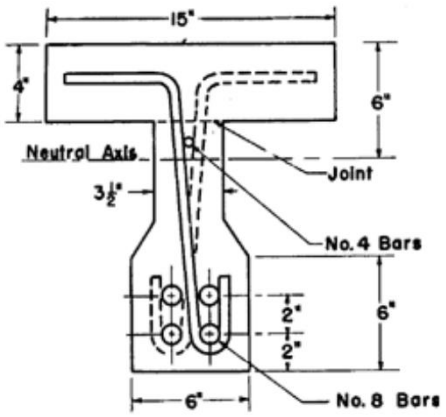

Figure 2-6: Beam cross-section in Saemann and Washa (1964).

The webs were cast and wet cured with burlap for 7 days and then the slab was cast on top. The composite specimen was wet cured again for 7 days and tested 21 days later. The two beams with unreinforced interfaces had intermediate roughness. This roughness was achieved by first screeding off the top surface. A retarding agent was then applied to allow brushing of the mortar between the coarse aggregate. The resulting roughness had an amplitude of approximately 1/8-inch.

Beam 15C was eleven-foot long and beam 16C was eight-foot long. Both were loaded under flexure by two point loads, each offset by one foot from the center. Horizontal shear stress was calculated using the sectional method. Beam 15C reported a horizontal shear stress of 420 psi and beam 16C reported a horizontal shear stress of 606 psi when the beam failed in shear. Shear failure is described as diagonal cracks traveling toward the top-center of the beam. Once a crack meets the interface, it travels along the

joint. At ultimate loading the shear cracks traveled on both ends of the beam. Final failure usually had crushing of concrete in the web. The ultimate horizontal shear stress of beams 15C and 16C were 420 psi and 606 psi, respectively.

In addition to these horizontal shear stresses at ultimate loading, the paper states the horizontal shear stress at 0.005 inch slip. The value of 0.005 inches was credited to Hanson (1960) and described to be a critical value at which the beam deflection curves deviate from a smooth curve. The horizonal shear stress for beam 15C at 0.005-inch slip was 329 psi and for beam 16C was 443 psi. The results of these specimens are summarized in Table 2-3.

Table 2-3: Results from specimens with unreinforced interfaces from Saemann and Washa (1964).

Specimen ID	**Reinforcement Across the Interface**	**Interface Roughness Technique**	**Failure mode**	**Method for Calculating Horizontal Shear Stress**	**Reported Horizontal Shear Stress at Horizontal Shear Failure (psi)**
15C	None	Intermediate roughness (1/8" brushing)	Both specimens reported to fail by a shear crack traveling along the interface.	Sectional	420
16C	None	Intermediate roughness (1/8" brushing)		Sectional	606

Saemann and Wahsa (1964) proposed an equation to calculate the horizontal shear capacity based on the findings of their study. This equation (shown below as Equation 2.5) is simplified for unreinforced interfaces.

$$Y = \frac{2700}{X + 5}$$

Equation 2-4

where,

$Y =$ ultimate shear strength [psi]

$X =$ the ratio of shear span to effective depth

This proposed equation provides a significant increase for unreinforced interfaces. The shear span to depth ratio would need to exceed 33 to have a design capacity of 80psi. Roughness is not considered in this equation, but the paper does conclude that the ultimate shear strength does increase as roughness of the surface is increased.

2.2.4 Seibel and Latham (1988)

Seibel and Latham investigated interface bond on concrete interfaces by testing fourteen shear block tests and twelve slab panel tests (under flexure). The shear block specimens are discussed in section 2.4.

The slab panel testing program included four slab panels with unreinforced interfaces (SP-1A, SP-2, SP-3, and SP-4). The specimen number represents the roughness as follows: 1- Monolithic, 2- Lubricated, 3- Surface rough, and 4- Scarified. The slab panel test reinforcement and setup are shown in Figure 2-7 and Figure 2-8.

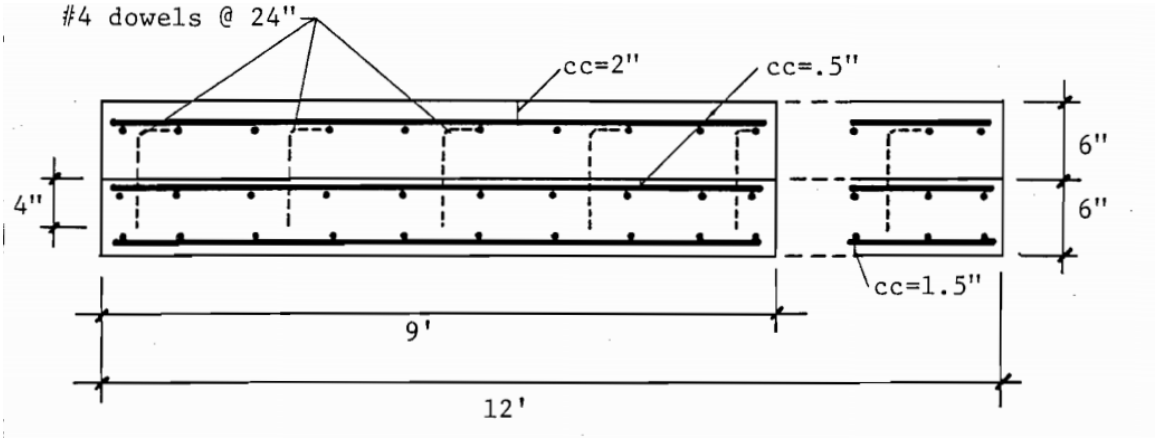

Figure 2-7: Elevation reinforcement layout for slab panel tests by Seibel and Latham (1988).

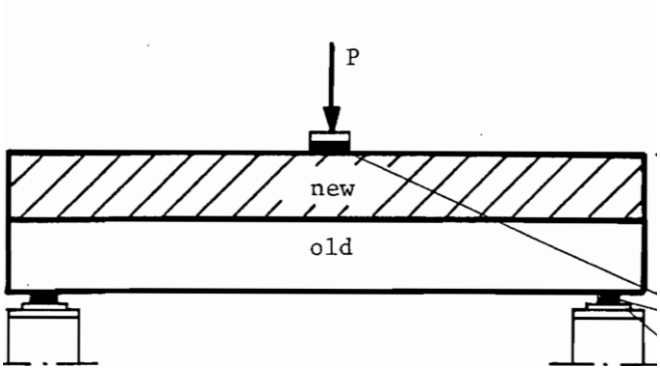

Figure 2-8: Load application for slab panel tests by Seibel and Latham (1988).

The initial behavior of all slab panel specimens was identical to that of a control monolithic specimen, except the lubricated specimen which failed due to sliding at the horizontal interface. The horizontal shear stress was not stated, but instead the maximum load, load at yield, and load when the interface delamination began. Using the simplified elastic method, the following shear stresses were calculated using the load when interface delamination began (horizontal shear failure or interface failure). The specimen results are summarized in Table 2-4.

This study concluded that using dowels to reinforce the interface while practicing appropriate placement techniques, such as wet curing, are necessary to avoid horizontal shear failures.

Table 2-4: Results from specimens with unreinforced interfaces from Seibel and Latham (1988).

Specimen ID	**Reinforcement Across the Interface**	**Interface Roughness Technique**	**Failure mode**	**Method for Calculating Horizontal Shear Stress**	**Reported Horizontal Shear Stress at Horizontal Shear Failure (psi)**
SP-2	None	Lubricated	Complete interlayer delamination + crushing	Simplified elastic	16.4
SP-3	None	Surface Rough	Interlayer delamination of left side + crushing	Simplified elastic	28.8
SP-4	None	Scarified	Crushing + flexural shear failure	-	-

2.2.5 Kovach and Naito (2008)

Kovach and Naito performed a two-phase study of interface bond in precast beam applications. The study consisted of nineteen composite beams in Phase 1 and twenty-two composite beams in Phase 2. All beams with unreinforced interfaces.

The first phase investigated the impact of roughness and compressive strength on the horizontal shear stress capacity. The interface roughness types were typical for precast applications including as-placed, broom, ¼" rake, and sheepsfoot. The web was fabricated

at a precast/prestressing manufacturer. The slabs were poured one day after the web was poured. Measures were taken to assure the surface was clean and free of laitance.

The beams were tested in two loading configurations: seven beams were tested under five-point loading (Beams 1 through 7) and twelve beams were tested under two-point loading (Beams 8 through 19). The five-point configuration was to represent an approximately uniform loading condition. The interface was unbonded in some regions of Beams 8-19 to create a higher stress at the bonded region. The unbonded region was on the outside of the beam. The cross-section and elevation of the beams used in Phase 1 are shown in Figure 2-9.

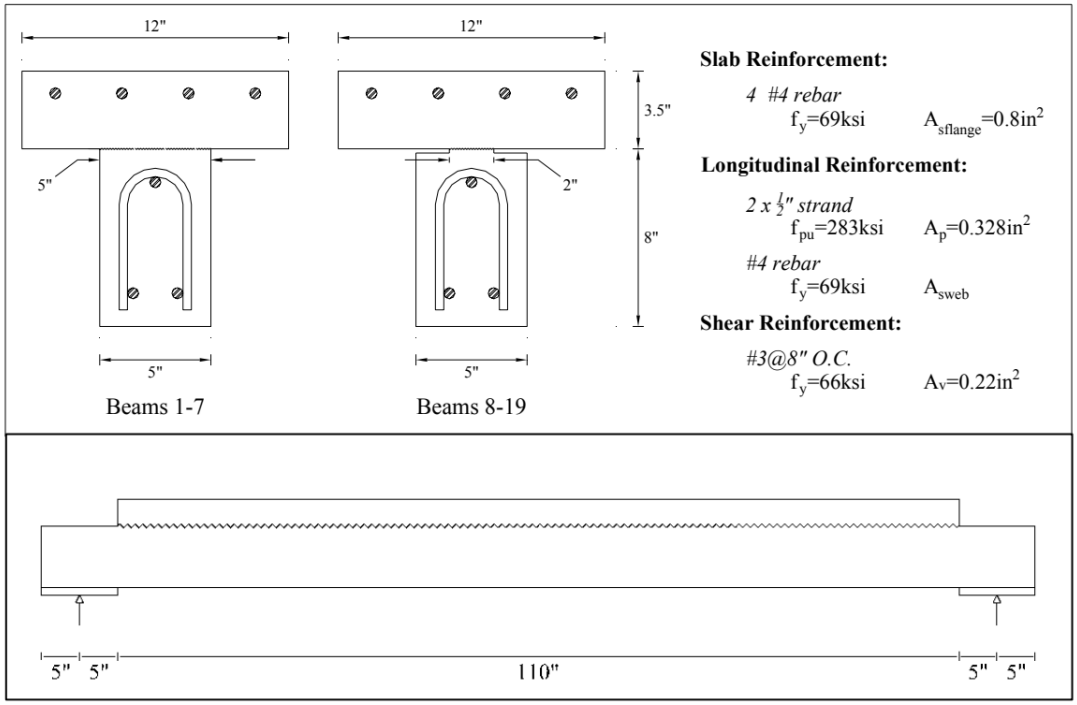

Figure 2-9: Cross-section and elevation of T-beam specimens in Phase 1 tested by Kovach and Naito (2008).

Slip gauges and surface mounted strain gauges were used to measure the beam deformations during testing. Using the strain values from the instrumentation and stress-strain relations from concrete cylinder tests a stress profile was developed at failure. The horizontal shear stress was then calculated using segment method (global force equilibrium). It was not mentioned what length or location of segment was used.

Eleven of the twelve two-point loaded specimens failed in horizontal shear. The horizontal shear stresses for those specimens are shown in Table 2-5. The values presented are found using the strain described earlier. The remaining specimens, including all those tested under five-point loading, failed in flexure or combined flexure-shear, as shown in Table 2-5.

Table 2-5: Horizontal shear stress from phase 1 beams tested by Kovach and Naito (2008).

Specimen ID	Reinforcement Across the Interface	Interface Roughness Technique	Failure mode	Method for Calculating Horizontal Shear Stress	Reported Horizontal Shear Stress at Horizontal Shear Failure (psi)
1	None	As-Placed	Flexure-Shear	-	-
2	None	Broom	Flexure-Shear	-	-
3	None	Monolithic	Flexure-Shear	-	-
4	None	Rake	Flexure-Shear	-	-
5	None	Rake	Flexure	-	-
6	None	Rake	Flexure-Shear	-	-
7	None	Sheepsfoot	Flexure-Shear	-	-
8	None	As-Placed	Horizontal Shear	From Strain (C/Lb_v)	482.2
9	None	As-Placed	Horizontal Shear	From Strain (C/Lb_v)	814
10	None	Broom	Horizontal Shear	From Strain (C/Lb_v)	915.6
11	None	Monolithic	Horizontal Shear	From Strain (C/Lb_v)	1075
12	None	Monolithic	Flexure-Shear	-	-
13	None	Rake	Horizontal Shear	From Strain (C/Lb_v)	639
14	None	Rake	Horizontal Shear	From Strain (C/Lb_v)	1182
15	None	Rake	Horizontal Shear	From Strain (C/Lb_v)	1348
16	None	Rake	Horizontal Shear	From Strain (C/Lb_v)	1245
17	None	Rake	Horizontal Shear	From Strain (C/Lb_v)	1054
18	None	Rake	Horizontal Shear	From Strain (C/Lb_v)	1194
19	None	Smooth	Horizontal Shear	From Strain (C/Lb_v)	787.4

While there was no quantification of the roughness, results from Phase 1 suggest there is a positive correlation between the intensity of the roughness and the horizontal shear strength. For best composite performance, this study suggested using a rake finish.

Phase 2 tested twenty-two composite beams under two-point loading of precast webs with toppings. The typical cross-section for these beams is shown in Figure 2-10.

The width of the interface was cut in these beams as well by debonding the outer two edges.

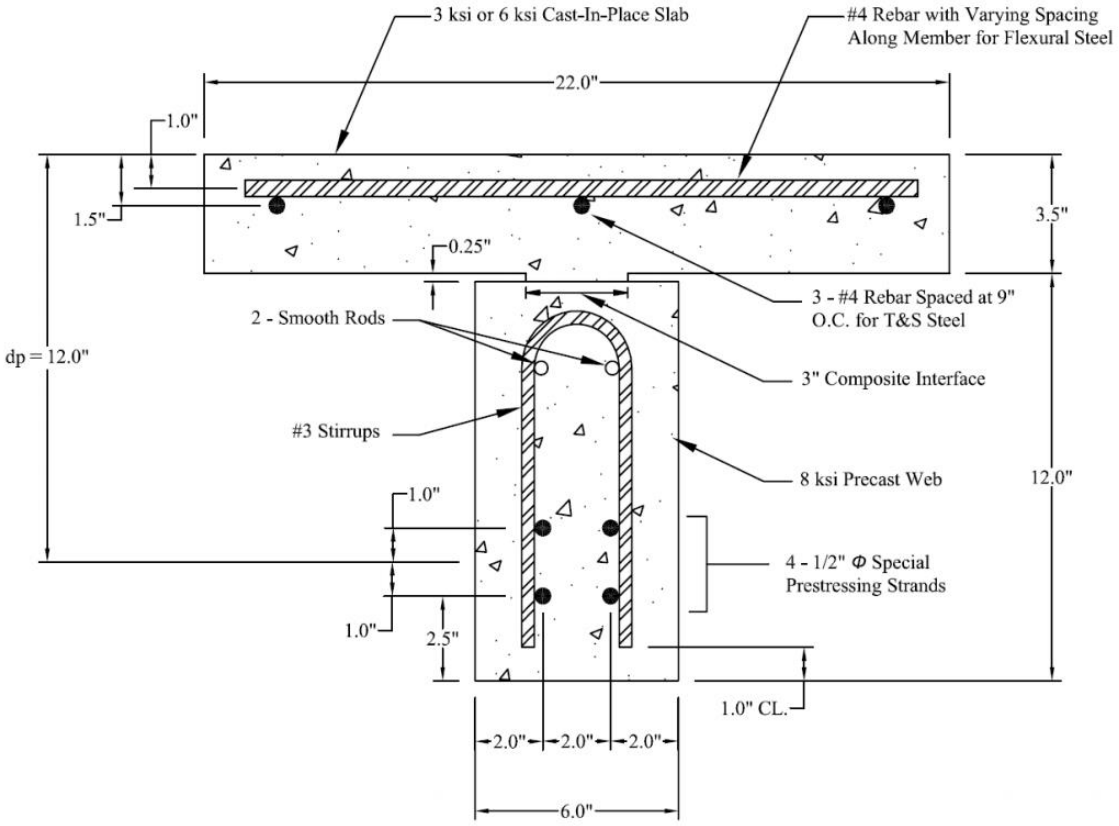

Figure 2-10: Cross-section of T-beam in Phase 2 tested by Kovach and Naito (2008).

Based on the conclusions from the previous phase, Phase 2 reduced the number of variables to obtain more dependable results. The different surface finishes used were smooth, broom, as-placed, and rake. Two different slab strengths were tested representing low (3 ksi) and high (6 ksi) strengths.

The beams in Phase 2 were fabricated differently than in Phase 1. There was a several month gap in between placement of the topping slab and the fabrication of the

precast/prestressed web. This was done to capture greater differential shrinkage between the two members. The webs were steam cured for three days and let to sit for a few months. The topping slab was poured and vibrated on top of the webs. The slab was wet cured with burlap for seventeen days and then left to air dry for ten days before testing.

Similar to Phase 1, the strain profile was found using strain data from the test. Then the segment method was using stress-strain relationships to find the compressive forces in the topping. The results of Phase 2 are summarized in Table 2-6.

Table 2-6: Results from Phase 2 beams specimens tested by Kovach and Naito (2008).

Specimen ID	**Reinforcement Across the Interface**	**Interface Roughness Technique**	**Failure mode**	**Method for Calculating Horizontal Shear Stress**	**Reported Horizontal Shear Stress at Horizontal Shear Failure (psi)**
6B3-E	None	Broom	Horizontal Shear	From Strain (C/Lb_v)	294
6B3-W	None	Broom	Horizontal Shear	From Strain (C/Lb_v)	297
6B4-E	None	Broom	Horizontal Shear	From Strain (C/Lb_v)	326
6B4-W	None	Broom	Horizontal Shear	From Strain (C/Lb_v)	364
6B5-E	None	Broom	Horizontal Shear	From Strain (C/Lb_v)	363
6B5-W	None	Broom	Horizontal Shear	From Strain (C/Lb_v)	405
6B6-E	None	Broom	Horizontal Shear	From Strain (C/Lb_v)	329
6B6-W	None	Broom	Horizontal Shear	From Strain (C/Lb_v)	311
3A1-E	None	As-Placed	Horizontal Shear	-	-
3A1-W	None	As-Placed	Horizontal Shear	-	-
3A2-E	None	As-Placed	No-data	-	-
3A2-W	None	As-Placed	Horizontal Shear	From Strain (C/Lb_v)	589
6A3-E	None	As-Placed	Horizontal Shear	From Strain (C/Lb_v)	502
6A3-W	None	As-Placed	Horizontal Shear	From Strain (C/Lb_v)	549
6A4-E	None	As-Placed	Horizontal Shear	From Strain (C/Lb_v)	558
6A4-W	None	As-Placed	Horizontal Shear	From Strain (C/Lb_v)	550

Specimen ID	Reinforcement Across the Interface	Interface Roughness Technique	Failure mode	Method for Calculating Horizontal Shear Stress	Reported Horizontal Shear Stress at Horizontal Shear Failure (psi)
6A5-E	None	As-Placed	Horizontal Shear	From Strain (C/Lb_v)	476
6A5-W	None	As-Placed	Horizontal Shear	From Strain (C/Lb_v)	375
6A6-E	None	As-Placed	Horizontal Shear	From Strain (C/Lb_v)	555
6A6-W	None	As-Placed	Horizontal Shear	From Strain (C/Lb_v)	449
6A7-E	None	As-Placed	Horizontal Shear	From Strain (C/Lb_v)	409
6A7-W	None	As-Placed	Horizontal Shear	From Strain (C/Lb_v)	457
6A8-E	None	As-Placed	Horizontal Shear	From Strain (C/Lb_v)	514
6A8-W	None	As-Placed	Horizontal Shear	From Strain (C/Lb_v)	592
3R1-E	None	Rake	Horizontal Shear	From Strain (C/Lb_v)	782
3R1-W	None	Rake	Horizontal Shear	From Strain (C/Lb_v)	668
6R3-E	None	Rake	Horizontal Shear	From Strain (C/Lb_v)	560
6R3-W	None	Rake	Horizontal Shear	From Strain (C/Lb_v)	603
6R4-E	None	Rake	Horizontal Shear	From Strain (C/Lb_v)	579
6R4-W	None	Rake	Horizontal Shear	From Strain (C/Lb_v)	742
6R5-E	None	Rake	Horizontal Shear	From Strain (C/Lb_v)	487
6R5-W	None	Rake	Horizontal Shear	From Strain (C/Lb_v)	476
6R6-E	None	Rake	Horizontal Shear	From Strain (C/Lb_v)	664
6R6-W	None	Rake	Horizontal Shear	From Strain (C/Lb_v)	664
6R7-E	None	Rake	Horizontal Shear	From Strain (C/Lb_v)	652
6R7-W	None	Rake	Horizontal Shear	From Strain (C/Lb_v)	665
6R8-E	None	Rake	Horizontal Shear	From Strain (C/Lb_v)	478
6R8-W	None	Rake	Horizontal Shear	From Strain (C/Lb_v)	567

This study concluded that the horizontal shear strength obtained from beam tests were approximately six to ten times larger than the limit established in the ACI-318 code. The study also concluded that with an increase of surface roughness, the horizontal shear capacity increases.

2.2.6 Swan (2011)

Swan evaluated interface shear strength by testing twelve beams with Iosipescu tests and six beams in three-point flexural tests. All interfaces were unreinforced. The Iosipescu tests are discussed in section 2.4 and the beam tests are discussed here.

Six beams with three different surface treatments were fabricated for the flexural tests. The following are the surface roughnesses with corresponding CSP values smooth (CSP 2-3), bush-hammer (CSP 6) jackhammer (CSP 10). CSP is defined in Phase 1 of the current study in section 4.2.1 of this thesis.

The cross-section of the beams is shown in Figure 2-11. PVC wall paneling sheet was used as a bond breaker on the outer edges. In preparation of the topping layer, the substrate was sprayed with water for saturated surface-dry (SSD) conditions.

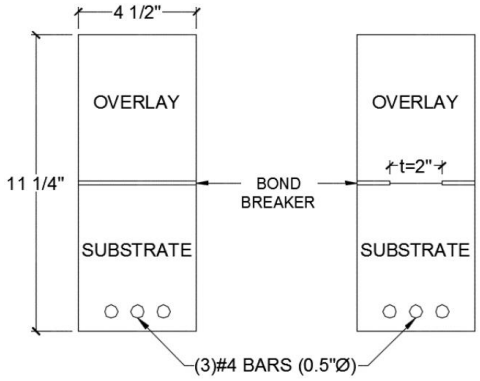

Figure 2-11: Cross-section of beams tested by Swan (2011).

One beam of each roughness was tested in flexural compression (shown on the left of Figure 2-12) and the other in flexural tension (shown on the right of Figure 2-12). This literature review will only discuss the three beams tests in flexural compression.

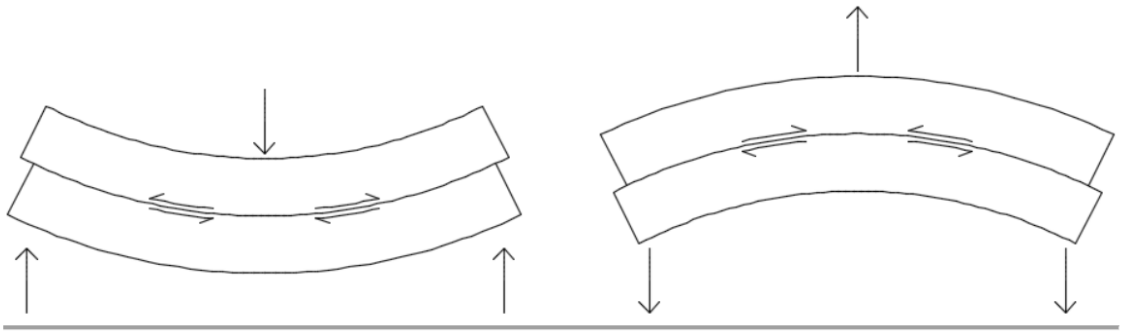

Figure 2-12: Beam loading conditions tested in Swan (2011).

The beams were tested with one point load at the center. The results from these tests are summarized in Table 2-7. Beam 1 and Beam 2 failed in diagonal tension. This was a diagonal crack (assumed to be from vertical shear) that traveled across the interface without causing any cracking along the interface. Beam 3 had a flexural crack that traveled up to the interface and then continued along the interface to the edge of the beam causing horizontal shear failure. The sectional method was used to find the horizontal shear stress at failure.

Table 2-7: Results from beams specimens tested by Swan (2011).

Specimen ID	**Reinforcement Across the Interface**	**Interface Roughness Technique**	**Failure mode**	**Method for Calculating Horizontal Shear Stress**	**Reported Horizontal Shear Stress at Horizontal Shear Failure (psi)**
1	None	Rake	Diagonal tension	-	-
2	None	Bush Hammer	Diagonal tension	-	-
3	None	Smooth	Flexural Shear	Sectional	637

2.2.7 Summary of previous beam tests on unreinforced interfaces

Table presents a summary of the beam tests presented in this section. Many studies were not able to fail the beam specimens in horizontal shear. The most comprehensive data on interface failure is obtained from the study by Kovach and Naito (2008), who cut parts of the bonded interfaces of their specimens with de-bonding material. As shown, most of the tests presenting interface failures presented horizontal shear strengths between 300 psi and 1000 psi. A few smooth or lubricated interfaces presented lower values.

Table 2-8: Summary of horizontal shear tests on beams with unreinforced interfaces.

Study	Specimen ID	Reinforcement Across the Interface	Interface Roughness Technique	Failure mode	Method for Calculating Horizontal Shear Stress	Reported Horizontal Shear Stress at Horizontal Shear Failure (psi)
Revesz (1953)	L	None	Smooth	Steel Fracture	-	-
	G	None	Smooth	Steel Fracture	-	-
	F	None	Smooth	Steel Fracture	-	-
	N	None	Smooth	Steel Yield	-	-
	J	None	Smooth	Horizontal Shear	Sectional	134
Hanosn (1960)	BR-1	None	Rough & Bonded	Shear-compression	Sectional	310
Saemann and Washa (1964)	15C	None	Intermediate roughness	The reported horizontal shear stress represents horizontal shear stress ultimate failure.	Sectional	329
	16C	None	Intermediate roughness		Sectional	443
Seibel and Latham (1988)	SP-2	None	Lubricated	Complete interlayer delamination + crushing	Simplified elastic	16.4
	SP-3	None	Surface Rough	Interlayer delamination of left side + crushing	Simplified elastic	28.8

Study	Specimen ID	Reinforcement Across the Interface	Interface Roughness Technique	Failure mode	Method for Calculating Horizontal Shear Stress	Reported Horizontal Shear Stress at Horizontal Shear Failure (psi)
Seibel and Latham (1988)	SP-4	None	Scarified	Crushing + flexural shear failure	-	-
Kovach and Naito Phase 1 (2008)	1	None	As-Placed	Flexure-Shear	-	-
	2	None	Broom	Flexure-Shear	-	-
	3	None	Monolithic	Flexure-Shear	-	-
	4	None	Rake	Flexure-Shear	-	-
	5	None	Rake	Flexure	-	-
	6	None	Rake	Flexure-Shear	-	-
	7	None	Sheepsfoot	Flexure-Shear	-	-
	8	None	As-Placed	Horizontal Shear	From Strain (C/Lb_v)	482.2
	9	None	As-Placed	Horizontal Shear	From Strain (C/Lb_v)	814
	10	None	Broom	Horizontal Shear	From Strain (C/Lb_v)	915.6
	11	None	Monolithic	Horizontal Shear	From Strain (C/Lb_v)	1075
	12	None	Monolithic	Flexure-Shear	-	-
	13	None	Rake	Horizontal Shear	From Strain (C/Lb_v)	639
	14	None	Rake	Horizontal Shear	From Strain (C/Lb_v)	1182
	15	None	Rake	Horizontal Shear	From Strain (C/Lb_v)	1348
	16	None	Rake	Horizontal Shear	From Strain (C/Lb_v)	1245
	17	None	Rake	Horizontal Shear	From Strain (C/Lb_v)	1054
	18	None	Rake	Horizontal Shear	From Strain (C/Lb_v)	1194
	19	None	Smooth	Horizontal Shear	From Strain (C/Lb_v)	787.4
Kovach and Naito Phase 2 (2008)	6B3-E	None	Broom	Horizontal Shear	From Strain (C/Lb_v)	294
	6B3-W	None	Broom	Horizontal Shear	From Strain (C/Lb_v)	297
	6B4-E	None	Broom	Horizontal Shear	From Strain (C/Lb_v)	326
	6B4-W	None	Broom	Horizontal Shear	From Strain (C/Lb_v)	364

Study	Specimen ID	Reinforcement Across the Interface	Interface Roughness Technique	Failure mode	Method for Calculating Horizontal Shear Stress	Reported Horizontal Shear Stress at Horizontal Shear Failure (psi)
Kovach and Naito Phase 2 (2008)	6B5-E	None	Broom	Horizontal Shear	From Strain (C/Lb_v)	363
	6B5-W	None	Broom	Horizontal Shear	From Strain (C/Lb_v)	405
	6B6-E	None	Broom	Horizontal Shear	From Strain (C/Lb_v)	329
	6B6-W	None	Broom	Horizontal Shear	From Strain (C/Lb_v)	311
	3A1-E	None	As-Placed	Horizontal Shear	-	-
	3A1-W	None	As-Placed	Horizontal Shear	-	-
	3A2-E	None	As-Placed	No-data	-	-
	3A2-W	None	As-Placed	Horizontal Shear	From Strain (C/Lb_v)	589
	6A3-E	None	As-Placed	Horizontal Shear	From Strain (C/Lb_v)	502
	6A3-W	None	As-Placed	Horizontal Shear	From Strain (C/Lb_v)	549
	6A4-E	None	As-Placed	Horizontal Shear	From Strain (C/Lb_v)	558
	6A4-W	None	As-Placed	Horizontal Shear	From Strain (C/Lb_v)	550
	6A5-E	None	As-Placed	Horizontal Shear	From Strain (C/Lb_v)	476
	6A5-W	None	As-Placed	Horizontal Shear	From Strain (C/Lb_v)	375
	6A6-E	None	As-Placed	Horizontal Shear	From Strain (C/Lb_v)	555
	6A6-W	None	As-Placed	Horizontal Shear	From Strain (C/Lb_v)	449
	6A7-E	None	As-Placed	Horizontal Shear	From Strain (C/Lb_v)	409
	6A7-W	None	As-Placed	Horizontal Shear	From Strain (C/Lb_v)	457
	6A8-E	None	As-Placed	Horizontal Shear	From Strain (C/Lb_v)	514
	6A8-W	None	As-Placed	Horizontal Shear	From Strain (C/Lb_v)	592
	3R1-E	None	Rake	Horizontal Shear	From Strain (C/Lb_v)	782
	3R1-W	None	Rake	Horizontal Shear	From Strain (C/Lb_v)	668
	6R3-E	None	Rake	Horizontal Shear	From Strain (C/Lb_v)	560
	6R3-W	None	Rake	Horizontal Shear	From Strain (C/Lb_v)	603

Study	Specimen ID	Reinforcement Across the Interface	Interface Roughness Technique	Failure mode	Method for Calculating Horizontal Shear Stress	Reported Horizontal Shear Stress at Horizontal Shear Failure (psi)
Kovach and Naito Phase 2 (2008)	6R4-E	None	Rake	Horizontal Shear	From Strain (C/Lb_v)	579
	6R4-W	None	Rake	Horizontal Shear	From Strain (C/Lb_v)	742
	6R5-E	None	Rake	Horizontal Shear	From Strain (C/Lb_v)	487
	6R5-W	None	Rake	Horizontal Shear	From Strain (C/Lb_v)	476
	6R6-E	None	Rake	Horizontal Shear	From Strain (C/Lb_v)	664
	6R6-W	None	Rake	Horizontal Shear	From Strain (C/Lb_v)	664
	6R7-E	None	Rake	Horizontal Shear	From Strain (C/Lb_v)	652
	6R7-W	None	Rake	Horizontal Shear	From Strain (C/Lb_v)	665
	6R8-E	None	Rake	Horizontal Shear	From Strain (C/Lb_v)	478
	6R8-W	None	Rake	Horizontal Shear	From Strain (C/Lb_v)	567
Swan (2011)	1	None	Rake	Diagonal tension	-	-
	2	None	Bush Hammer	Diagonal tension	-	-
	3	None	Smooth	Flexural Shear	Sectional	637

2.3 EXPERIMENTAL STUDIES ON HORIZONTAL SHEAR CAPACITY OF UNREINFORCED INTERFACES - BOND TESTS

This section summarizes research that has studied the shear strength of concrete to concrete interfaces by various bond testing. Currently there is no standard test in the industry to determine shear bond strength for unreinforced interfaces in repair or new construction. Research studies have evaluated various shear test methods including the slant shear test, torsion or friction-transfer test, bi-surface or triplet test, and single-shear tests including the guillotine test, each illustrated in Figure 2-13. The goal of these tests is to characterize interfacial strength with confidence and low variability. It is also desirable

to be able to correlate these results with actual horizontal shear strength of composite members. The eventual goal would be to use these bond tests to calculate an appropriate design strength.

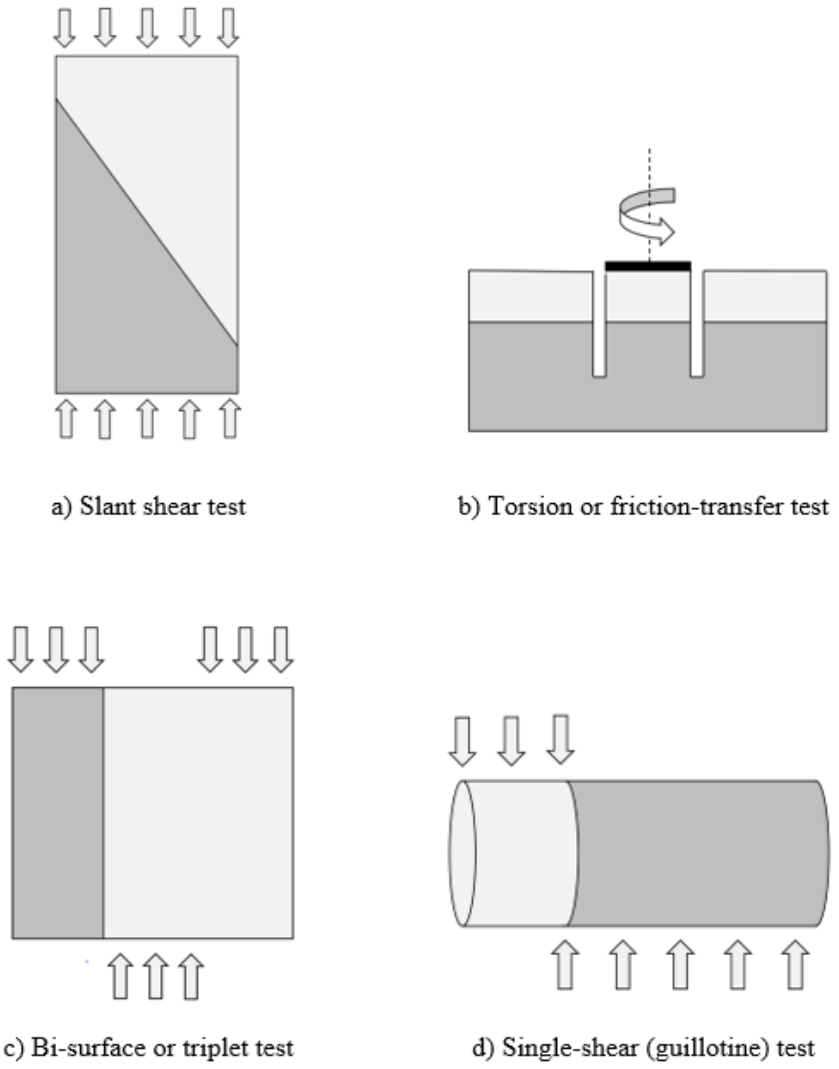

Figure 2-13: Shear test methods.

2.3.1 Comparison between bond test methods

Several research studies have compared different shear test methods to one another or to tensile bond strength by pull-off test or splitting tensile test.

Silfwerbrand (2003) investigated the use of an in-situ torsion test to assess interface shear strength and reported ratios of average shear strength to average tensile bond pull-off strength ranging from 1.9 to 3.1.

Rosen (2016) studied interface bond testing methods including the guillotine test, slant shear test, and tensile pull-off test. Slab specimens were fabricated with various roughening and consolidation techniques. The substrate roughening techniques include broom, rake, and bush hammer. Two specimens of each roughening technique were fabricated, one with a vibrated topping and the other hand consolidated. Rosen reported ratios of average slant shear strengths to average pull-off tensile strength ranging from 7.6 to 10.2. and ratios of average guillotine shear strengths to average pull-off tensile strength ranging from 1.3 to 2.2.

Momayez et al. (2005) studied different test methods for evaluating bond strength, including tensile bond pull-off, splitting prism, slant shear and direct shear. The direct shear test used involved lab cast rectangular prisms rather than core samples. Several concrete types were considered, and interface roughness was characterized as low (3 mm to 4 mm amplitude) or high (7 mm to 8 mm amplitude). Momayez et al. reported ratios of direct (single) shear to tensile pull-off bond strength of 1.6 to 2.2 and 1.7 to 2.4 for low and high roughness interfaces, respectively. The slant shear strength results produced higher ratios of shear to tensile pull-off strength of 5.1 to 7.5 and 5.4 to 8.8 for low and high roughness interfaces, respectively. The comparison of shear strength results and

splitting tensile strengths rather than pull-off tensile strengths showed similar ratio ranges (i.e. tensile pull-off strengths are similar to splitting tensile strengths).

Santos (2009) studied interface bond strength by slant shear and splitting tensile testing. The experimental program tested specimens with various time gaps between substrate and topping casting (28-days, 56-days, 84-days) and curing conditions (interior or exterior). Ratios of average slant shear strengths to average splitting tensile strengths range from 5.1 to 6.3. This range is consistent with the average slant shear to average tensile bond strength found in Momayez et. al. (2005) and Rosen (2016).

Rosen (2016) also reported ratios of average slant shear strengths to average guillotine shear strengths ranging from 3.8 to 6.4. Momayez et al. (2005) reported ratios of average slant shear strengths to average bi-surface shear strengths ranging from 3.2 to 3.5 and 3.3 to 3.7 for low and high roughness interfaces, respectively. These results indicate that slant shear strengths are consistently higher (on the order of at least three times higher) than direct shear strengths determined using the guillotine test or bi-surface shear test. They also illustrate the significant effect of compression across the interface in the slant shear test on the resulting shear strength. Since many repair and new construction topping applications do not have sustained compression across the unreinforced interface, the use of slant shear tests to establish interface shear strength for design may not be appropriate.

2.3.2 Variability of different bond test methods

The variability of the strength results for the different test methods is illustrated by the reported coefficient of variation (CoV). Two studies that have used guillotine shear are Sprinkel (2016) and Rosen (2016). Sprinkel (2016) tested two groups of cores with

samples sizes of 10 and 7 and reported CoV of 30% and 23%. Rosen (2016) tested six groups of cores each with a sample size of 2 and reported CoV ranging from 14.3% to 36.9%.

The CoV values for slant shear tests and bi-surface shear tests from previous studies are also variable. Santos (2009) reported CoV from slant shear tests from 2.0% to 38.3% for laboratory cured specimens and from 6.7% to 28.4% for exterior cured specimens. Momayez et al. (2005) reported CoV for slant shear specimens ranging from 4.7% to 15.8% and CoV from bi-surface shear test ranging from 6.5% to 13.3%.

The CoV for shear strength are higher than those normally associated with concrete compressive strength or splitting tensile strength results. However, this this not unexpected given the complex nature of interface shear failure and tests performed on samples obtained by coring. Different bond tests methods have shown similar levels of variability, and there is no sufficient data to arrive to a general conclusion about what method(s) provide lower uncertainty.

2.4 Other Shear Tests on Unreinforced Interfaces

This section includes studies on interface shear strength for concrete-to-concrete interfaces based on tests other than beam tests and basic bond tests. The tests included in this section comprise push-off tests, shear-block tests, and Iosipescu tests. Unlike the bond tests in section 2.3, these tests require unique formwork and test setups. The results are useful for research studies, but the test design is not practical for quality control and assessments in the construction industry.

2.4.1 Hanson (1960)

The Hanson study tested push-off specimens in addition to the girder specimens discussed in section 2.2. A typical cross-section of the push-off specimens is shown in Figure 2-14. Several variables were tested in this study, one of them being reinforcement across the interface. Nineteen of the sixty-two specimens had no reinforcement across the interface.

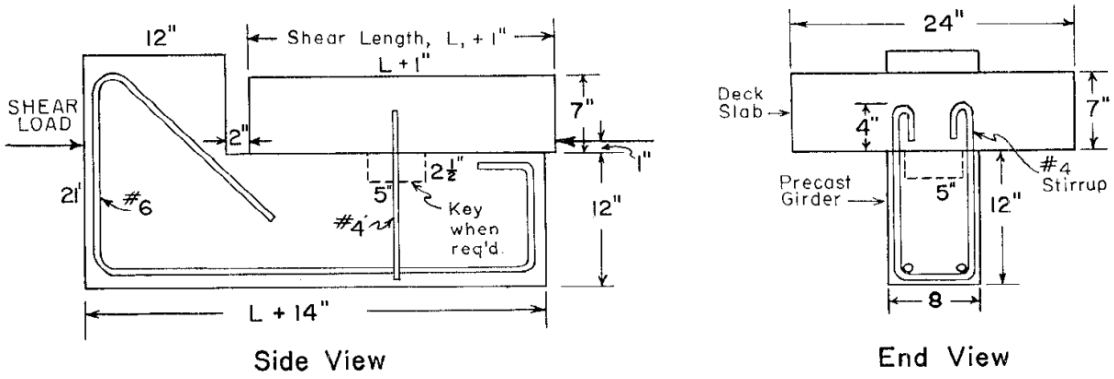

Figure 2-14: Push-off specimens tested by Hanson (1960).

These tests were done to explore load-deformation characteristics of various contact surfaces subject to a shearing force. Amongst the specimens with no shear reinforcement across the interface, the specimens had other variables such as:

- Interface Length: Length of interface or shear length, either 6”, 12”, or 24”
- Smooth: Contact surface troweled
- Rough: Contact surface roughness by scraping with steel, approximate roughness amplitude of ¼”
- Bond: No attempt made to destroy adhesive bond
- Unbonded: Contact surface coated with silicone

- Smooth Aggregate Bare: After trowel, a retarding compound applied leaving aggregate bare
- Rough Aggregate Bare: After roughening with scraping with steel, the surface paste was prevented from setting and removed with a water jet 24-hours later
- Keys: The keys were 2-1/2" deep divots into the substrate surface and 5" long along the shearing surface forming an interlocking hole that the topping layer will form into.

The results from the push-off tests are summarized in Table 2-9.

Table 2-9: Push-off specimen results from tests by Hanson (1960).

Specimen ID	Reinforcement Across the Interface	Interface Roughness Technique	Failure mode	Method for Calculating Horizontal Shear Stress	Reported Horizontal Shear Stress at Horizontal Shear Failure (psi)
BR12-1	None	Rough and Bonded	Interface Failure	0.005" Slip	416
BR12-2	None	Rough and Bonded	Interface Failure	0.005" Slip	555
BR12-3	None	Rough and Bonded	Interface Failure	0.005" Slip	455
BR12-4	None	Rough and Bonded	Interface Failure	0.005" Slip	350
BR12-5	None	Rough and Bonded	Interface Failure	0.005" Slip	362
BR12-6	None	Rough and Bonded	Interface Failure	0.005" Slip	410
BR12-7	None	Rough and Bonded	Interface Failure	0.005" Slip	408
BR12-8	None	Rough and Bonded	Interface Failure	0.005" Slip	405
B12-1	None	Bond Only	Interface Failure	Before 0.005" Slip	125
B12-2	None	Bond Only	Interface Failure	Before 0.005" Slip	230
B12-3	None	Bond Only	Interface Failure	Before 0.005" Slip	130
B12-4	None	Bond Only	Interface Failure	Before 0.005" Slip	90

Specimen ID	Reinforcement Across the Interface	Interface Roughness Technique	Failure mode	Method for Calculating Horizontal Shear Stress	Reported Horizontal Shear Stress at Horizontal Shear Failure (psi)
B12-5	None	Bond Only	Interface Failure	Before 0.005" Slip	120
B24-1	None	Bond Only	Interface Failure	Before 0.005" Slip	109
B24-2	None	Bond Only	Interface Failure	Before 0.005" Slip	94
B24-3	None	Bond Only	Interface Failure	Before 0.005" Slip	100
RSK12-1	None	Rough	Interface Failure	0.005" Slip	270
BRK12-1	None	Keys in Rough and Bonded	Interface Failure	0.005" Slip	420
BRK12-2	None	Keys in Rough and Bonded	Interface Failure	-	-

Specimens with keys indicated that bond must be destroyed for the keys to be engaged therefore it was concluded that it was desirable to avoid the use of keys and to rely on a combination of bond and roughness (and stirrups for reinforced interfaces) to have sufficient interface bond strength. The results show a consistent increase in strength when the surface is roughened to a ¼" amplitude.

2.4.2 Seibel and Latham (1988)

The Seibel and Latham study tested shear block specimens in addition to the flexural specimens discussed in section 2.2. The shear block test setup included two interface planes as shown in Figure 2-15. A total of eight unreinforced shear block specimens were tested: specimens 1A, 1B, 2A, 2B, 3A, 3B, 4A, and 4B. The numbering is the same as defined in section 2.2.4 and the letter represents the first (A) and second (B) test of that interface type. The shear stress is calculated by force P divided by the area

of both interface surfaces between “new” and “old” material. The reported nominal ultimate shear stress is shown in Table 2-10.

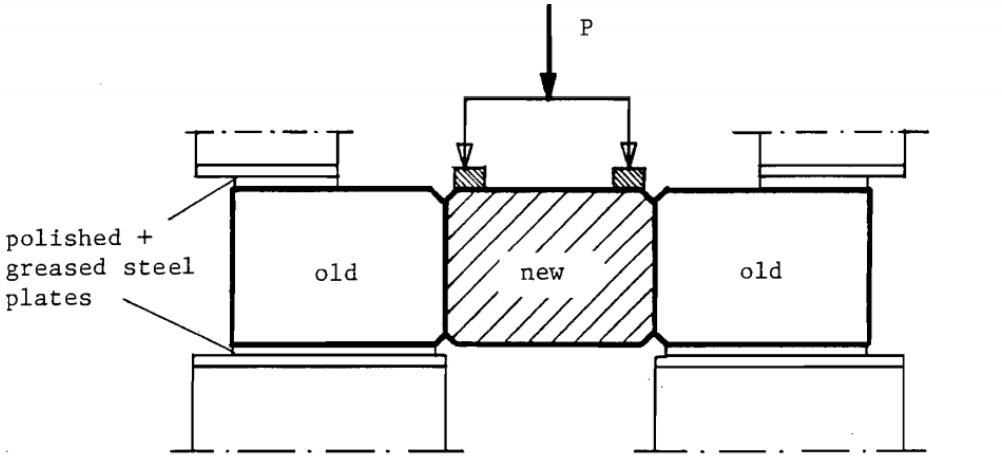

Figure 2-15: Load application of shear block tests by Seibel and Latham (1988).

Table 2-10: Push-off test results from Seibel and Latham (1988).

Specimen ID	**Reinforcement Across the Interface**	**Interface Roughness Technique**	**Failure mode**	**Method for Calculating Horizontal Shear Stress**	**Reported Horizontal Shear Stress at Horizontal Shear Failure (psi)**
1A	None	Monolithic	-	-	-
1B	None	Monolithic	-	-	-
2A	None	Lubricated	Horizontal Shear	Force/ Interface Area	6
2B	None	Lubricated	Horizontal Shear	Force/ Interface Area	28
3A	None	Surface Rough	Horizontal Shear	Force/ Interface Area	33
3B	None	Surface Rough	Horizontal Shear	Force/ Interface Area	79
4A	None	Scarified	Horizontal Shear	Force/ Interface Area	99
4B	None	Scarified	Horizontal Shear	Force/ Interface Area	110

2.4.3 Swan (2011)

The Swan study tested Iosipescu specimens in addition to the flexural specimens discussed previously in this literature review. The Iosipescu apparatus is shown in Figure 2-16. This is a type of direct shear test that places steel rods of the bottom and top of the specimen both on opposite sides of the interface. A compressive force is applied and increased until failure.

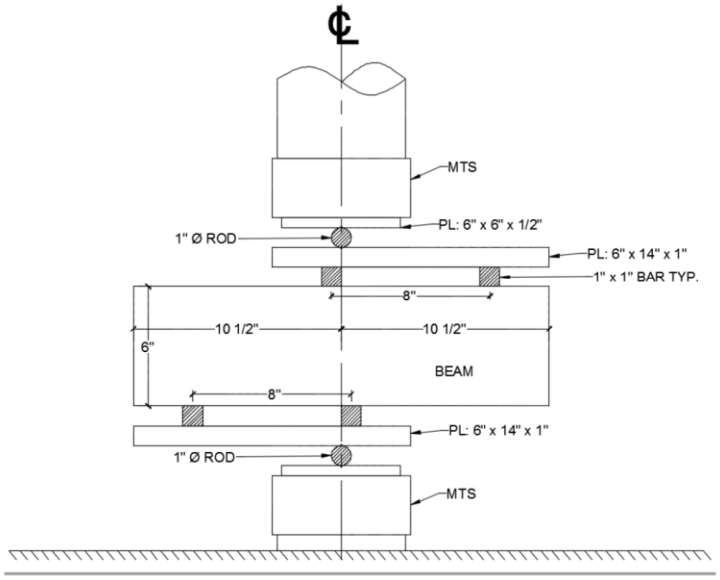

Figure 2-16: Iosipescu test setup in Swan (2011).

For the Iosipescu specimens, the substate was cast in plywood forms, vibrated, and cured for 28 days. In preparation of topping placement, the surface was moistened to SSD conditions. The topping was vibrated and left to cure 28 days before testing.

Four Iosipescu specimens were tested for each interface roughness. The average horizontal shear stress at failure is shown in Table 2-11.

Table 2-11: Average shear stresses from Iosipescu specimens tested by Swan (2011).

Substrate Roughness	Average Horizontal Shear Stress (psi)
Smooth	303
Bush Hammer	354
Jackhammer	404

2.5 CODE PROVISIONS FOR CALCULATING HORIZONTAL SHEAR CAPACITY

Horizontal shear provisions for composite beams and composite girders were first developed by ACI-ASCE Committee 333 in 1960 (ACI-ASCE 1960). The recommendations were based on experimental results from Hanson (1960), Ozell and Cochran (1956), Revesz (1953), and Karr and Hognestad (1960). Only two of these studies, Revesz (1953) and Hanson (1960), included unreinforced specimens. In total, there were 78 composite beams considered, 9 of which failed in horizontal shear failure, and 2 of which had no reinforcement across the interface. These 9 beams that failed in horizontal shear were the basis for the first recommendations for horizontal shear design.

Horizontal shear recommendations from Committee 333 were adopted into ACI 318-63 (ACI 1963) building code. The next change to the horizontal shear provision in the building code was in ACI 318-71 (ACI 1971), where the allowable stresses were rounded up but are essentially the same as those published in ACI 318-63. The code requirement has remained mostly unchanged since then. A progression of the ACI 318 horizontal shear standard is summarized in Table 2-12.

Table 2-12: Evolution of the ACI 318 horizontal shear capacity (psi).

Surface	Ties	ACI 318-63	ACI 318-71	ACI 318 -19
Intentionally Rough	None	76*	80	80
Not Intentionally Rough	Minimum	76*	80	80
Intentionally Rough	Minimum	304*	350	290**

*based on allowable stress reported multiplied by factor of 1.9 for capacity of bond at ultimate load
**based on a concrete compressive strength of 4,000 psi

The current version of the ACI code, ACI 318-19, refers to test results by Saemann & Washa (1964), Kaar et al. (1960), and Hanson (1960). Of all the specimens in these three studies, only three of the flexural (beam) tests had unreinforced interfaces.

The horizontal shear design provisions for ACI 318-19 and ACI 562-19 are summarized in this section.

2.5.1 American Concrete Institute 318- Building Code Requirements for Structural Concrete (ACI 318-19)

The design requirements for horizontal shear transfer in composite concrete flexural members are defined in section §16.4 in ACI 318-19. The design for a section without tension must satisfy Equation 2-5 in section §16.4.3.1 stating where shear capacity with strength reduction factor, ϕ, must be larger than the factored shear demand Vu.

$$\phi V_{nh} \geq V_u$$

Equation 2-5

For an unreinforced interface V_{nh} is capped at 80 psi, or 80 multiplied by b_v, interface width, and d, the distance from extreme compression fiber to the centroid of

tension reinforcement. This 80 psi limit is stated in ACI 318-19 table §16.4.4.2 and below in Equation 2-6.

$$\phi V_{nh} = 80 b_v d$$

Equation 2-6

where,

$V_{nh} =$ Nominal horizontal shear capacity [lb.]

$\phi =$ Strength reduction factor [typically taken as 0.75 for shear strengths]

$b_v =$ Width of interface [in.]

$d =$ Distance from extreme compression fiber to tension reinforcement but not less 0.80h for prestressed concrete members. [in.]

The code also states that the contact surface must intentionally roughened, clean and free of laitance. The commentary suggests the surface should be roughened to a ¼ inch amplitude as suggested by previous studies (Hanson 1960, Saemann and Washa 1964, and Karr et. al. 1960).

2.5.2 American Concrete Institute 562- Code Requirements for Assessment, Repair, and Rehabilitation of Existing Concrete Structures and Commentary (ACI 562-19)

The Code Requirements for Assessment, Repair, and Rehabilitation of Existing Concrete Structures and Commentary (ACI 562) provides provisions for interface bond in section §7.4 titled “Interface bond of cementitious repair materials”. The interface horizontal shear must satisfy Equation 2-7. This is the same equation stated in ACI 318-19.

$$\phi V_{nh} \geq V_u$$

Equation 2-7

ACI 562-19 is in accordance with ACI 318-19 with additional provisions for shear stresses less than 80 psi. It is identical in which it limits the capacity of unreinforced interfaces to a shear stress of 80 psi multiplied by a reduction factor (ϕ). Yet it already accounts for strength reduction factor, ϕ=0.75. Therefore, any stress less than 60 psi (ϕ* 80psi) does not require reinforcement, but if the factored shear stress is higher than 30 psi it requires quantitative bond testing. The method of quantitative bond testing is not specified, but it is common to employ tension pull-off testing defined in ASTM C1583. If the factored demand is less than 30 psi, there is still no need for reinforcement, and now does not require quantitative bond testing, but instead it requires bond integrity testing. Bond integrity testing is to test for intimate contact, which can be done by hammer sounding, ground-penetrating radar or impact-echo.

The commentary states when the nominal interface shear stress is lower than 80 psi and where there is good surface preparation, placement, repair material, and curing then you will likely achieve composite behavior without interface reinforcement.

Chapter 3 : Phase 1 - Experimental Program

3.1 Overview

Phase 1 experimental program was designed to produce a data set of direct shear bond strengths and tensile bond strengths for a range of interface conditions in precast topping and concrete repair applications. The goal of Phase 1 is to examine the following:

- Interface bond shear strengths on core specimens as measured by guillotine shear tests.
- Correlation between interface bond shear strength and tensile bond pull-off strength.
- Correlation between interface bond shear strength and a range of interface surface conditions.
- Correlation between interface tensile bond strength and a range of interface surface conditions.
- Different approaches for characterizing interface surface conditions (i.e., texture/roughness).

3.2 Specimen Design and Test Variables

A total of twenty composite slabs with unreinforced interfaces were fabricated and tested. The test variables were interface preparation and concrete material characteristics. Parameter combinations for each specimen are described in Table 3-1 (Note: two slabs per parameter were fabricated and tested). Interface preparation techniques were selected to provide a range of different conditions expected for both precast topping slab applications and partial-depth repair applications. The following interface conditions have been selected for new precast construction: smooth (float), tining-raked, and broomed.

The following interface conditions have been selected for concrete repair: sandblasting, mechanical removal followed by sandblasting, and hydrodemolition. The three repair techniques were intended to produce concrete surface profiles of CSP 2-3, CSP 5-7, and CSP 9-10, respectively, according to ICRI No. 310.2R (ICRI 2013). Concrete material characteristics including workability and consolidation method are discussed in section 3.3. Interface conditions are discussed in more detail in section 3.4.

The composite slab dimensions were approximately 3 foot by 3 foot with a thickness of 8.5 inches (2.5-inch topping cast on top of a 6-inch substrate). Direct tensile pull-off tests were conducted on the composite slabs, and direct shear (guillotine) tests were conducted on cores which had been previously extracted from the slabs. On average, 12 direct shear tests were performed on cores from each slab, and 6 direct tensile pull-off tests were conducted on each slab. The general slab dimension and testing layout are shown in Figure 3-1.

Table 3-1. Phase 1 testing program matrix.

Slab Category	Substrate Interface Preparation Technique	Concrete Placement Technique		Specimen ID
		Concrete Workability (Slump)	Consolidation Technique	
Repair	Sandblast	Moderate	Hand Consolidated	A
Repair	Bush Hammer + Sandblast	Moderate	Hand Consolidated	B
Repair	Hydrodemolition	Moderate	Hand Consolidated	C
Precast	Float	Lower	Screed Only	D
Precast	Broom	Lower	Screed Only	E
Precast	Tine	Lower	Screed Only	F
Precast	Broom	Moderate	Hand Consolidated	G
Precast	Tine	Moderate	Hand Consolidated	H
Precast	Broom	Moderate	Vibrated	I
Precast	Tine	Moderate	Vibrated	J

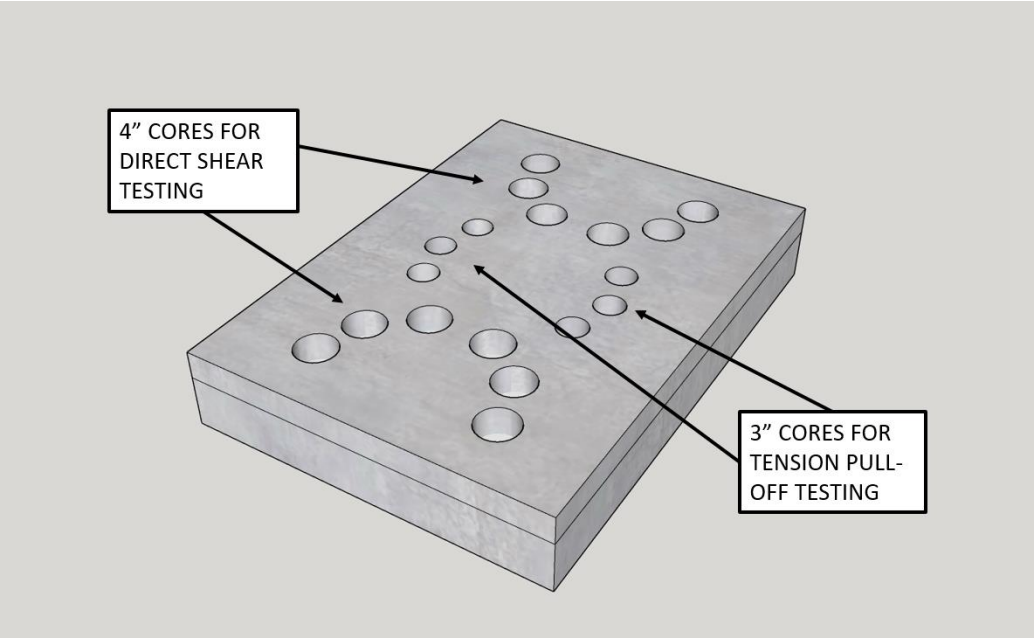

Figure 3-1: Slab specimen general layout.

3.3 CONCRETE MIXTURES AND PLACEMENT PROCEDURES

Concrete mixtures for the slabs were chosen to be representative for typical design and repair applications. Two different mixtures were initially considered for the overlay concrete representing repair and new construction topping applications. Ultimately, it was decided to use the same concrete for both the topping slab and partial depth repair applications to limit the number of variables in the testing program and allow the interface condition to be the primary focus when interpreting the shear and tensile bond strength results. Ready-mixed concrete was used for all slab specimens (substrate, repair and topping concrete). All concrete had a specified compressive strength of 4,000 psi and a maximum coarse aggregate size of 3/4 inch. However, the mixtures for the substrate and topping/overlay had a specified slump of 4.5 inch and 5 inch, respectively.

The substrate slabs were placed with an actual slump of 3 to 6 inches. All concrete substrate placements were consolidated using hand tools followed by wooden screed (hand consolidation). The concrete for the partial-depth repair specimens was placed at a slump of at least 5 inches (termed moderate workability herein). All partial-depth repair placements were consolidated on the substrate slab by placing in two lifts followed by wooden screed (hand consolidation). The first lift was worked into the substrate by hand using trowels, while the second lift was worked into the first using hand tools (shovels and trowels) followed by screeding.

The precast topping specimens investigated topping workability and placement technique as research parameters in addition to interface conditions. Two workability levels were considered: lower workability with a slump less than 4 inches, and moderate workability with a slump greater than 5 inches. Three placement techniques were investigated: screed only, hand consolidated (same technique as described above for repair

series specimens) and vibrated. The latter condition was performed using a pencil vibrator inserted in the topping concrete on a 6-inch (approximate) grid pattern, followed by screeding.

The concrete surface treatment immediately prior to placement of the repair concrete or topping concrete may affect the shear and tensile bond strength. Other researchers have compared dry or untreated surfaces to those that are saturated-surface dry, as well as the use of bonding agents (Mones and Brena 2013). The surface treatment was not considered a variable in the current study; all substrate slabs were prepared to produce saturated-surface dry conditions prior to placement of the repair or topping concrete. First, the surface was cleaned to remove any dust, laitance, or loose material. The cleaning was followed by wetting of the substrate concrete approximately 24 hours prior to repair or topping placement and covering using wet burlap. The concrete surface was exposed to drying by evaporation over a period of approximately 1 hour prior to concrete placement, and compressed air was used to ensure that there was no standing water on the substrate surface.

Table 3-2. Concrete workability and placement techniques

Series	**Repair or Topping Concrete Workability**	**Consolidation Method**
Repair	Moderate (Slump 5”)	Hand consolidation (HC): two lifts followed by wooden screed
Precast	Lower (Slump < 4”)	Screed only (SC): one lift followed by wooden screed
	Moderate (Slump > 5”)	Hand consolidation (HC): two lifts followed by wooden screed
	Moderate (Slump > 5”)	Vibrated (V): two lifts vibrated followed by wooden screed

3.4 INTERFACE CONDITIONS

The interface conditions were selected to represent common surface preparation practices used in industry. For new precast construction this includes substrates that are smooth (floated), tined (raked), and broomed before the concrete has set. The tining rake profile and its corresponding substrate finish are shown in Figure 3-2 and Figure 3-3, respectively. Likewise, the stiff-bristle broom profile and its corresponding substrate finish are shown in Figure 3-4 and Figure 3-5.

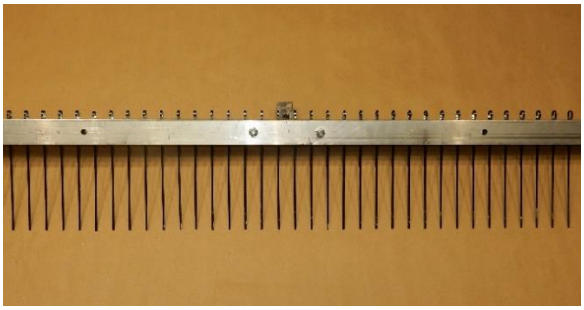

Figure 3-2. Tining rake.

Figure 3-3. Substrate roughened with tining rake.

Figure 3-4. Stiff-bristle broom.

Figure 3-5. Substrate roughened with broom.

For repair construction, the two main practices for surface roughening are hydrodemolition and mechanical removal. Mechanical removal can damage the surface causing microcracking or "bruising" therefore it is specified to be followed by an abrasive

blasting technique such as sandblasting. This research study considered three different surface conditions with the following range of CSP roughness values:

- Hydrodemolition - CSP of 9 to 10.
- Mechanical removal by bush hammer followed by sandblasting - CSP of 6 to 7.
- Sandblasting only - CSP of 2 to 3.

Although sandblasting alone is not a common practice for concrete repair, a range of CSP values was desired for research purposes, and sandblasting was included to provide a lower bound of surface roughness. An experienced repair contractor was engaged to perform the surface preparation by sandblasting, bush-hammering, and hydrodemolition. Photos of each demolition technique are shown in Figure 3-6 through Figure 3-11.

Figure 3-6. Typical repair surface prepared by hydrodemolition (CSP 9-10).

Figure 3-7. Hydrodemolition procedure.

Figure 3-8. Typical repair surface condition prepared by mechanical abrasion (bush hammer followed by sand blasting – CSP 6-7).

Figure 3-9. Bush hammer bit.

Figure 3-10. Typical repair surface prepared by sandblast only. (CSP 3).

Figure 3-11. Sandblast procedure.

3.5 CONCRETE PLACEMENT SEQUENCE

The slab specimens for Phase 1 were fabricated in three groups, which had a separate concrete placement for the substrate and topping. The complete slab specimen program is shown in Table 3-3, including casting order.

All substrate slabs were cured for 28-days prior to placement of the topping or repair material. This duration was selected to provide a balance between the maturity of the substrate concrete and early-age drying shrinkage and the project schedule. The three topping placements occurred four to six weeks after the substrate cast.

Each concrete placement (substrate or topping) was moist-cured for 7-days using saturated burlap covered by a plastic sheet to seal in the moisture. The specimens were then placed outside for the remainder of the 28-day curing period. Both direct tensile and direct shear testing were performed after the topping or repair material reached 28-day strengths.

Table 3-3: Slab specimen parameters.

Cast Number	Slab Category	Substrate Roughening Technique	Topping Workability (Slump) Level	Topping Consolidation Technique	Specimen ID
Cast 1 (Substrate) / Cast 2 (Topping)	Repair	Sandblast	Medium	HC	A
Cast 1 (Substrate) / Cast 2 (Topping)	Repair	Bush Hammer + Sandblast	Medium	HC	B
Cast 1 (Substrate) / Cast 2 (Topping)	Repair	Hydro-demolition	Medium	HC	C
Cast 3 (Substrate) / Cast 4 (Topping)	Precast	Float	Low	SC	D
Cast 3 (Substrate) / Cast 4 (Topping)	Precast	Broom	Low	SC	E
Cast 3 (Substrate) / Cast 4 (Topping)	Precast	Tine	Low	SC	F
Cast 5 (Substrate) / Cast 6 (Topping)	Precast	Broom	Medium	HC	G
Cast 5 (Substrate) / Cast 6 (Topping	Precast	Tine	Medium	HC	H
Cast 5 (Substrate) / Cast 6 (Topping	Precast	Broom	Medium	V	I
Cast 5 (Substrate) / Cast 6 (Topping	Precast	Tine	Medium	V	J

SC: Screed Only
HC: Hand Consolidated
V: Vibrated

3.6 SURFACE ROUGHNESS CHARACTERIZATION

Previous research and practice have shown that surface roughness can influence interface bond strength. ACI 318-19 and ACI318-562 code requirements for design of horizontal shear transfer at interfaces require intentional roughening of the substrate

surface. To characterize the surface conditions considered in the current study, the following qualitative (visual) and quantitative approaches were used:

- CSP by Visual Comparison to ICRI CSP Comparators.
- Mean Texture Depth by Sand Patch Test (ASTM E965-15).
- Mean Texture Depth by Analysis of 3D Data from Line Laser Scanner (LLS).

3.6.1 CSP by Visual Comparison

The International Concrete Repair Institute (ICRI) provides a means of visually comparing a concrete surface to 10 concrete surface profiles (CSP) comparators for a qualitative assessment of roughness. The repair specimens were compared to the comparators shown in Figure 3-12.

Figure 3-12. ICRI CSP Comparators.

3.6.2 Mean Texture Depth by Sand Patch Test

The mean texture depth (MTD) is a measure of surface texture using a volumetric technique. A common approach to measure MTD is performing a sand patch test (SPT)

following ASTM E965 (2015). This technique was developed to measure the macrotexture depth of concrete pavement surfaces. It involves spreading a known volume of sand in a circular manner as uniformly as possible. Once the sand does not spread further, four diameter measurements are taken. These steps are shown in Figure 3-13 and Figure 3-14. The MTD is calculated based on the volume and diameter of the sand patch using the following equation:

$$MTD = \frac{4V}{\pi D^2}$$

Equation 3-1

where,

V= Volume of sand

D=Average measured diameter

The sand patch test is not commonly used to characterize surface preparation in repair or new construction for structures. Furthermore, there are no established correlations between MTD determined by sand patch test and shear or tensile bond of concrete repairs or topping slab applications. However, since it provides a quantitative indication of surface roughness, the sand patch test was included in the current study as a means of obtaining a quantitative comparison between the surface roughness of the interface types considered.

Figure 3-13. Measuring volume of sand for ASTM E965 Sand Patch Test.

Figure 3-14. Measuring diameter of sand circle after spreading onto concrete surface per ASTM E965.

3.6.3 Mean Texture Depth by Analysis of 3D Data from Line Laser Scanner

Surface roughness measurements were taken by researchers from the Infrastructure Materials Group at the University of Texas at Austin using a using a line laser scanner (LLS) technology developed by for pavements. The LLS, shown in Figure 3-15, measures surface height (elevation) data over a selected area to create a 3D representation of the surface. An example of a 3D surface plot is shown in Figure 3-16. The 3D data are used along with an algorithm developed by El Hachem and Prozzi (2019) to calculate an equivalent MTD.

The LLS was used in the current study to scan all substrates (precast and repair surfaces). The 3D data were used to calculate equivalent MTD values for each surface condition.

Figure 3-15. Line Laser Scanner on the tined substrate specimen.

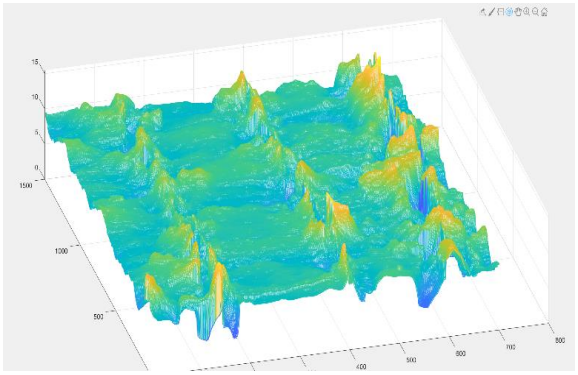

Figure 3-16. Sample LLS 3D scan data for tined substrate specimen.

3.7 Bond Strength Testing Methods

The interface bond strengths were assessed using direct shear (guillotine) tests conducted on cores extracted from the slabs and direct tensile pull-off tests conducted directly on the slabs.

3.7.1 Direct Shear (Guillotine) Testing

Direct shear testing was performed using 4-inch-diameter cores extracted from the slabs. The core specimens were subjected to direct shear loading using a guillotine shear jig as shown in Figure 3-17 through Figure 3-20. In this test setup, core samples are inserted into the circular opening of the jig and thin metal shim sheets are used to ensure a snug fit and maintain the correct alignment of the core sample during testing. The core sample is placed in the jig such that the interface between the substrate and topping is aligned with the line of applied direct shear force. Once the core sample is secured in the jig, a loading block is placed into the jig against the sample and the entire assembly is placed into a concrete compression testing machine. The cores were loaded at a rate of 5 ± 2 psi per second per ASTM C1583 (2013).

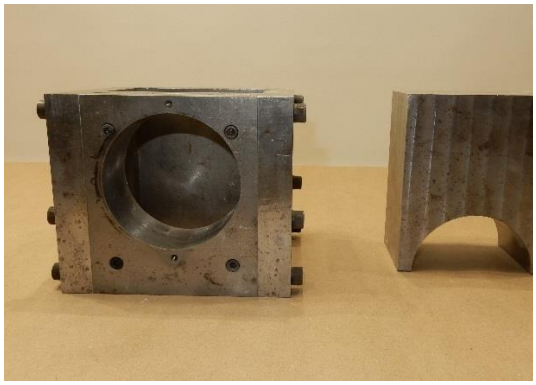

Figure 3-17. Guillotine shear jig – side view.

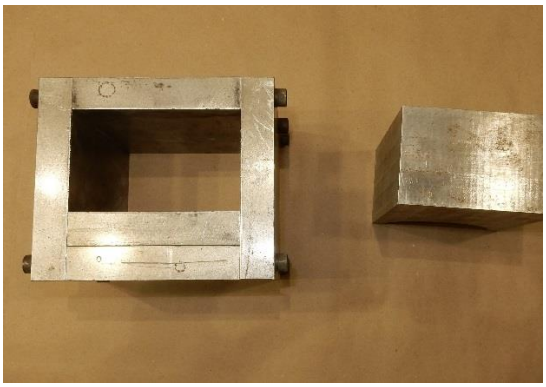

Figure 3-18. Guillotine shear jig – top view.

Figure 3-19. Core sample inside guillotine jog placed within concrete compression testing machine.

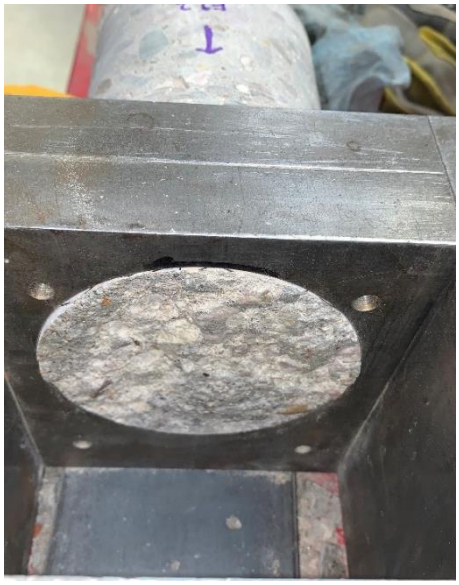

Figure 3-20. Core sample shear failure interface after testing (loading head removed).

3.7.2 Direct Tensile Pull-off Testing

Direct tensile pull-off testing was performed in general accordance with ASTM C1583. Preparation for the test involves coring of the slab to a depth of approximately 1 inch below the interface level, and attachment of a metal disk to the concrete surface at the cored location using epoxy. Once the epoxy has cured, a pull-off force is applied perpendicular to the interface to measure the interface bond strength in tension. All pull-off tests were performed using a Proceq DY-216 automated pull-off tester.

ASTM C1583 specifies the use of a 2-inch core and metal disk for direct tensile pull-off testing. Preliminary tests in the current study using the standard disk size showed highly variable results, possibly due to the 2-inch core diameter relative to the 2.5-inch interface depth. ATSM C1583 specifies a circular cut or core depth of at least 0.5 inches below the interface between the substrate and overlay, requiring a minimum 3-inch core depth for the specimens in this study. It is possible that stresses due to core barrel twist or wobble affected the integrity of bond at the interface, increasing the variability of the apparent tensile strength result. It is expected that the effect of barrel twist is more significant as the depth of coring is increased for thicker topping or repair material placements, such as in the case of the 3-inch core depth required in the current study. ASTM C1583 does not provide guidance on this matter, nor does it address disk sizes other than 2 inches. For the purposes of the current study, the test method was changed to use a 3-inch core and disk, which resulted in more consistent test results. All data reported herein are based on a 3-inch core and disk.

Figure 3-21. Direct tensile pull-off testing device.

Figure 3-22. Direct tensile pull-off testing sample.

Chapter 4 : Phase 1 - Experimental Results and Discussion

This chapter presents and discusses Phase 1 experimental results, including material testing data, surface roughness characterization, interface shear strength results obtained from guillotine tests, and interface tensile strength results obtained from direct tensile pull-off tests.

4.1 MATERIAL TESTING DATA

As discussed in Chapter 3, the slab specimens in Phase 1 were fabricated in three groups, each of which having a separate concrete placement for the substrate and topping. Concrete slump as well as compressive and tensile strengths for each concrete placement are presented here.

4.1.1 Slump

The concrete slump was measured for each concrete placement in accordance with ASTM C143 (2015); results are listed in Table 4-1. As described previously, two levels of concrete workability were considered for the topping used on the precast specimens. These are termed lower workability and moderate workability for the purposes of presenting and discussing results herein.

Table 4-1. Measured concrete slump.

Cast Number	Slump
Cast 1 (Substrate - Partial Depth Repair)	2.75”
Cast 2 (Topping - Partial Depth Repair)	5”
Cast 3 (Substrate- Lower workability precast topping)	4”
Cast 4 (Topping - Lower workability precast topping)	3.75”
Cast 5 (Substrate- Moderate workability precast topping)	6”
Cast 6 (Topping - Moderate workability precast topping)	5.5”

4.1.2 Compressive Strength

Concrete compressive strength tests were conducted using 4-inch by 8-inch cylinders in accordance with ASTM C39 (2018). The strength was tested at seven and twenty-eight days after casting as well as on the day of shear/tensile testing of specimens. The compressive strengths for each concrete cast are shown in Table 4-2.

Table 4-2. Concrete compressive strength results.

Cast Number	7-Day (psi)	28-Day (psi)	Day of Testing (psi)
Cast 1 (Substrate)	3550	5550	5700
Cast 2 (Topping - Partial Depth Repair)	4450	5400	5400
Cast 3 (Substrate)	4400	5750	6700
Cast 4 (Topping - Lower workability precast topping)	4600	5400	5700
Cast 5 (Substrate)	4100	5200	5100
Cast 6 (Topping - Moderate workability precast topping)	4150	5350	5950

4.1.3 Splitting Tensile Strength

Concrete splitting tensile strength tests were conducted using 4-inch by 8-inch cylinders in accordance with ASTM C496 (2017). The strength was tested at seven and twenty-eight days after casting as well as the day of shear/tensile testing of specimens. The splitting tensile strengths for each cast are shown in Table 4-3.

Table 4-3: Splitting Tensile Strength Results.

Cast Number	7-Day (psi)	28-Day (psi)
Cast 1 (Substrate)	470	550
Cast 2 (Topping - Partial Depth Repair)	520	540
Cast 3 (Substrate)	510	590
Cast 4 (Topping - Lower workability precast topping)	510	550
Cast 5 (Substrate)	510	540
Cast 6 (Topping - Moderate workability precast topping)	460	580

4.2 SURFACE ROUGHNESS CHARACTERIZATION RESULTS

As described previously, four techniques characterizing surface roughness were used on the substrate surfaces to help distinguish the roughness of each interface condition:

- CSP by Visual Comparison to ICRI CSP Comparators
- Mean Texture Depth by Sand Patch Test (ASTM E965)
- Mean Texture Depth by Analysis of 3D Data from Line Laser Scanner (LLS)

4.2.1 CSP by Visual Comparison Results

The ICRI CSP Comparators were only used on repair specimens. The CSP results are summarized in Table 4-4.

Table 4-4: ICRI CSP Values for repair interface conditions.

Interface Condition	CSP Range
Sandblast	2-3
Bush Hammer + Sandblast	7-8
Hydrodemolition	9-10

4.2.2 Mean Texture Depth by Sand Patch Test and Line Laser Scanner

The Sand Patch Test (SPT) was performed on selected substrate specimens with repair interface conditions, followed by use of the Line Laser Scanner (LLS) on the same specimens. As shown in Table 4-5, the Mean Texture Depth (MTD) values were similar for the two methods. Since the LLS is quicker, cleaner, and has shown to be more consistent than the SPT, the LLS was the only method used to determine MTD for the remaining slabs. Each slab had measurements of MTD by LLS at 4 different locations. The complete summary of MTD values for all specimens based on LLS can be found in Table 4-6.

Hypothesis testing using a Student's t-test statistical analysis indicates that there is a statistically significant difference between the MTD values found by LLS for the repair surfaces (hydrodemolition versus bush hammer + sandblast, and bush hammer + sandblast versus sandblast only). Hypothesis testing also showed a statistically significant difference between MTD average of the broom and tined surfaces. These results indicate that MTD can differentiate between the different surface preparation techniques investigated in this study.

Table 4-5: Comparison of MTD from line laser scanner and sand patch test.

Interface Condition	**MTD Average from LLS (mm)**	**MTD Average from SPT (mm)**
Sandblast	0.2	-
Bush Hammer + Sandblast	0.82	0.83
Hydrodemolition	1.33	1.4

Table 4-6: Average mean texture depth for each interface condition based on LLS measurements.

Interface Condition	MTD Average from LLS (mm)	Standard Deviation (mm)	Coefficient of Variation	Sample Size
Broom	1.14	0.21	18%	16
Tine (Rake)	2.23	0.44	20%	16
Sandblast	0.2	0.012	6%	8
Bush Hammer + Sandblast	0.82	0.1	12%	8
Hydrodemolition	1.33	0.13	10%	8

4.3 DIRECT SHEAR (GUILLOTINE) RESULTS

The direct shear tests results for all Phase 1 specimens are shown in Table 4-7 and Figure 4-1. Most of the tested cores failed at the interface bond line. In some cases the failure plane was straight across the bond line as shown in Figure 4-2 and Figure 4-3, while in other cases the failure plane initiated at the interface and propagated into the topping or substrate as shown in Figure 4-4 and Figure 4-5. A limited number of cores did not fail in shear at the interface, but rather failed in flexure near the mid-length of the core. These results are not included in the data set provided in this report.

Table 4-7. Phase 1 Direct shear strength results.

Slab Category	Substrate Roughening Technique	Topping Workability Level	Topping Consolidation Technique	Direct Shear Strength			
				Average (psi)	Std. Dev. (psi)	CoV	Sample Size
Repair	Sandblast	Moderate	HC	815	209	26%	19
Repair	Bush Hammer + Sandblast	Moderate	HC	682	237	35%	18
Repair	Hydro-demolition	Moderate	HC	1009	214	21%	24
Precast	Float	Lower	SC	415	308	74%	2
Precast	Broom	Lower	SC	454	285	63%	35
Precast	Tine	Lower	SC	453	330	73%	33
Precast	Broom	Moderate	HC	855	185	22%	10
Precast	Tine	Moderate	HC	737	254	34%	20
Precast	Broom	Moderate	V	840	511	25%	21
Precast	Tine	Moderate	V	676	206	30%	17

HC: Hand Consolidated
V: Vibrated
SC: Screed Only

Std. Dev.: Sample standard deviation
CoV: Coefficient of variation

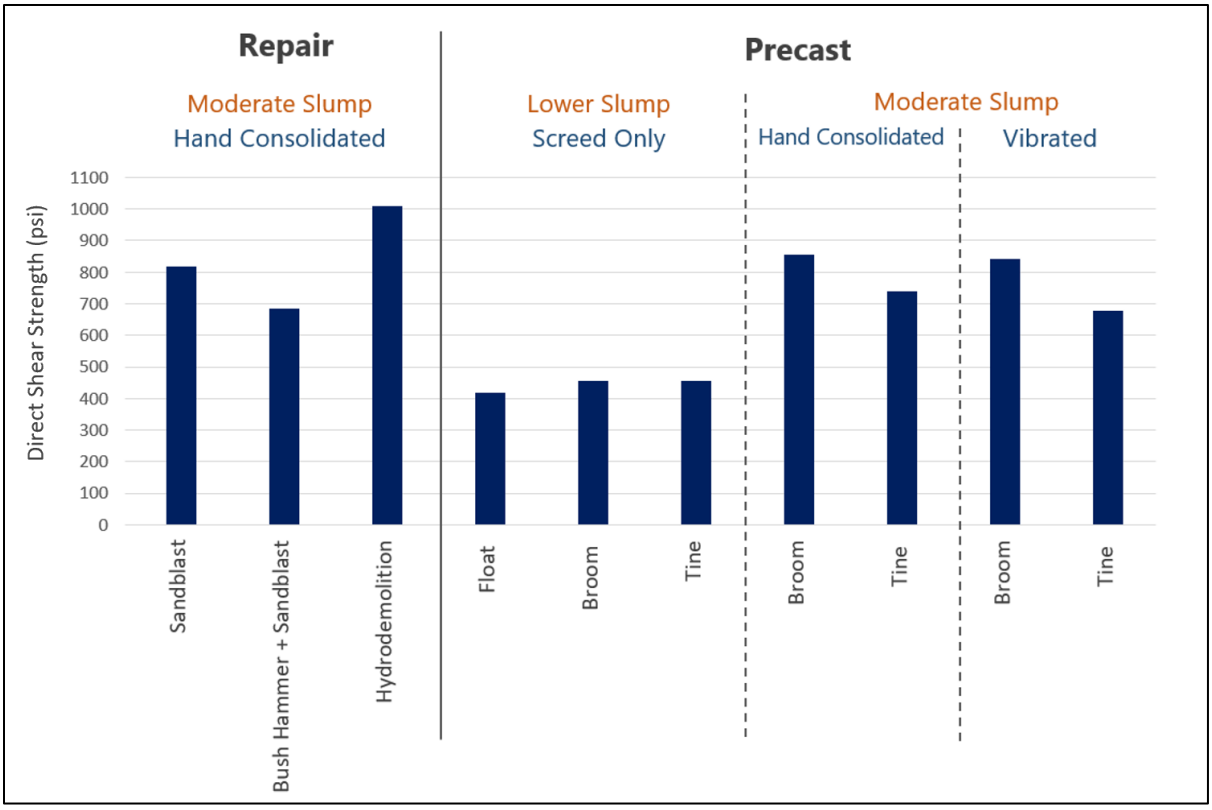

Figure 4-1. Average direct shear (guillotine) strength results (psi). Note current ACI interface nominal shear strength for design is 80 psi.

Figure 4-2. Direct shear failure plane at interface bond line (whole specimen).

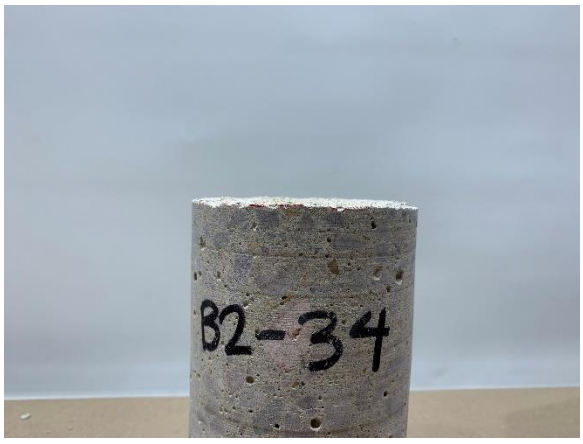

Figure 4-3. Direct shear failure plane at interface bond line (only substrate portion of core shown).

Figure 4-4. Direct shear failure plane propagating into topping layer (whole specimen).

Figure 4-5. Direct shear failure plane propagating into topping layer (only substrate portion of core shown).

As shown in Table 4-7, the hydrodemolition interface had the highest average shear bond strength of the three repair interfaces investigated at 1009 psi; this was the highest measured shear strength of all interfaces (repair and precast) considered in the current study. Hypothesis testing using a Student's t-test indicated a statistically significant difference between the shear bond strengths of the three repair interfaces. The lowest shear strength in the repair series was obtained for the bush hammer + sandblast interface, which had an average shear strength of 682 psi in comparison to 815 psi for sandblast alone. This suggests that mechanical removal using a bush hammer may be damaging or "bruising" the concrete substrate to a degree that cannot be compensated for by follow-up sandblasting; this is a known concern related to the use of bush hammering for concrete removal. It is also notable that the bush hammer + sandblast had the greatest variability of shear test results for the three repair interfaces, with a coefficient of variation

(CoV) of 35% in comparison to 26% and 21% for the sandblast and hydrodemolition interfaces, respectively.

The precast series investigated topping concretes with two different workability levels (termed lower and moderate) as well as different placement techniques as described previously. As expected, a pronounced difference was measured for shear strengths of precast samples with topping placed with lower slump and consolidated by screed only in comparison to topping with moderate slump and hand consolidated or vibrated. The average shear strengths of the float, broom and tined interfaces with lower slump/screed only placement did not show a significant effect of interface preparation and exhibited very high variability with coefficients of variation ranging from 63% to 74%, as indicated in Table 4-7. Furthermore, the average strengths for these specimens were on the order of 35% to 45% lower than the strengths of the same interfaces where the topping was placed with a moderate slump and hand consolidation or vibration.

The difference between the workability levels and placement techniques was visibly apparent at the bond interface observed after testing, as illustrated in Figure 4-6. Incomplete consolidation of the topping against the substrate concrete was visibly apparent in specimens with lower slump topping placed by screed only. Where moderate slump topping was consolidated by hand or vibration, instances of entrapped air or incomplete consolidation at the interface were significantly reduced. In addition, filling of tine grooves in the substrate by the topping was improved such that the groove lines were much less visible after testing to failure.

Substrate Topping

(a) Tined surface, lower slump topping with screed only placement

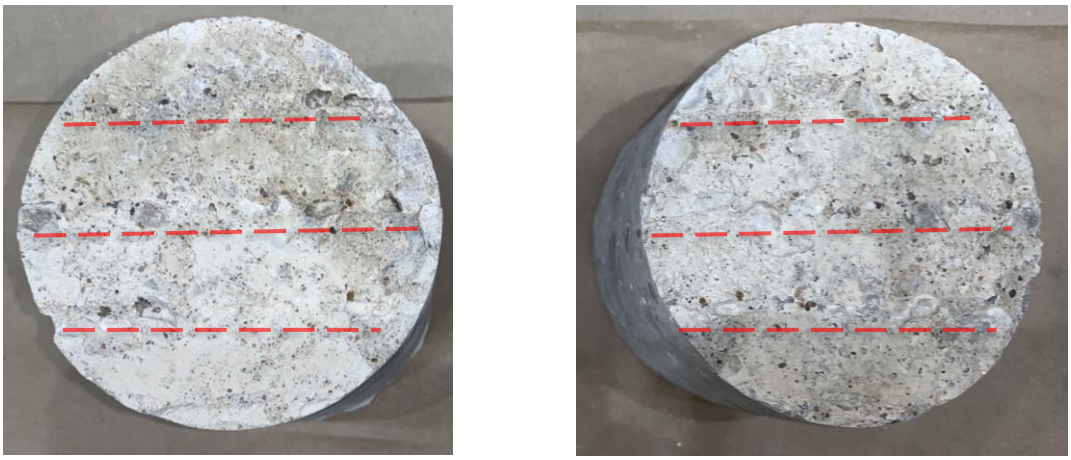

Substrate Topping

(b) Tined surface, moderate slump topping with hand consolidated placement (note tining lines have been accented using dashed lines in the figure)

Figure 4-6. Visual comparison of interface conditions for precast specimens with topping concrete placed under different conditions.

The precast series specimens with moderate slump concrete had shear strengths comparable to the bush hammer + sandblast and sandblast only specimens from the repair series, as depicted from Table 4-7. The broom-hand consolidated and broom-vibrated had average direct shear strengths of 855 psi and 840 psi, respectively, while the tine-hand consolidated and tine-vibrated specimens had shear strengths of 737 psi and 676 psi, respectively. On average, the shear strengths of the broom finish were approximately 20% higher than those of the tine finish; hypothesis testing using a Student's t-test indicates that this difference is statistically significant. Furthermore, hypothesis testing indicates that there is no statistical difference between the hand consolidation and vibrated placement conditions for either the broom or tine surface.

The precast series specimens with moderate slump concrete were tested both parallel and perpendicular to the broom/tine direction as illustrated in Figure 4-7 and Figure 4-8. The average direct shear strengths for broom finish when loaded parallel and perpendicular were 893 psi and 786 psi, respectively (results for both vibrated and hand consolidated combined). For tine finish, the average direct shear strengths for parallel and perpendicular loading were 711 psi and 695 psi, respectively (combined results from both consolidation techniques). Hypothesis testing using Student's t-test indicates that the differences between the average direct shear strengths for the two loading directions are not statistically significant when both consolidation techniques are grouped.

The broom-vibrated parallel tests and broom-vibrated perpendicular tests had average direct shear strengths of 956 psi and 721 psi, respectively. The average direct shear strength of loading parallel to the roughening direction is approximately 30% higher than when loaded perpendicular for the broom-vibrated specimens. Hypothesis testing using Student's t-test shows this difference in average strength is statistically significant.

No other combination of consolidation or roughening technique indicated statistically different means.

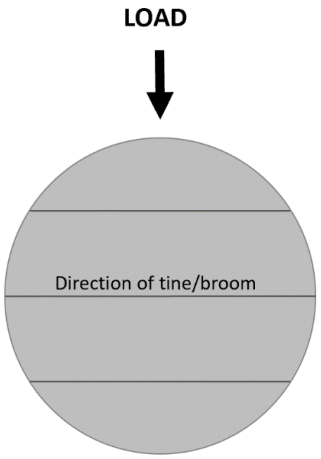

Figure 4-7. Direct shear test orientation for precast specimen loaded perpendicular to the roughening direction.

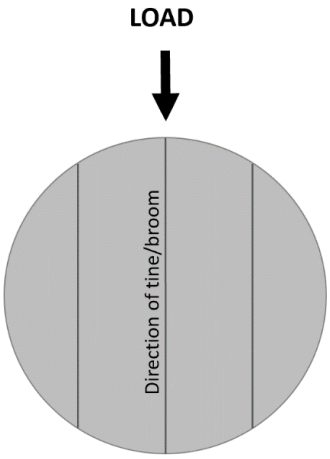

Figure 4-8. Direct shear test orientation for precast specimen loaded parallel to the roughening direction.

4.4 DIRECT TENSILE PULL-OFF RESULTS

Phase 1 direct tensile pull-off test results are presented in Table 4-8 and Figure 4-9. The precast series specimens with lower slump topping placed by screed only did not produce valid test results due to separation (debonding) of the topping from the substrate during coring in preparation for pull-off testing. This may have resulted from the limited bond between the topping and the substrate due to the lower slump topping and limited consolidation for these specimens, or the possible effect of differential shrinkage at the interface, or both. The coring action (i.e., shear stress due to torsion while coring or barrel wobble) to prepare for the pull-off test caused debonding of the topping. Therefore, pull-off test results for the precast series presented and discussed herein are only those for

moderate slump concrete placed by hand consolidation or vibration. Note that all pull-off tension tests were performed with 3-inch diameter disks as described previously.

Table 4-8: Phase 1 Direct tensile pull-off strength results.

Slab Category	Substrate Roughening Technique	Topping Workability Level	Topping Consolidation Technique	Direct Tensile Pull-off Strength			
				Average (psi)	Std. Dev. (psi)	CoV	Sample Size
Repair	Sandblast	Moderate	HC	280	66	24%	12
Repair	Bush Hammer + Sandblast	Moderate	HC	191	47	25%	12
Repair	Hydro-demolition	Moderate	HC	422	37	9%	12
Precast	Float	Lower	SC	-	-	-	-
Precast	Broom	Lower	SC	-	-	-	-
Precast	Tine	Lower	SC	-	-	-	-
Precast	Broom	Moderate	HC	339	81	24%	12
Precast	Tine	Moderate	HC	327	62	19%	12
Precast	Broom	Moderate	V	360	74	21%	12
Precast	Tine	Moderate	V	360	38	11%	12

HC: Hand Consolidated
V: Vibrated
SC: Screed Only

Std. Dev.: Sample standard deviation
CoV: Coefficient of variation

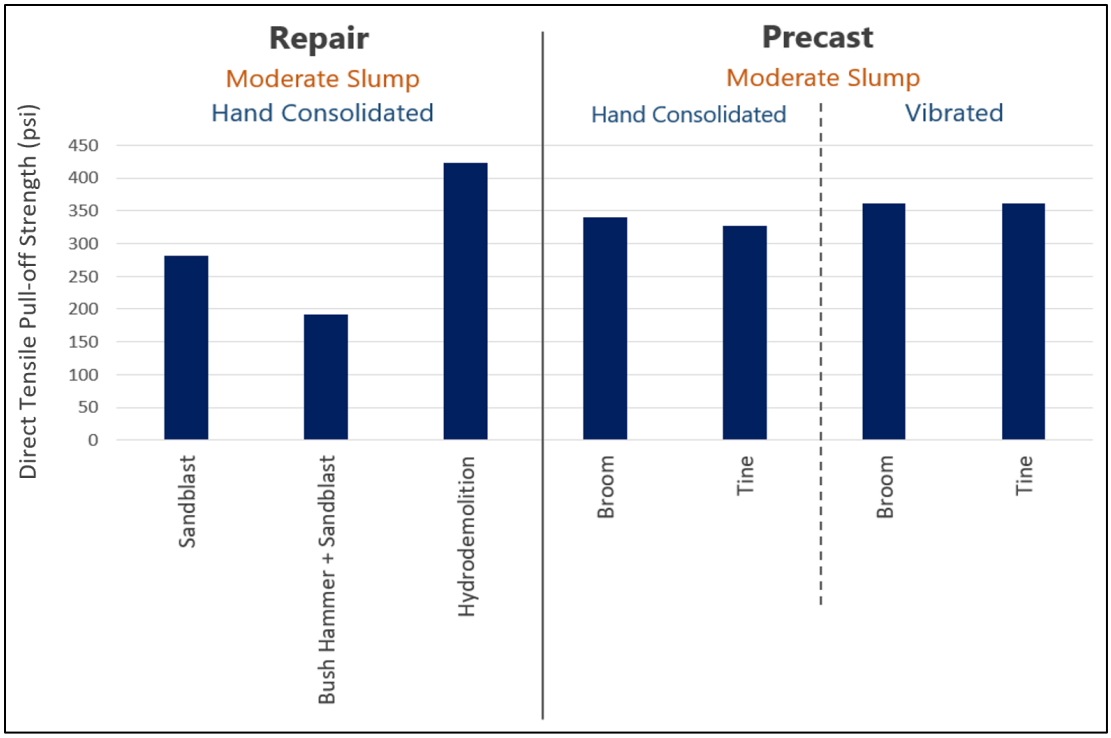

Figure 4-9: Average direct tensile pull-off results (psi).

The direct tensile pull-off test results exhibited the same overall trends in strength as shown in the direct shear strength results. In the repair series, hydrodemolition of the interface resulted in the highest tensile bond strength with an average of 422 psi, followed by sandblast alone at 280 psi and bush hammer + sandblast at 191 psi, as shown in Table 4-8. Hypothesis testing (Student's t-test) indicates that the differences between the average tensile bond strengths for the three repair interfaces were statistically significant. The variability of the test results from the hydrodemolition interfaces was significantly lower than that of the other repair interfaces, indicating more consistent interface conditions and improved tensile bond strength.

The precast series specimens with moderate slump concrete had lower tensile pull-off strengths than the hydrodemolition specimens from the repair series but had higher

strengths than the sandblast alone and bush hammer + sandblast repair specimens. The broom-hand consolidated and broom-vibrated specimens had average direct tensile strengths of 339 psi and 360 psi, respectively, while the tine-hand consolidated and tine-vibrated specimens had shear strengths of 327 psi and 360 psi, respectively. Hypothesis testing indicates that the differences between the tensile bond strength results for the broom and tine finishes are not statistically significant. Similarly, there is no statistical difference in tensile strength between the hand consolidation and vibrated placement conditions.

4.5 PHASE 1 - DISCUSSION

The precast series with float surface preparation and lower slump topping were not able to achieve consistent measurable results in either the direct shear or tensile bond pull-off tests, and thus are excluded from further discussion. This combination of surface preparation and concrete placement was included for comparison purposes to represent a lower bound condition in the precast series. It is not used in practice, nor is it recommended for use in precast or other construction with unreinforced interfaces.

The test results presented in the preceding sections for the precast series indicate that the differences in interface direct shear and tensile bond strength for topping placed by hand consolidation and by vibration were not statistically significant. Accordingly, the data sets for hand consolidated and vibrated precast series specimens have been combined for the purposes of the following discussion.

4.5.1 Effectiveness of Surface Preparation Techniques Investigated

The influence of the surface preparation technique on the interface shear and tensile strengths from Phase 1 is analyzed and discussed here.

Repair Interfaces

As expected, the substrate prepared by hydrodemolition provided the highest direct shear and tensile pull-off strengths in the repair series specimens. The hydrodemolition achieved a CSP of 9-10 based on the ICRI CSP comparators and had the highest MTD of the repair series specimens as determined by LLS. Hydrodemolition is a widely used method for concrete removal and can produce a surface profile with a high degree of surface roughness with a low risk for microcracking or bruising,

The bush hammer + sandblast interface had the lowest shear and tensile bond strengths in the repair series. The use of a hand-held bush hammer is a form of scabbling for concrete removal. While removal by bush hammer can produce a concrete profile of CSP 7 to 9 (a CSP of 7 to 8 was achieved in this project), the scabbling action can cause microfractures in the cement paste and loosening of the coarse aggregate at the substrate surface, creating a weakened or bruised layer. The use of abrasive blasting (sandblasting) after concrete removal by bush hammering is intended to remove the weakened layer. Despite having a CSP 7-8 surface profile, the low shear and tensile bond strength test results for the bush hammer + sandblast specimen suggest that microcracking was present and that the sandblasting was unable to remove weakened surface layer at the interface. This surface preparation type had the highest ratio of shear-to-tensile bond strength of all interfaces investigated, suggesting that the (presumed) presence of microcracking had a more significant effect on the tensile pull-off strength than on the direct shear strength.

The sandblast only interface was included to provide a lower bound for surface roughness; a surface profile of CSP 2-3 was achieved in this study. The sandblast only surface could be considered to meet the ACI 318-19 Cl. 16.4.4.2 surface preparation definition of "intentionally roughened," but would not meet the requirement for "intentionally roughened to a full amplitude of approximately 1/4-inch." This latter condition is required for design conditions with interface shear reinforcement. In spite of this lower degree of surface roughness, the sandblast only interface achieved higher direct shear and tensile pull-off strengths than the bush hammer + sandblast interface and had comparable strength results to the broom and tine interfaces in the precast series. These results illustrate the benefits of limited "intentional roughening" that removes laitance and minor surface defects while opening the paste pore structure at the repair interface.

Precast Interfaces

The float only interface was included along with lower slump concrete and screed only placement as a lower bound interface condition and does not represent typical or recommended practice. Viable shear or tensile pull-off strengths could not be achieved for this interface preparation and topping placement, and it was not studied further.

The broom interface developed an average direct shear strength approximately 20% higher than the tine interface (considering all data for moderate slump concrete placed by hand consolidation and moderate slump concrete consolidated by vibrating). The average tensile pull-off strength was similar for the two interfaces (i.e., the differences in the test data were determined to be not statistically significant). The broom interface shear strength results were slightly less variable than the results for the tine surface, although the opposite trend was noted for the tensile pull-off strength results.

It is generally assumed that a tine or rake finish will provide more surface roughness than a broom finish, and thus the tine finish is expected to provide improved interface bond strength. The direct shear strength results from this study contradict this assumption. Previous research comparing the shear strength of broom and tine or rake finishes has also been contradictory. Mones and Breña (2013) performed push-off tests for 24 specimens with two hollow-core slab concrete types and six different slab finishes, including broom and raked. The highest shear strength values were obtained for specimens with transverse broomed finish, at 278 psi, while the longitudinally raked finish with an amplitude of about 1/4 inches had an average strength of 198 psi. While these findings are consistent with the current study, Kovach and Naito (2008) observed the opposite trend in a study involving 32 composite T-beam flexural experiments to assess shear transfer. In specific, they observed a strong correlation between shear strength and surface roughness and recommended design horizontal shear strength values of 435 psi for broom finish and 571 psi for rake finish.

The contradictory conclusions regarding the shear bond strength of broom and rake finishes in unreinforced interfaces may result from several factors, including substrate and topping properties and placement procedures, variability in the surface textures created by raking or tining the substrate, and differences in shear test methods.

4.5.2 Correlation Between Strength Test Results and Mean Texture Depth

The mean texture depths of the various substrate surface preparations are shown in Figure 4-10 along with the average shear and tensile bond strengths. The relations between MTD and direct tensile pull-off strength, and MTD and direct shear strengths are

shown in Figure 4-11 and Figure 4-12, respectively. As shown, there is no apparent correlation between interface bond strength and MTD.

The precast tine surface had the highest MTD due to the large grooves in the surface macrotexture created by the tining rake, b this surface did not have the highest shear or tensile bond strength. The repair hydrodemolition interface had the highest average shear and tensile bond strength, but had an MTD of 1.33 mm, or only 60% of the 2.23 mm MTD for the precast tine surface. The repair bush hammer + sandblast surface preparation achieved the lowest shear and tensile bond strengths of all interface types, but had only the second lowest MTD at 0.82 mm in comparison to the sandblast only interface at an MTD of 0.20 mm.

The MTD for the precast tine surface was approximately double that of the precast broom surface, while there was no difference in tensile bond strengths for these surfaces and the broom finish had a higher shear bond strength. The high MTD for the tine interface results from the deep, narrow grooves created by the tining rake. The grooves are pronounced but are spaced father apart than the surface undulations created by the broom. Examination of the tine grooves under optical microscope (Figure 4-13) shows that the mortar from the topping concrete may not be fully consolidated in the substrate grooves. This condition, in combination with the wide spacing of the grooves, does not appear to provide improved bond in comparison to the broom substrate finish in spite of having a high MTD. The more uniform and shallower surface roughness of the broom finish may facilitate more thorough consolidation of the topping concrete at the interface, resulting in improved bond.

Published research typically shows a strong correlation between shear strength and surface roughness (Kovach and Naito 2008), although most studies do not quantitatively

characterize surface roughness. From a qualitative perspective, there is a subtle correlation between surface texture roughness and interface shear strength in the repair series; the increased surface roughness (higher CSP) of the hydrodemolition interface provided a significant increase in shear and tensile bond strength in comparison to the sandblast only and bush hammer + sandblast interfaces, which have lower surface roughness (CSP values). However, the comparison of the bush hammer + sandblast and sandblast only interfaces provides a contradictory conclusion, most likely due to microcracking or bruising of the substrate due to concrete removal by bush hammer that may have reduced bond strength.

The results of the current study indicate that for the interface types and topping placement conditions investigated, the shear and tensile bond strength of an unreinforced interface does not appear to be influenced by the degree of surface macrotexture roughness measured by MTD. This contrasts with most published research, although the published correlations are primarily qualitative indications of relative surface roughness rather than the quantitative measure of MTD used in the current study. The results in the current study suggest that the interface bond strength in shear may be less dependent on degree or magnitude of surface roughness, and more dependent on having a uniformly roughened surface that is sound (i.e., no laitance or surface defects) and having well consolidated repair or topping concrete. The favorable results obtained for the sandblast only interface in the repair series also suggest that removal of the finished surface of the concrete and opening of the pore structure may improve bond in spite of having very low surface roughness or texture.

The limited influence of surface roughness on shear and tensile bond strength results for the unreinforced interfaces considered in this study contrasts with shear transfer

mechanisms were friction is engaged. For example, surface roughness is known to have a significant influence on shear transfer by shear friction across interfaces with reinforcement, or for unreinforced interfaces subjected to a permanent normal force such that friction can develop.

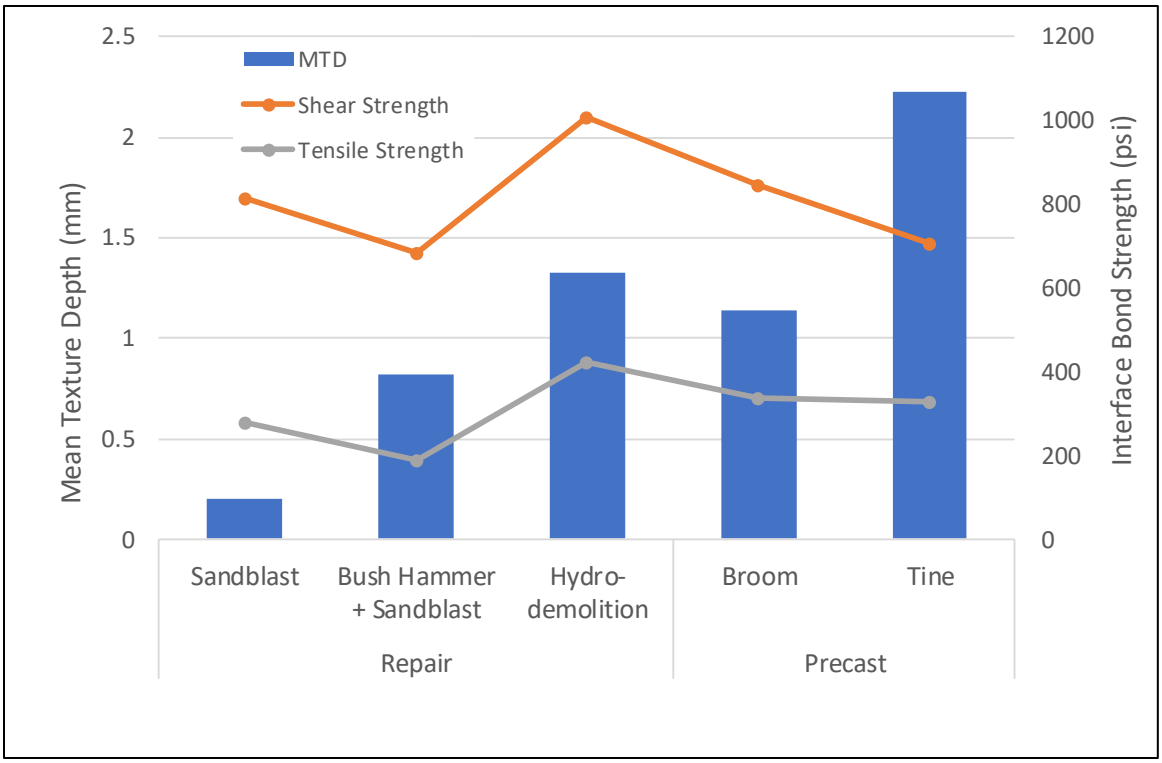

Figure 4-10. Measured mean texture depths and bond strengths for difference surface preparation techniques.

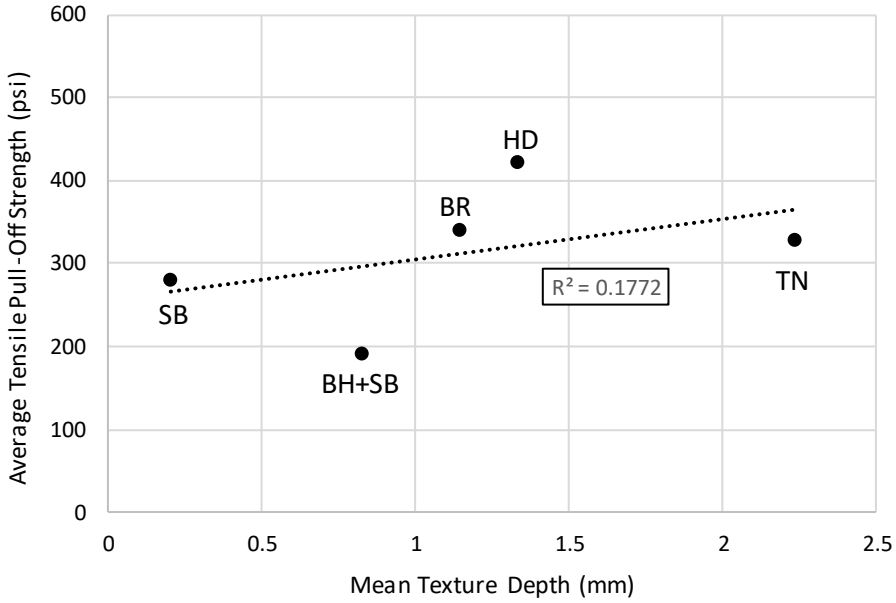

SB: Sandblast only BR: Broom

BH+SB: Bush hammer + sandblast TN: Tine

HD: Hydro-demolition

Figure 4-11: Mean texture depth vs. direct tensile pull-off strength.

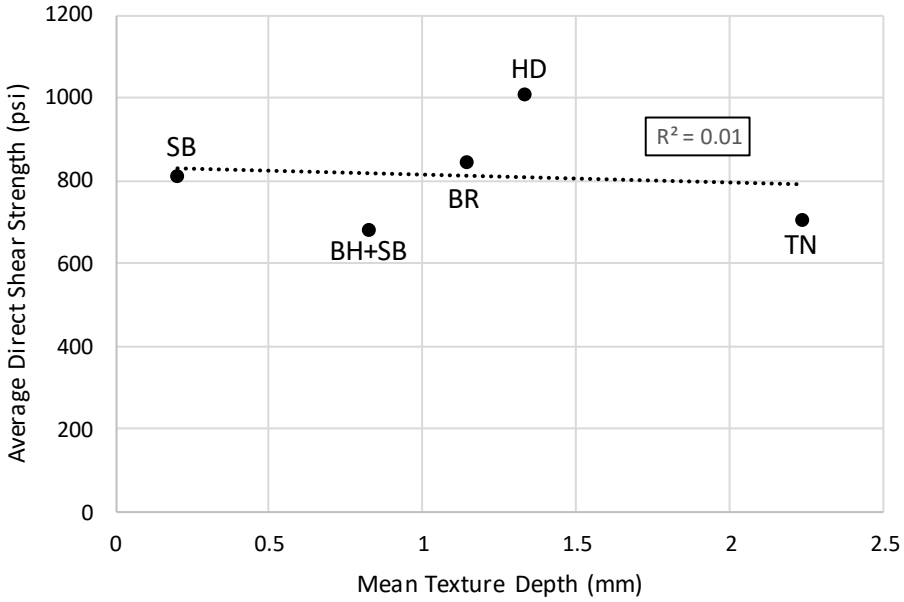

SB: Sandblast only BR: Broom

BH+SB: Bush hammer + sandblast TN: Tine

HD: Hydro-demolition

Figure 4-12: Mean texture depth vs. direct shear strength.

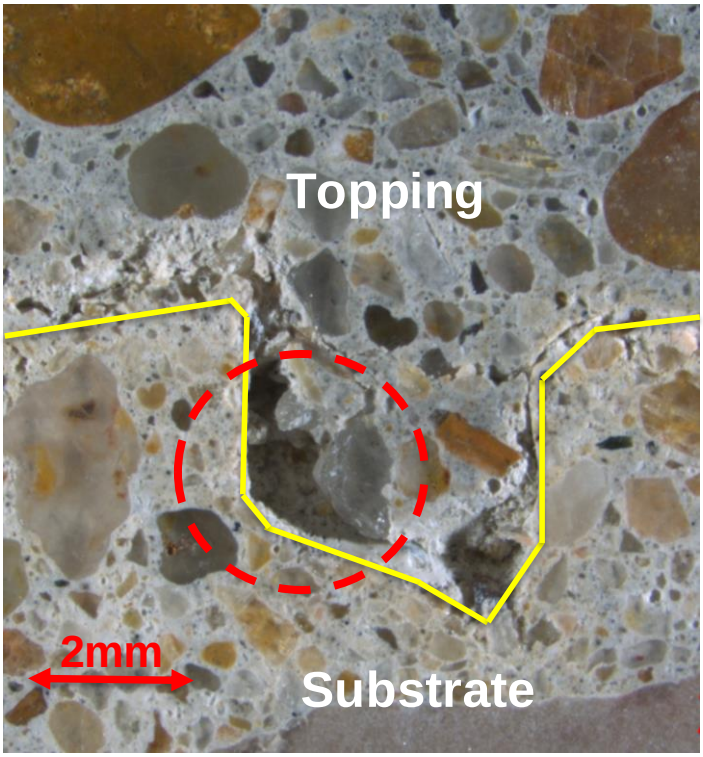

Figure 4-13. Precast Series Tine Interface: Close up view of topping consolidation in substrate groove created by tining rake.

4.5.3 Comparison of Shear and Tensile Strength Results

The correlation between average direct shear strength determined by guillotine shear test and average direct tensile pull-off strength is shown in Figure 4-14. Individual ratios of interface shear-to-tensile pull-off strength for each interface type tested are listed in Table 4-9 and are plotted as a function of MTD in Figure 4-15. Note that the average results used to create this table and these figures were based on a sizeable data set of 129 direct shear guillotine tests and 84 direct tensile pull-off test results.

The ratios of shear-to-tensile strength range from 2.16 to 3.57, with an average value of 2.7 and standard deviation of 0.55. Figure 4-14 includes a linear regression trendline and indicates a modest linear correlation between interface shear and tensile

strength with a coefficient of determination (R^2) value of 0.69. Note that the regression trendline is based on a non-zero y-intercept; correlation is decreased using a zero y-intercept.

The ratios of shear-to-tensile strength vary with surface roughness with an overall decreasing trend in strength ratio with increasing MTD (Figure 4-15). The results for the repair series bush hammer + sandblast interface have the highest ratio of shear-to-tensile strength of 3.57, while having the second lowest MTD. If the results for this data set are removed, a nearly linear relationship between ratio of shear-to-tensile strength and MTD is obtained ($R^2 = 0.97$).

Table 4-9. Ratio of average interface direct shear strength to direct tensile pull-off strength

Slab Category	**Surface Preparation Technique**	**Mean Texture Depth, MTD (mm)**	**Average Shear Strength (psi)**	**Average Tensile Strength (psi)**	**Ratio of Shear-to-Tensile Strength**
Repair	Sandblast	0.2	815	280	2.91
Repair	Bush Hammer + Sandblast	0.82	682	191	3.57
Repair	Hydro-demolition	1.33	1009	422	2.39
Precast	Broom-All	1.14	848	339	2.5
Precast	Tine-All	2.23	707	327	2.16
				Average	**2.71**

Numerous previous research studies (e.g., Momayez et. al. 2005, Santos 2009, Rosen 2016) have explored the correlation between different test methods used to assess interface shear bond strength, and some have examined the correlation between interface shear strength and interface tensile bond pull-off strength. A limited review of previous

research reveals that the actual correlation is dependent on the test methods used and interface parameters investigated, as discussed in the literature review.

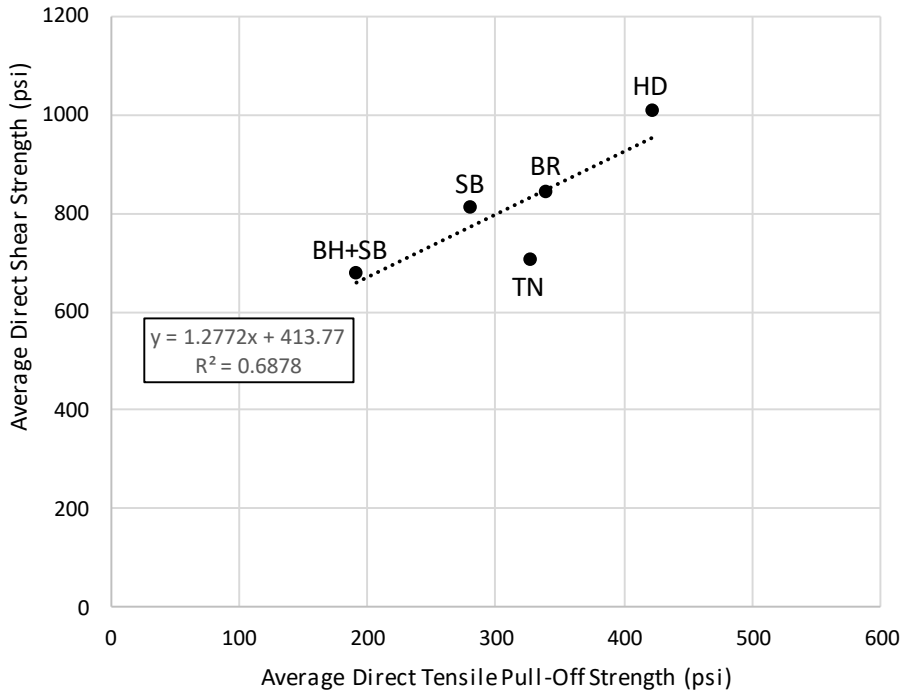

SB: Sandblast only
BH+SB: Bush hammer + sandblast
HD: Hydro-demolition
BR: Broom
TN: Tine

Figure 4-14: Correlation between interface direct shear strength and direct tensile pull-off strength.

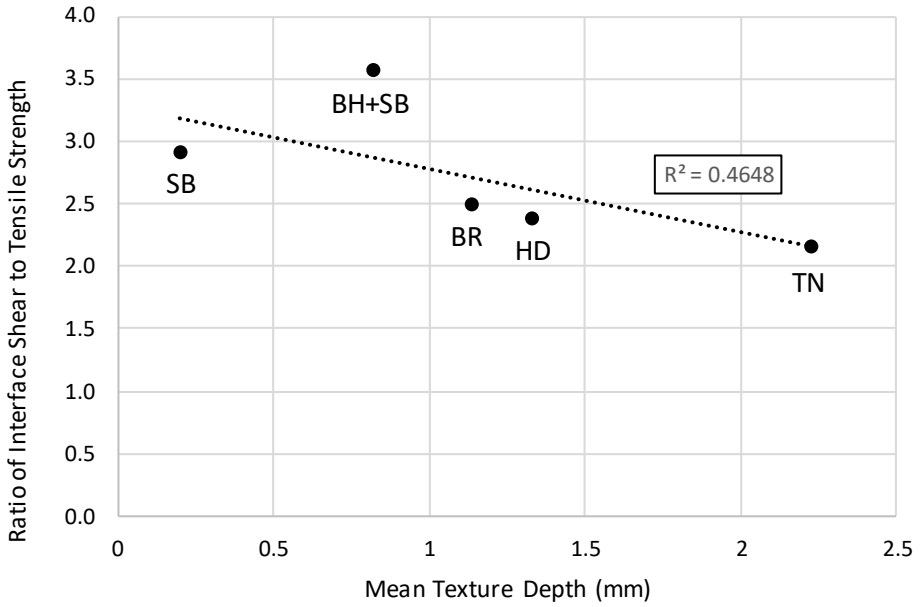

SB: Sandblast only
BH+SB: Bush hammer + sandblast
HD: Hydro-demolition
BR: Broom
TN: Tine

Figure 4-15. Variation of ratio of shear-to-tensile bond strength with respect to mean texture depth.

The shear-to-tensile pull-off strength results from the current study are consistent with the range of values for direct shear or torsion shear tests from previous studies. The slant shear test produces significantly higher apparent shear strengths due to the effect of normal force across the interface tested.

Many research studies and repair design guides conclude that tensile bond pull-off testing is the preferred method for assessing in-situ interface bond conditions in practice based on its relative simplicity and ability to be performed entirely in the field. ACI 562-19 Clause 7.4.3 requires the use of quantitative bond strength testing to verify performance of cementitious repairs for unreinforced interfaces where the factored shear stress (demand) is between 30 psi and 60 psi. Direct tension pull-off tests are one method

permitted by ACI 562 for this purpose. The commentary for Clause 7.4.3 states that "*typically direct shear strengths are larger than direct tension strengths,"* although it goes on to indicate that *"it is generally adequate to assume that the repair to substrate bond will resist an interface shear equal to the direct tensile pull-off test result."* The ratios of measured interface direct shear strength to tensile pull-off strength are consistently greater than the assumed ratio of 1:1 noted in the ACI 562 commentary; presumably the commentary is intended to provide a conservative lower bound.

The data from the current study and other published research show that the ratio of shear strength to tensile pull-off strength is influenced by interface preparation condition including surface roughness and mean texture depth. This observation, in combination with the dependence of the shear-to-tensile strength ratio on test methods used to obtain the strength results and the general variability of shear and tensile bond strength results, indicates that a generally applicable single value, or even a range of values, for ratio of shear-to-tensile strength suitable for quality control purposes may not achievable. Rather, the ratio would need to be determined based on test data on a case-by-case basis in order to effectively use it for quality control purposes in a performance-based design approach for interface shear.

4.5.4 Comparison of Shear Strength Results to Design Values

In all cases, the average direct shear strengths determined by guillotine shear testing were significantly higher than the nominal interface shear strength for design of 80 psi per ACI 318 and ACI 562. It is important to note that average material strength test results are not typically appropriate for use in structural design or evaluation.

The Tolerance Factor Method is one approach that is often used to estimate equivalent specified or characteristic material or element strengths for design based on test data (ACI 214.4R 2010, ACI 228.1R 2019, ACI 335.4 R-19). While Phase 1 of the current study does not include sufficient data to develop a modified interface shear strength for design, estimating the characteristic shear strength using the tolerance factor method provides an indication of the potential for increased shear strength design values based on interface bond testing.

Characteristic design interface shear strengths were estimated based on a 10% fractile using the Tolerance Factor Method; results for 90% and 95% confidence levels are shown in Table 4-10. The 10% fractile (i.e., 90% probability of exceedance) is commonly used for evaluating concrete strength test data. Note that the data presented in Table 4-10 for the precast series have been combined for the moderate slump concrete placed by hand consolidation and vibration since these data sets were not shown to be statistically different. Furthermore, the table does not include the results for precast specimens with lower slump topping placed by screed only, as the variability of these results was too large to provide meaningful results.

Table 4-10. Estimated characteristic design interface shear strengths based on Tolerance Factor Method (10% Fractile).

Slab Category	Substrate Roughening Technique	Direct Shear Strength - Test Data				Characteristic Strength (psi)	
		Average (psi)	Std. Dev. (psi)	CoV	Sample Size	90% Confidence	95% Confidence
Repair	Sandblast	815	209	26%	19	443	408
Repair	Bush Hammer + Sandblast	682	237	35%	18	255	214
Repair	Hydro-demolition	1009	214	21%	24	643	612
Precast	Broom	838	205	24%	31	498	474
Precast	Tine	703	236	34%	37	320	294

Std. Dev.: Sample standard deviation
CoV: Coefficient of variation

The estimated characteristic design shear strengths at a 95% confidence level range from 2.7 to 7.6 times higher than the current 80 psi nominal interface shear strength in ACI 318-19 and ACI 562-19. These results suggest that partial depth repairs and precast topping applications with good interface surface preparation and well-consolidated repair or topping concrete may justify the use of a higher interface shear bond strength for design.

The characteristic design shear strengths also reflect the significant influence of variability in the test results on the resulting design strength. Notably, the characteristic interface shear strength for the broom finish is 60% higher than that for tine finish, while the mean strength of the broom finish was only 20% higher than that of the tine finish. In this case, the tine finish had a greater coefficient of variation than the broom finish (Table 4-10), which results in a larger difference between the mean and characteristic strengths. A similar punitive result occurs for the bush hammer + sandblast repair

interface, which had a coefficient of variation of 35% resulting in a characteristic strength less than half of the mean strength.

Chapter 5 : Phase 2 - Test Program

5.1 Overview

The experimental program of Phase 2 comprised five composite RC beams tested under three bending to study the horizontal shear capacity of unreinforced interfaces. Each of the beams had a different interface roughness representative of common precast (new construction) and partial depth repair techniques. A monolithic beam was also tested as a control specimen. In addition to the beams, five composite slabs were fabricated at the same time to obtain cores for guillotine shear and direct tensile pull-off tests for the five different interface roughnesses.

This chapter describes the experimental variables, specimen design and fabrication, test setup and instrumentation for Phase 2.

5.2 Experimental Variables

The surface roughness conditions chosen for the five composite beams were sandblast, hydrodemolition, broom, tine, and float. Five companion plain concrete composite slabs were fabricated with the same surface roughness as the composite beams. The topping workability and consolidation technique were consistent for all the composite specimens using a moderate topping slump and vibrating the topping for consolidation. A monolithic beam with the same geometry and reinforcement as the composite beams was also included in the program. The complete test program of Phase 2 with corresponding cast number is summarized in Table 5-1 and Table 5-2. Photos of the various roughness techniques are shown in Figure 5-1 through Figure 5-4.

Table 5-1: Phase 2 Beam Specimen Test Matrix

Beam Number	Substrate Roughening Technique	Category	Topping Workability (Slump) Level	Topping Consolidation Technique	Concrete Cast Number
B0	Monolithic beam	-	-	-	Cast 7
B1	Sandblast	Repair	Medium	V	Cast 7 (Substrate) / Cast 9 (Topping)
B2	Hydrodemolition	Repair	Medium	V	Cast 7 (Substrate) / Cast 9 (Topping)
B3	Float	Precast	Medium	V	Cast 7 (Substrate) / Cast 9 (Topping)
B4	Broom	Precast	Medium	V	Cast 7 (Substrate) / Cast 9 (Topping)
B5	Tine	Precast	Medium	V	Cast 7 (Substrate) / Cast 9 (Topping)

V: Vibrated

Table 5-2: Phase 2 Slab Specimen Test Matrix

Slab Number	Substrate Roughening Technique	Category	Topping Workability (Slump) Level	Topping Consolidation Technique	Concrete Cast Number
S1	Sandblast	Repair	Medium	V	Cast 8 (Substrate) / Cast 9 (Topping)
S2	Hydrodemolition	Repair	Medium	V	Cast 8 (Substrate) / Cast 9 (Topping)
S3	Float	Precast	Medium	V	Cast 8 (Substrate) / Cast 9 (Topping)
S4	Broom	Precast	Medium	V	Cast 8 (Substrate) / Cast 9 (Topping)
S5	Tine	Precast	Medium	V	Cast 8 (Substrate) / Cast 9 (Topping)

Figure 5-1. Hydrodemolition

Figure 5-2. Sandblast

Figure 5-3. Tine

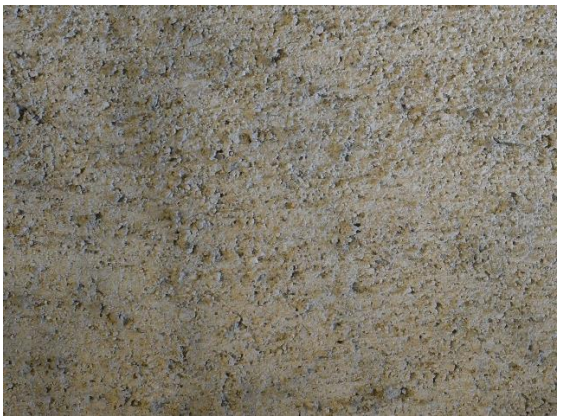

Figure 5-4. Broom

5.3 SPECIMEN DESIGN

The dimensions and reinforcement of the beam specimens are presented in Figure 5-5, Figure 5-6, and Figure 5-7. The specimens were designed so that the horizontal shear capacity of the interface in one span could be exceeded prior to reaching the flexural and vertical shear capacities of the beam. The beam substrates had an 18-inch width and a height of 13 inches. The beam toppings had an 18-inch width with a height of 5 inches. The beam longitudinal reinforcement comprised eight #8 bars as tension reinforcement,

four #4 bars to cage the stirrups at the top of the substrate, and three #4 bars at mid-height of the topping as compression reinforcement. The transverse reinforcement comprised four legs of #3 bars spaced at 4.5 inches in the longitudinal direction of the beam.

To ensure a horizontal shear failure, one shear span of the beam (failure end) had an unreinforced interface which was also partially debonded to reach higher levels of horizontal shear stress. As shown in Figure 5-5, only the central 8 inches of the interface were bonded in the failure end. The other shear span (non-failure end) had the stirrups extending into the topping slab acting as interface reinforcement and the interface was bonded across the entire width, as shown in Figure 5-6. The toppings were designed to end 18 inches (equivalent to the beam depth) from the center of the support. This was done to prevent potential interface failures caused by propagation of diagonal shear cracks originating at the supports. This idea was originally proposed in Loov and Patnaik (1994) and has been implemented in other horizontal shear beam test studies such as Kovach and Naito (2008).

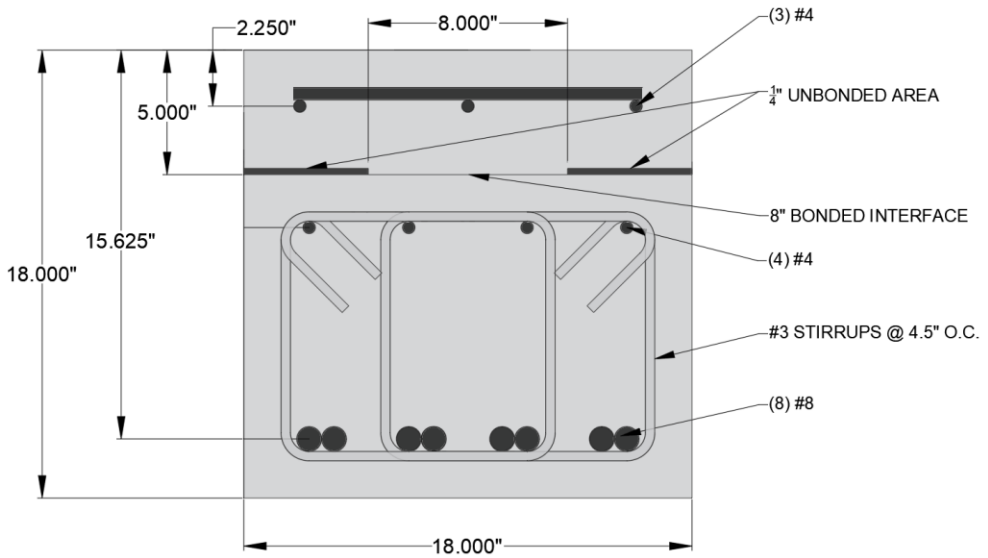

Figure 5-5: Beam specimen cross-section – Failure end

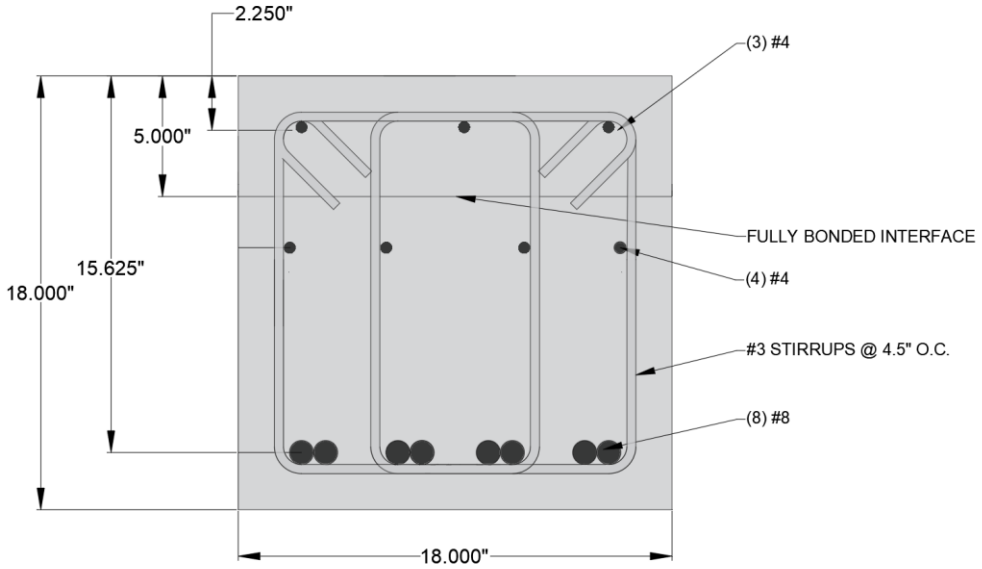

Figure 5-6: Beam specimens cross-section – Non-failure end.

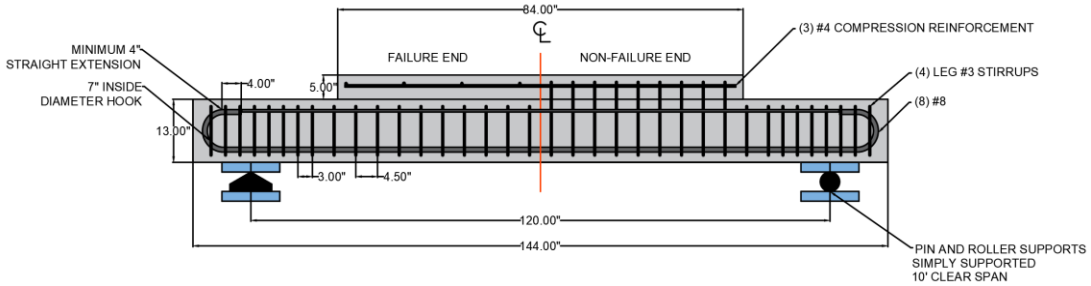

Figure 5-7: Beam specimen elevation view.

The same slab specimen design used in Phase 1 was used for Phase 2. The slabs had a 4" substrate with a 2.75" topping. The specimens were 3' foot by 3.5' to provide adequate space for (9) 4" diamter direct shear cores and (6) 3" direct tensile pull-off cores.

5.4 Specimen Fabrication

Fabrication of Phase 2 specimens was done at the Ferguson Structural Engineering Laboratory at the University of Texas at Austin. The same mix designs as in Phase 1 were selected for the substrate and toppings.

5.4.1 Substrate Fabrication

The composite beam substrates and monolithic beam were cast at the same time. The concrete mix used had a design strength of 4,000 psi, design slump of 4.5", and maximum aggregate size of ¾ inches. Photos of the rebar cages before the pour are shown in Figure 5-8 and Figure 5-9.

Figure 5-8: Beam substrate rebar cages ready for casting.

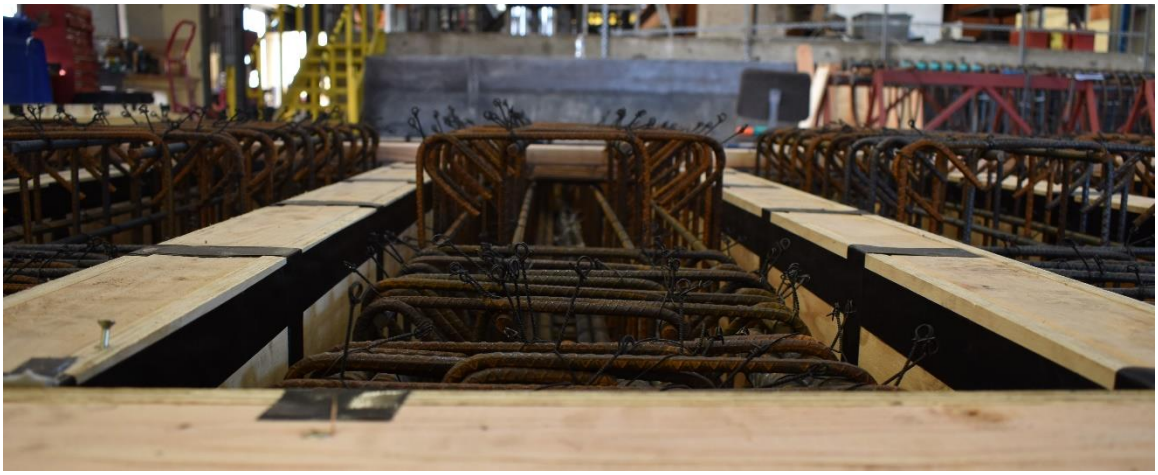

Figure 5-9: Beam substrate showing stirrups on non-failure end that extend into topping as interface reinforcement.

The specimens were vibrated and screeded for consolidation. Once the concrete had set up, all surfaces were floated on the failure end and the broom and tine specimens

were roughened. The non-failure end surface was left as-placed. Saturated burlap was placed on the beams and covered with a plastic tarp. The beams were left to wet cure for 7 days. Due to a time constraint during the cast, the slab substrates were poured separately one week later. The same mix design, and finishing and curing procedures were used.

When both the beam and slab substrates had exceeded their specified 28-day strength, the sandblast and hydrodemolition surface conditions were executed in the corresponding specimens. This procedure was done by the same repair contractor as in Phase 1. These two surfaces are shown along with CSP comparators in Figure 5-10 and Figure 5-11.

Once the five surface roughness conditions had been completed, roughness measurements were taken using the same linear laser scanner used in Phase 1 to determine their MTD values.

Figure 5-10: Hydrodemolition compared to CSP 10 comparator.

Figure 5-11: Sandblast compared to CSP 3 comparator.

5.4.2 Method for interface debonding

As previously described, the failure end of the interface of composite beams was partially debonded to enforce a horizontal shear failure. A variety of techniques have been used in previous studies to debond portions of concrete interfaces, including plastic wall paneling secured with tape (Swan 2011) and polyethylene foam tape (Kovach and Naito 2008). The debonding material needs to be thick enough to prevent aggregate interlock between the substrate and topping, but also be flexible to adhere to the peaks and valleys of each surface so that it stays in place during casting. In the present study, one layer of ¼-inch polyethylene foam tape was chosen as the debonding material. Figure 5-12 shows the debonding tape installed on the hydrodemolition beam substrate. Prior to the beam casting, the effectiveness of the debonding foam tape was tested on mock-up cylinders with roughened surfaces. The roughened substrate of the mock-up was covered by the foam tape and a topping was cast on top of the foam tape. Once the forms for the topping were removed, the concrete topping could be easily pulled off due to self-weight.

Figure 5-12: Hydrodemolition substrate with debonding foam tape.

5.4.3 Topping Fabrication

The concrete toppings for the composite beams and slabs were cast at the same time. The beams specimens prior to the topping pour are shown in Figure 5-13. Prior to casting, the substrates were covered with saturated burlap and left to soak for 24 hours to achieve SSD conditions (Figure 5-14). Before the concrete arrived for the topping the surfaces were cleaned and patted dry. Any water puddles were blown with compressed air. The same mix design that was used for the substrates was used for the topping.

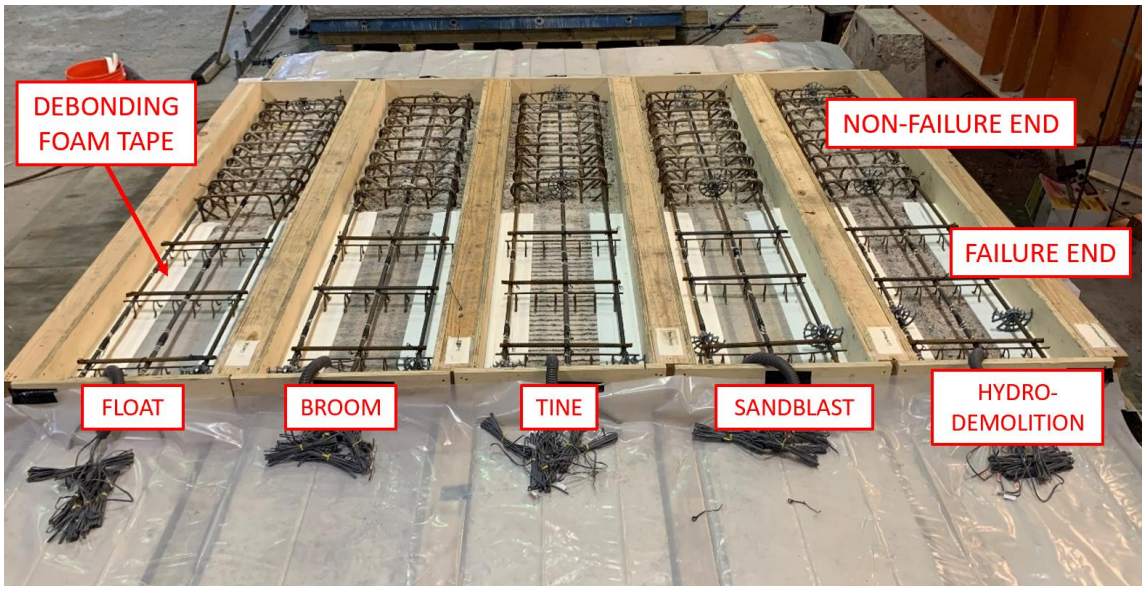

Figure 5-13: Beams ready for topping pour.

Figure 5-14: Soaking substrates before casting to achieve SSD conditions.

5.5 BEAM TEST SETUP AND LOADING PROTOCOL

The beams were simply supported and loaded with a single point load at midspan using the test setup shown in Figure 5-15. The supports were fabricated to act as pin and roller boundary conditions. The pin support (Figure 5-16) was created using a tilt saddle placed on top of a load cell to allow rotation in all directions. A steel plate was placed on top of the tilt-saddle to support the beam. The roller support (Figure 5-17) was created by placing a 3-inch diameter steel rod between two steel plates sitting on two load cells for stability. The roller allowed for translation and rotation in the longitudinal direction of the beam.

A 400-ton hydraulic actuator was used to apply a downward vertical load at the center of the beam. The actuator had a 12-inch stroke and a 9-inch diameter. A tilt saddle and steel plates were placed between the beam and the actuator to spread the load along the entire beam width, as shown in Figure 5-18. The actuator reacted against a steel frame anchored to the strong floor.

The beam was loaded under monotonic loading using a hydraulic pump. The load was applied at 10-kip increments. At the end of each load increment, the test was paused and the beam was examined for cracks.

Figure 5-15: Beam test setup.

Figure 5-16: Pin support

Figure 5-17: Roller support

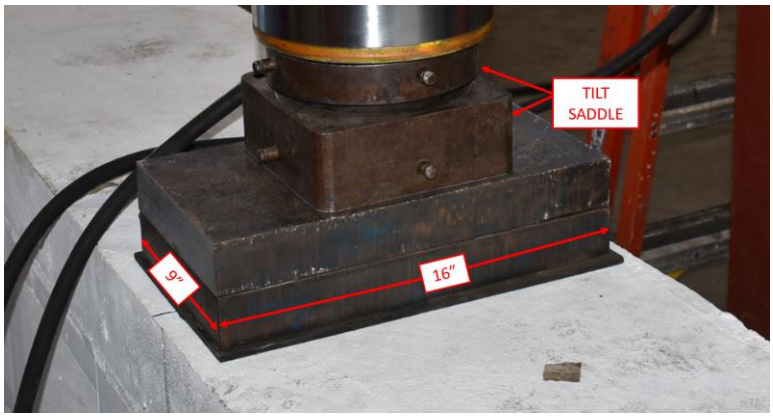

Figure 5-18: Loading plates

5.6 BEAM INSTRUMENTATION

During the beam tests, force and deformation data was collected from load cells, linear potentiometers, strain gauges on the reinforcement, and vision system to monitor strains and displacements of the beam.

Linear potentiometers (L-pots) were used to measure midspan deflection (LP01), end slip of the interface (LP02 and LP03), and slip of the interface along one side face of the beam (LP04, LP05, and LP06). Along the other side face, interface slip was monitored using a digital image correlation (DIC) system, but the analysis of DIC data is out of the scope of this thesis and will be not be discussed here. The position of the L-pots used to measure deflection and interface slip is indicated in Figure 5-19. The end slip L-pots are shown in Figure 5-20 and the side face L-pot is shown in Figure 5-21.

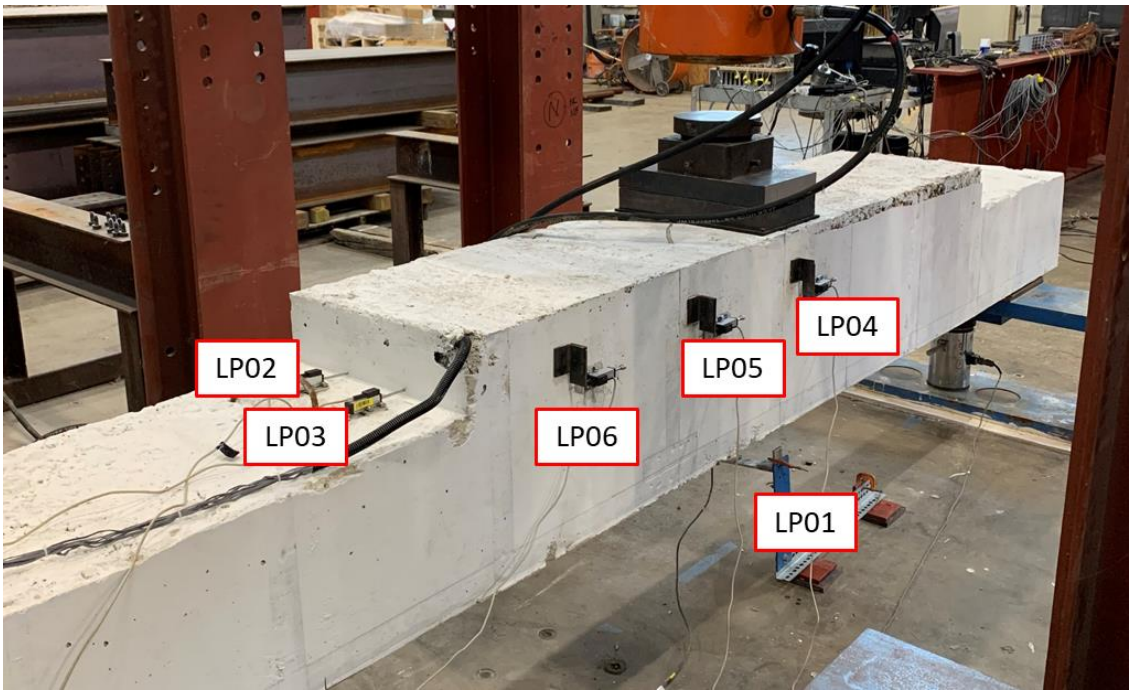

Figure 5-19: Linear potentiometer layout.

Figure 5-20: End-slip linear potentiometers.

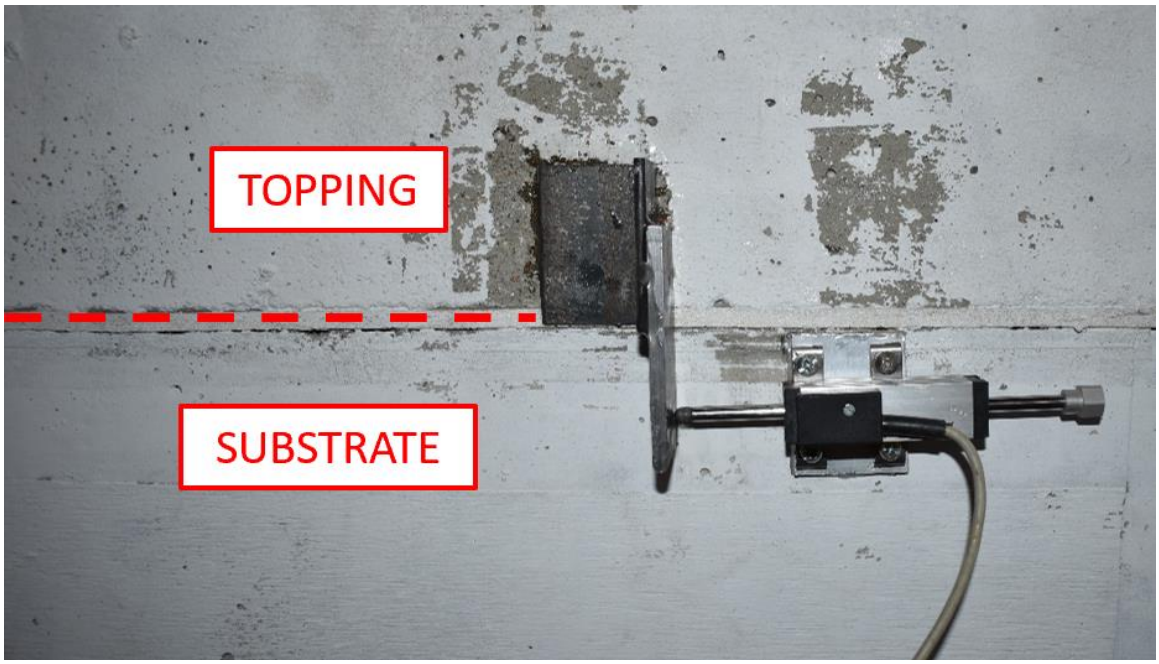

Figure 5-21: Side face linear potentiometer.

Each specimen had also nine strain gauges to measure strains in the longitudinal reinforcement. The strain gauges were placed at midspan, 16-inches from midspan, and 32-inches from midspan in one tension bar and two compression bars. The location of strain gauges along the beam length and cross section is shown in Figure 5-22.

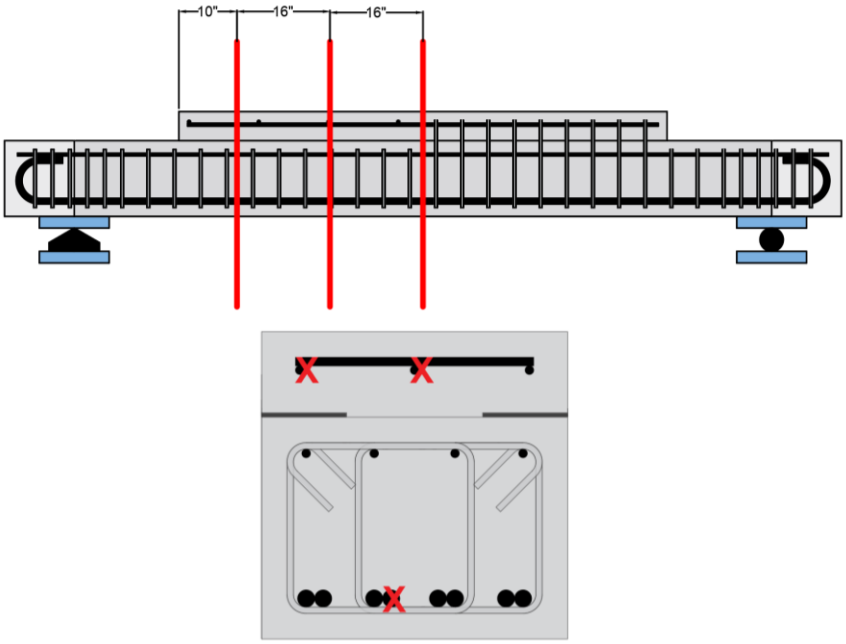

Figure 5-22: Strain gauge layout.

5.7 Testing of Slabs

Nine guillotine shear tests and six direct tensile pull-off tests were conducted on each composite slab. At the time of this report only four of the nine direct shear tests were performed for each slab.

Chapter 6 : Phase 2 - Experimental Results and Discussion

This chapter presents and discusses Phase 2 experimental results, including material test data, surface roughness characterization of slab and beam specimens, flexural testing of beam specimens, as well as guillotine tests and direct tensile pull-off tests of samples from composite slabs.

At the time of completion of this thesis, the six beam specimens included in the test program had been fabricated but only four (monolithic, broom, tine, and hydrodemolition) were tested. Only the results from these four specimens and the corresponding slab data are presented in this chapter.

6.1 Material Test Results

6.1.1 Concrete Slump

The concrete slump was measured for each concrete placement in accordance with ASTM C143-15; results are listed in Table 6-1. The target slump for each mix was aiming to represent a "moderate" slump used in industry being 4.5" and 5" for the substrate and topping, respectively.

Table 6-1. Phase 2 measured concrete slump.

Cast Number	Slump
Cast 7 (Substrate - Beams)	4.5"
Cast 8 (Substrate - Slabs)	4.75"
Cast 9 (Topping – Beams & Slabs)	5.75"

6.1.2 Compressive and Splitting Tensile Strengths

Concrete compressive strength and splitting tensile strength tests were conducted using 4-inch by 8-inch cylinders in accordance with ASTM C39-18 and ASTM C496-17, respectively. Strength tests were conducted at twenty-eight days after casting as well as on the day of beam testing. The compressive strengths and splitting tensile strengths for each concrete cast are shown in Table 6-2 and Table 6-3, respectively.

Table 6-2. Phase 2 concrete compressive strength results.

Cast Number	28-Day (psi)	Day of Testing-Monolithic Beam (psi)	Day of Testing-Broom and Tine Beams (psi)	Day of Testing-Hydro-demolition Beam (psi)
Cast 7 (Substrate - Beams)	5500	6100	6100	6100
Cast 8 (Substrate - Slabs)	5700	-	-	-
Cast 9 (Topping)	6000	-	6000	6200

Table 6-3: Phase 2 concrete splitting tensile strength results.

Cast Number	28-Day (psi)	Day of Testing-Monolithic Beam (psi)	Day of Testing-Broom and Tine Beam (psi)	Day of Testing-Hydrodemolition Beam (psi)
Cast 7 (Substrate - Beams)	550	700	700	700
Cast 8 (Substrate - Slabs)	650	-	-	-
Cast 9 (Topping)	650	-	650	700

6.2 Surface Roughness Characterization by Mean Texture Depth from Line Laser Scanner Results

The mean texture depth (MTD) results obtained from the Line Laser Scanner are presented in Table 6-4 and Figure 6-1. As shown, the MTD values for the float, broom, sandblast, and hydrodemolition surfaces in the beams are similar to the corresponding

MTD values for slab surfaces. The tine specimens present a larger disparity, with the beam having a 26% higher average MTD as compared to that of its companion slab.

Table 6-4: Phase 2 Mean Texture Depth obtained from LLS.

	Interface Condition	Average MTD (mm)	Standard Deviation (mm)	Coefficient of Variation	Sample Size
Slab	Float	0.08	0.011	13%	4
	Broom	0.60	0.072	12%	4
	Tine (Rake)	0.75	0.118	16%	4
	Sandblast	0.20	0.033	17%	4
	Hydrodemolition	1.33	0.139	10%	4
Beam	Float	0.16	0.038	24%	4
	Broom	0.70	0.065	9%	4
	Tine (Rake)	1.30	0.145	11%	6
	Sandblast	0.23	0.021	9%	5
	Hydrodemolition	1.46	0.170	12%	4

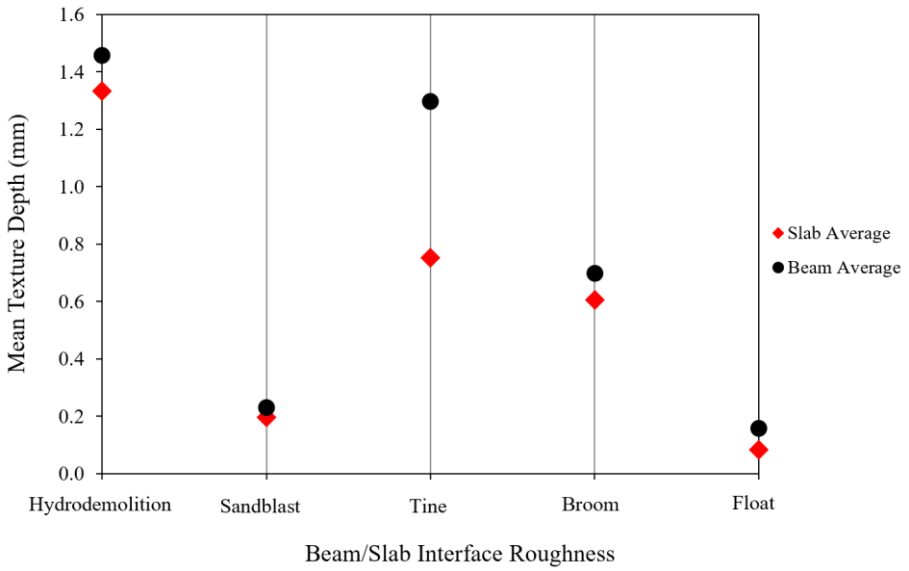

Figure 6-1: MTD results for Phase 2 specimens.

Using the MTD averages, the specimens were grouped into three levels of roughness: high, moderate, and low. The hydrodemolition beam, hydrodemolition slab, and tine beam are in the "high roughness" group with MTD averages of 1.46 mm, 1.33 mm, and 1.30 mm, respectively. The broom beam, broom slab, and tine slab are in the "moderate roughness" group with MTD averages of 0.70 mm, 0.60 mm, and 0.75 mm, respectively. The sandblast beam, sandblast slab, float beam, and float slab are in the "low roughness" group with MTD averages of 0.23 mm and 0.2 mm, 0.16 mm, and 0.08 mm, respectively.

These groups were defined by clear distinctions of the averages. Hypothesis testing with Student's t-test indicates the averages of all three specimens in the "high roughness" and "moderate roughness" groups are not statistically significant different from one another in their respective groups. The float and sandblast specimens in the "low roughness" group do have statistically different means according to Student's t-test, but

all MTD averages in this group are still clearly lower than those in the “moderate roughness” group. These groups are shown graphically in Figure 6-2.

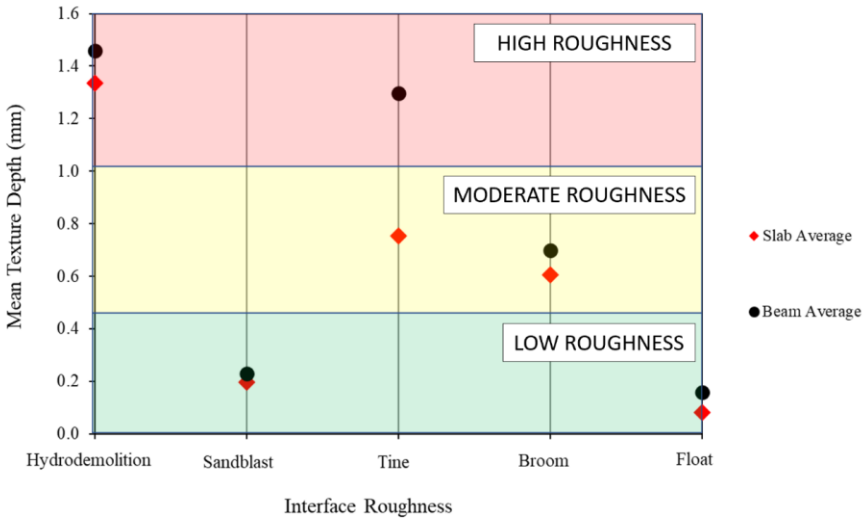

Figure 6-2: Phase 2 MTD groups.

Cracks along the interface have been observed in the specimens in the “low roughness” group. The damage was noticed approximately three weeks after topping placement, but the exact time of cracking is unknown. This effect can be attributed to the insufficient bond of these interfaces to restraint differential shrinkage between the substrate and topping. No cores were successfully taken from the two slabs in this group as the stress from coring caused a break at the interface. The two beams in this group were scanned using a Proseq Pundit 250 Array device that uses pulse echo technology to detect voids/delaminations in concrete. These scans indicated the beams were fully delaminated along a significant part of the unreinforced interface. As indicated earlier, these two beams remain to be tested and the results are not included in this report.

No cracks were observed in the moderate- and high-roughness beam specimens, and all cores taken from the moderate- and high-roughness slabs stayed intact. When only considering specimens from Phase 2, evidence seems to indicate that low-roughness interfaces are prone to debonding. This is not the case of Phase 1 sandblast specimens, which presented relatively high direct shear and direct tension strengths. Bond strength is dependent on many factors including surface preparation (roughness, cleaning, SSD), topping concrete slump, topping concrete water-to-cement ratio, topping concrete consolidation techniques, and concrete substrate/topping finishing. The use of petrography analysis is being explored to determine any other factors besides roughness that may have influenced interface delamination.

6.3 BEAM TEST RESULTS

The results of the flexural tests on four beam specimens (monolithic, broom, tine, and hydrodemolition) are presented and analyzed in terms of observed damage, load-vs.-deflection response, load-vs.-slip response, and steel strains. Using the data presented, the horizontal shear stresses at failure are also estimated using different analytical methods.

6.3.1 Observed damage

The four beam specimens were tested under a monotonically increasing vertical load applied at mid-span, as described in Chapter 5. The crack evolution for the monolithic beam, tine beam, and hydrodemolition beam is shown in Figure 6-3 through Figure 6-5. The crack evolution of the broom beam was similar to the tine and hydrodemolition specimens.

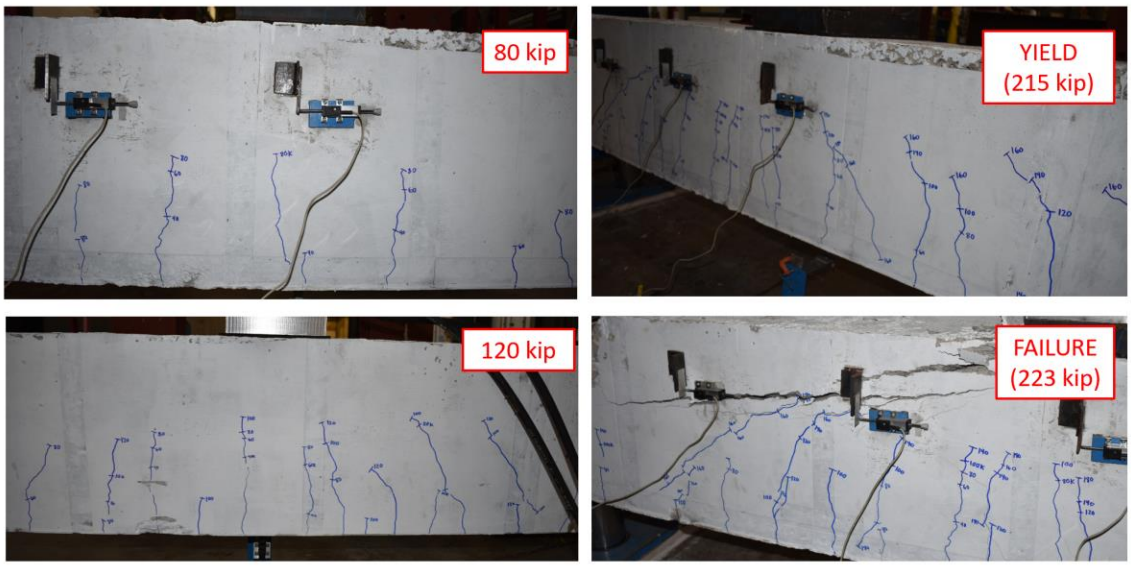

Figure 6-3: Crack progression of monolithic beam.

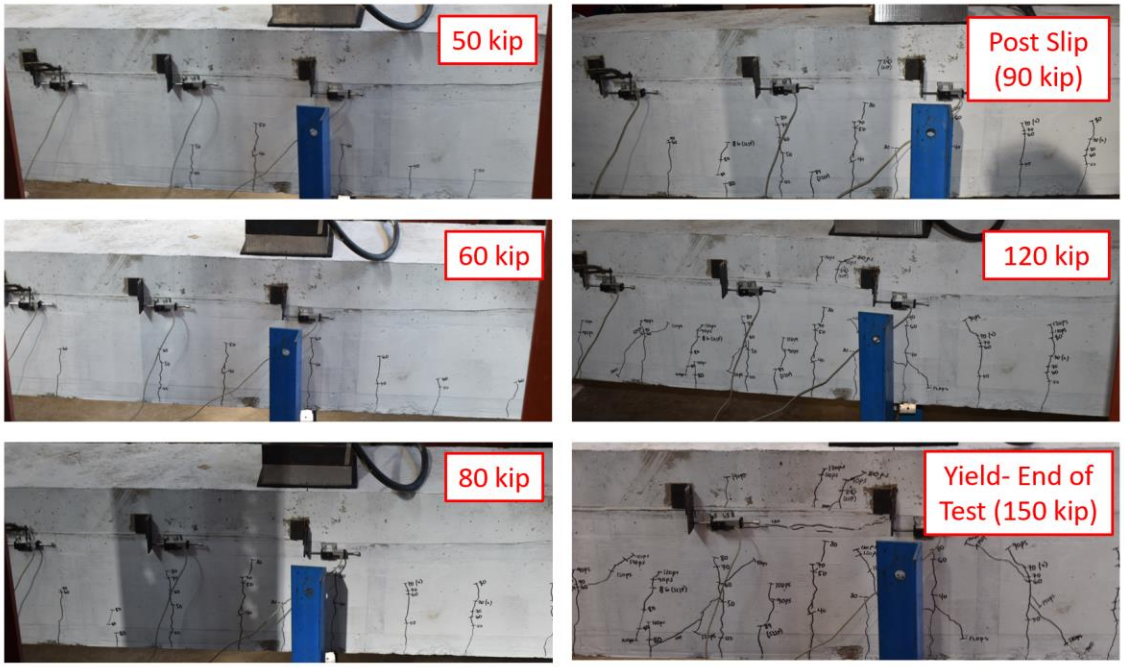

Figure 6-4: Crack progression of tine beam.

Figure 6-5: Crack progression of hydrodemolition beam.

As seen in the photos, flexural cracking was first observed in all beams after loading to 40 kips. As the load increased, more flexural cracks appeared and propagated upward but remained more than 3 inches below the interface until steel yielding and concrete crushing occurred.

The monolithic specimen presented a flexure-dominated behavior. However, after yielding the tension reinforcement at 215 kips and reaching a load of 223 kips, which is approximately equal to its theoretical flexural capacity, the beam failed due to propagation of a large crack between the end of the topping to the location of the vertical load, as shown in Figure 6-6. This crack had started at the support and propagated diagonally to the end of the topping, but failure ultimately occurred by the propagation and opening of this crack along the weak plane created by the short stirrups used in this shear span.

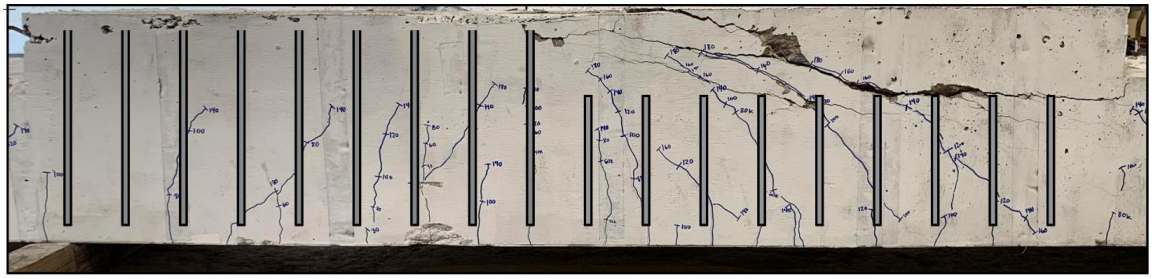

Figure 6-6: Failed monolithic beam with estimated location of stirrups.

The tine, broom, and hydrodemolition beams failed in horizontal shear at the substrate-topping interface when loaded to 86 kip, 89 kip, and 86 kip, respectively. Interface failures occurred prior to yielding the longitudinal steel. The failures were identified by a mild banging sound, a sudden drop in the lateral load capacity, and a jump in slip at the interface. Immediately after interface failure, cracks were observed at the bottom of the topping slab (Figure 6-7) and the end face of the interface (Figure 6-8). Due to the topping debonding on the sides of the section, it was not possible to visually identify longitudinal cracks along the interface. However, sudden increases of slip were measured at this point as it will be explained in Section 6.3.3.

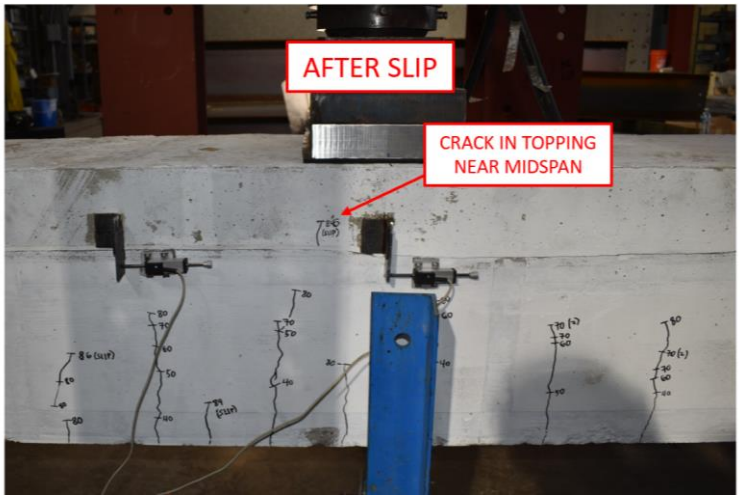

Figure 6-7: Crack pattern after interface slip.

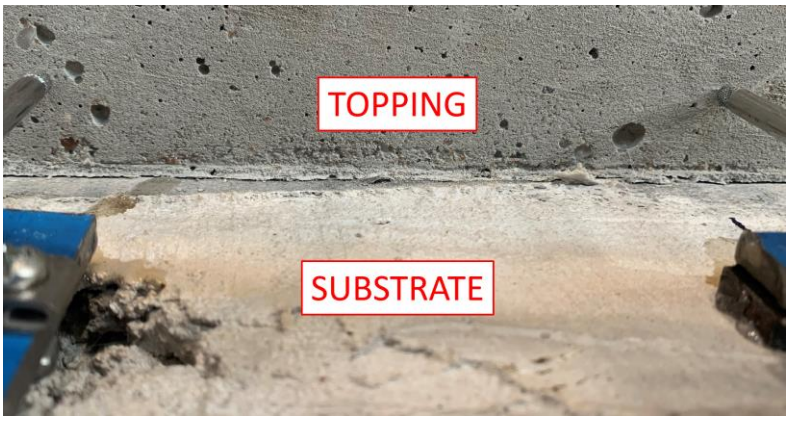

Figure 6-8: Interface crack after slip at end of topping slab.

After horizontal shear failure, the composite beams were loaded again at 10 kip intervals. The beam stiffness dropped and began exhibiting non-composite behavior. As the substrate continued to bend while subject to loading, the topping in the failure end appeared to remain straight beyond the mid-span region, causing a vertical gap to form at the interface (Figure 6-9). The tests were stopped after the tension steel yielded at approximately 160 kips. At this point, flexural cracks were widely open near the center of

the beam and concrete at the top of the substrate near mid-span began crushing (Figure 6-9).

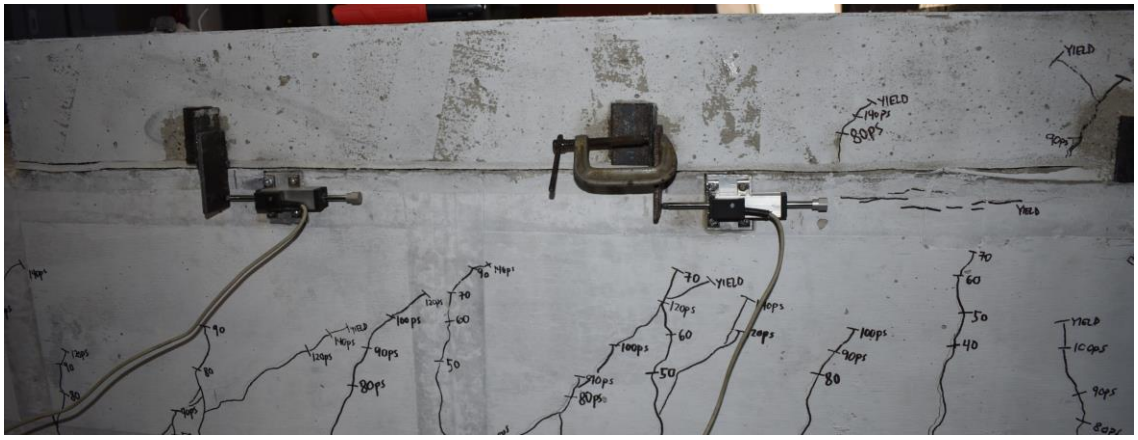

Figure 6-9: Top of substrate concrete crushing at midspan when tension steel yielded. Vertical gap seen between topping and substrate on left side of photo.

6.3.2 Load vs. Midspan Deflection Response

The load-vs.-midspan deflection responses of the monolithic, broom, tine and hydrodemolition specimens are shown in Figure 6-10. All four beams present very similar response until interface failure in the composite beams. The horizontal shear failure of the three composite beams (occurring at loads between 86 and 89 kips) is characterized by a sudden drop of the lateral load capacity of approximately 20 kips. This drop is caused by the reduction of stiffness as the beams loses composite action and the substrate and topping start to behave independently in the failure end. Beyond this point, the three beams with failed interfaces present a very similar response, with a lower stiffness and strength as compared to the monolithic beam due to the non-composite response along one span.

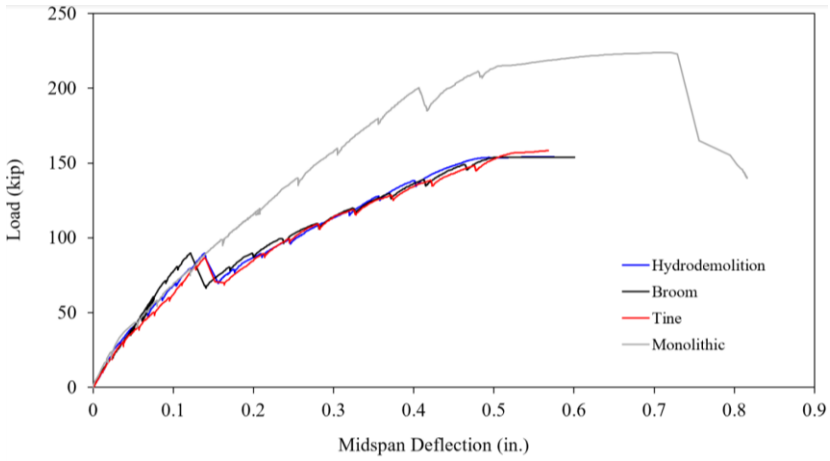

Figure 6-10: Load-vs.-deflection of monolithic, tine, broom, and hydrodemolition specimens.

6.3.3 Load vs. Slip Response

The relative horizontal displacement between the topping and the substrate was measured at midspan, 16" from midspan, 32" from midspan, and 42" from midspan (end of topping slab) as described in Chapter 5. The slip is plotted against the vertical load for each test in Figure 6-11 through Figure 6-14.

Relative displacement at the end of the topping slab increases linearly at early stages of loading for all the beams, including the monolithic specimen (Figure 6-14). This small displacement is not attributed to interface slip but to a small differential deformation caused by bending between the two points of measurement, which are not exactly at the same section and height. At interface failure, a sudden increase of slip is observed together with a small decay of the vertical load. Slip results from midspan, 16" from midspan, and 32" from midspan (Figure 6-11 through Figure 6-13) show no slip for the monolithic specimen, but the composite beams present a small and linear slip up until interface failure. This indicates these linear potentiometers that are placed on the side face of the beam are measuring slip of the topping relative to the substrate. At interface failure,

sudden slip jumps but with different magnitudes are also observed at midspan, 16” from midspan, and 32” from midspan.

The slip resulting from interface failure is calculated by subtracting the slip reading just before interface failure and just after (at the end of the load decay). A summary of slip from interface failure is shown in Figure 6-15. The behavior of each composite specimen was similar and each show slip increases as the distance from midspan increases.

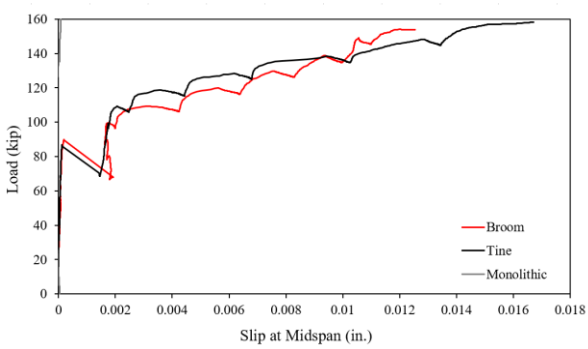

Figure 6-11: Vertical load versus substrate-to-topping slip measured at midspan.

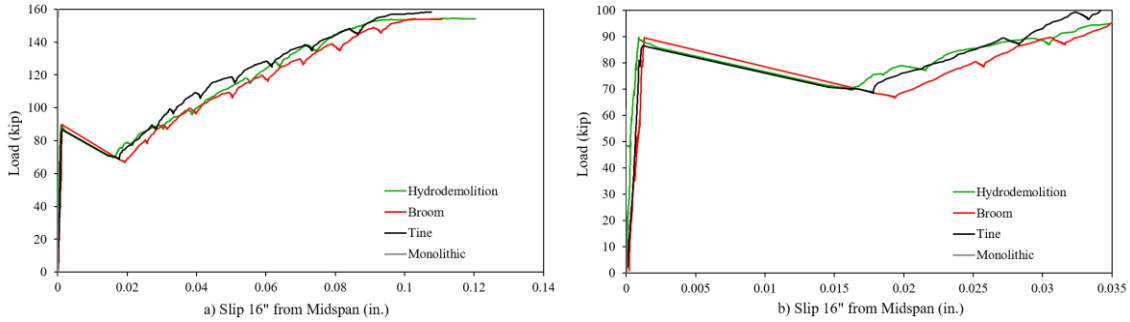

Figure 6-12: Vertical load versus substrate-to-topping slip measured 16” from midspan on the failure end: (a) full response, (b) close-up view of slip during interface failure.

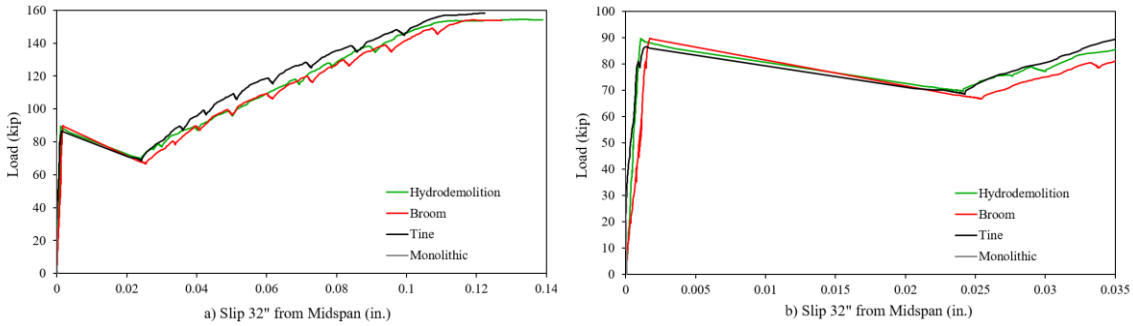

Figure 6-13: Vertical load versus substrate-to-topping slip measured 32” from midspan on the failure end: (a) full response, (b) close-up view of slip during interface failure.

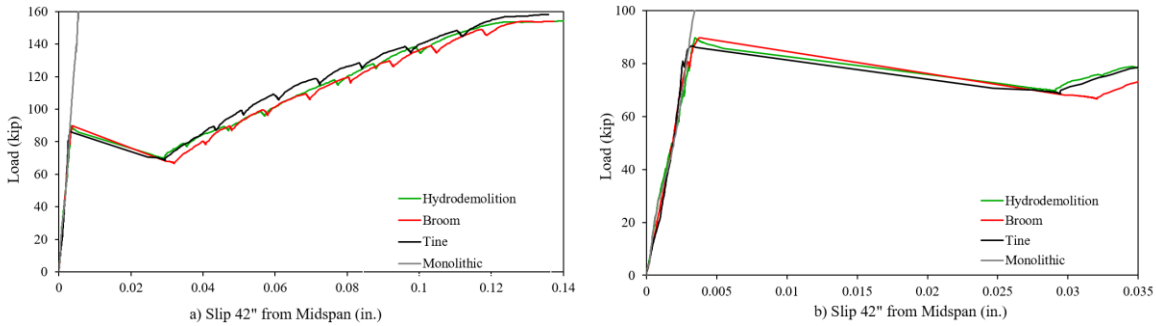

Figure 6-14: Vertical load versus substrate-to-topping slip measured 42” from midspan on the failure end: (a) full response, (b) close-up view of slip during interface failure.

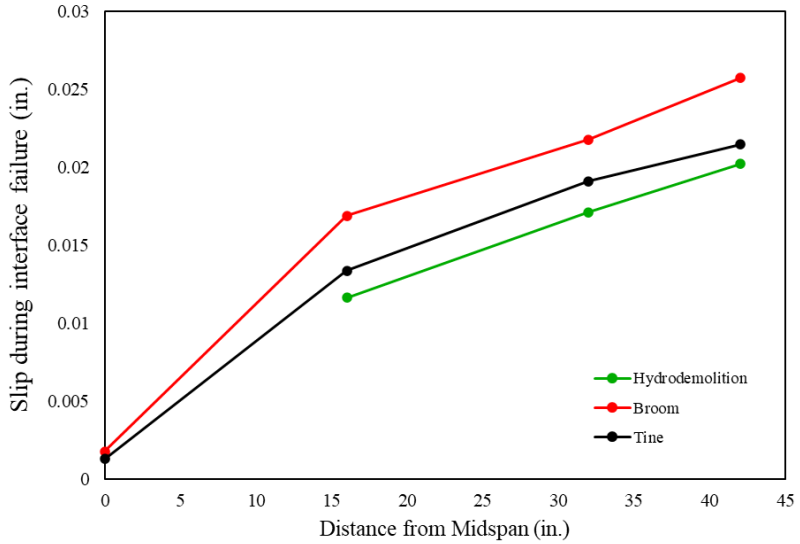

Figure 6-15: Slip during interface failure versus distance from midspan.

When increasing the load beyond this interface failure, the beams with interfaces clearly show a consistent increase of slip as a response to bending while the monolithic slip response remains small and trends linearly along the same initial slope (see Figure 6-14). This confirms that the measurements from the linear potentiometers at the end of topping (42" from midspan) includes a small component caused by the differential bending deformation.

6.3.4 Moment vs. strain response

The strains in tension and compression reinforcement are plotted against the applied moment at the specific cross-section in Figure 6-16, Figure 6-17, and Figure 6-18.

For the tension bars, the moment-strain relation is linear up to an approximate moment of 75 kip-ft, corresponding to cracking of the section. Beyond cracking, the stiffness of the curves decrease but the moment-strain relationship remains linear up until the interface failure for composite specimens. At interface failure, the moment capacity drops and strains deviate from the behavior of the monolithic beam. As the beams are loaded again, strains increase again linearly until reaching a yield strain of $\varepsilon_y = 0.0024$.

Compression strains increase linearly with moment until horizontal shear failure. When interface failure occurs, the compression steel in at midspan jumps from compression strains of approximately 0.0004 to near zero compression or in some cases, the midspan compression steel strain go into tension. The near zero or tension strains after interface slip indicates the topping is behaving independently from the substrate.

Compression strains were measured in a bar placed at the center of the topping (above bonded interface) and on a bar on the outer edge of the topping (above interface area debonded by foam tape). The strains in the center measured were higher than the

strains on the outer edge of the topping for all cross-sections. A summary of the percent difference between the strains is shown in Table 6-5. For the hydrodemolition and broom specimens, the difference between the strains increases the further from midspan. The tine beam has significantly larger percent difference in compression strains for all three cross-sections. The average of the compressive strains obtained from these bars is used for the analyses presented in the following section.

Table 6-5: Percent difference between compression strains in center of topping compared to outer edge of topping.

	Hydrodemolition	Tine	Broom
Midspan	5%	36%	3%
16" from Midspan	7%	18%	5%
32" from Midspan	21%	33%	13%

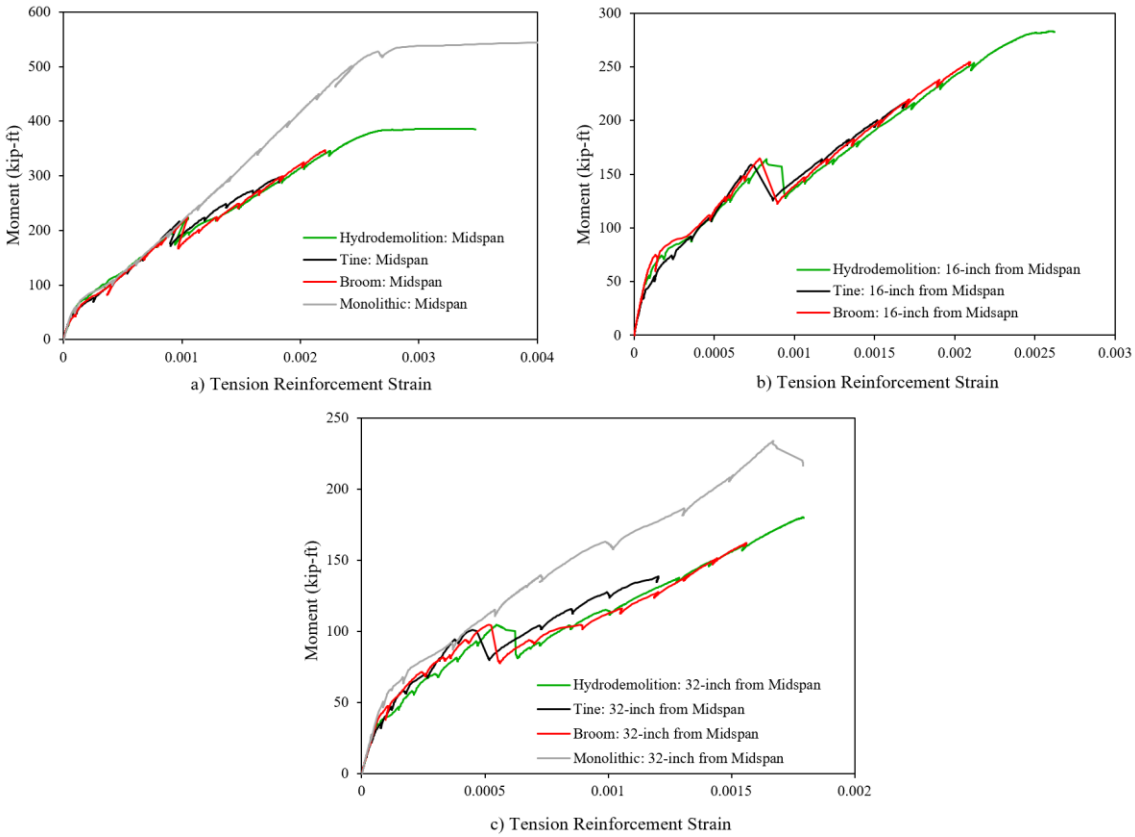

Figure 6-16: Strain in tension steel versus moment: (a) Midspan, (b) 16” from Midspan, and (c) 32” from Midspan.

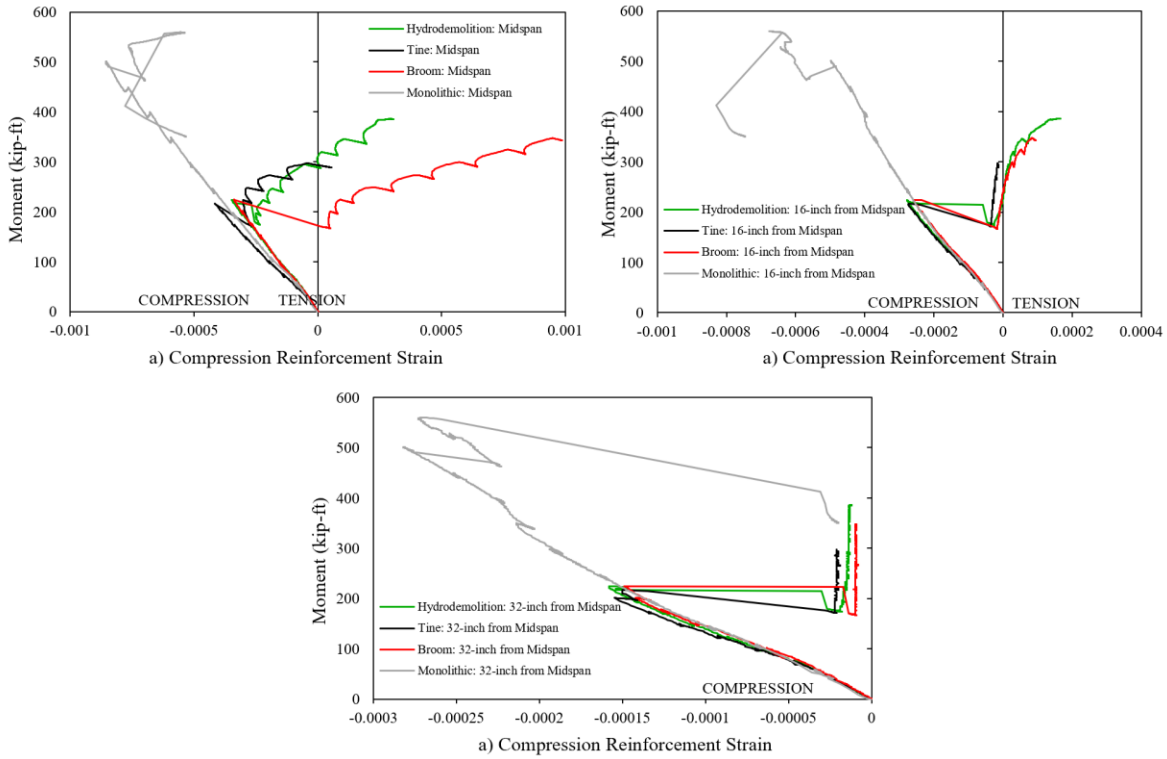

Figure 6-17: Strain in compression steel in center of topping slab versus moment: (a) Midspan, (b) 16” from Midspan, and (c) 32” from Midspan.

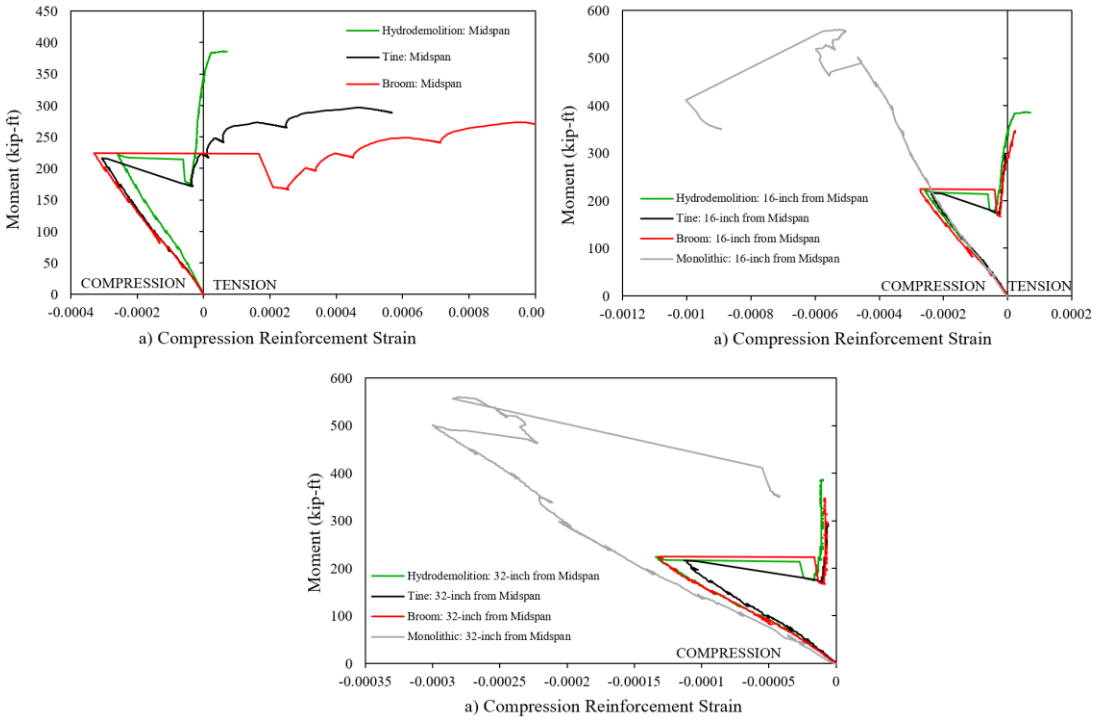

Figure 6-18: Strain in compression near outer edge of topping slab versus moment: (a) Midspan, (b) 16" from Midspan, and (c) 32" from Midspan.

6.3.5 Estimated interface shear stresses at failure

The horizontal shear stress along the interface is analytically estimated using strain data obtained from compression and tension steel immediately before interface slip. To convert steel strain data into horizontal forces resisted by the interface, a number of assumptions are made regarding the strain distribution along the section depth and the material stress-strain relations. Once the stress distribution at failure is obtained, average shear stresses at the interface are calculated based on equilibrium. Assumptions and estimated interface shear stress demands are described for three different methods.

Material stress-strain models

To compute compressive stresses in concrete, concrete is modeled with the stress-strain relations for short-term loading in compression proposed in section §5.1.8.1 of fib model code 2010 (fib 2010). The compressive stresses in the beams at interface failure did not to exceed 50% of the concrete compressive strength, which indicates the stress-strain relation is expected to be practically linear. The stress-strain relationship for the fib model vs. linear ($57{,}000 * \sqrt{f'_c}$) is shown in Figure 6-19.

The reinforcing steel does not yield before interface failure therefore the stress-strain behavior is assumed to be linear.

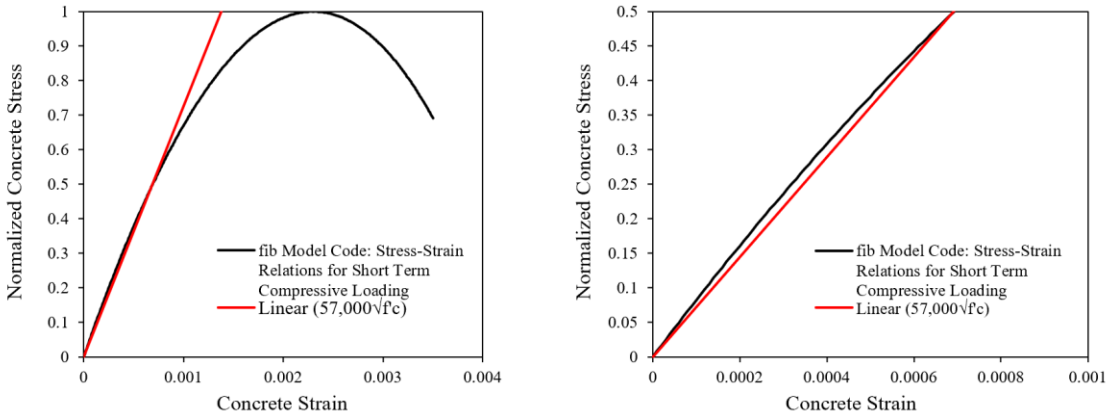

Figure 6-19: Concrete stress-strain model (fib 2010)

Method A: stress distribution based on linear strain profile

Assuming plane sections remain plane after deformation, strain gauge data from tension and compression steel is used to develop a linear strain profile along the beam depth for cross-sections at midspan, 16” from midspan, and 32” from midspan. The resulting strain profiles for the broom, tine, and hydrodemolition beams are shown in Figure 6-20.

From the linear strain profile, stresses in concrete and steel are calculated based on the material models previously described. Then, the resultant compression and tension forces acting on the section are calculated. The compression and tension forces for the three composite specimens are presented in Table 6-6. In almost all cases the tension force is larger than the compression, which does not satisfy equilibrium at the sectional level. At midspan, 16" from midspan, and 32" from midspan the tension force is greater than the compression force by ranges of 1% to 18%, 9% to 33%, and 36-60%, respectively. The results suggest the further the cross section is from midspan, the more strain distributions tend away from linear behavior along the beam depth.

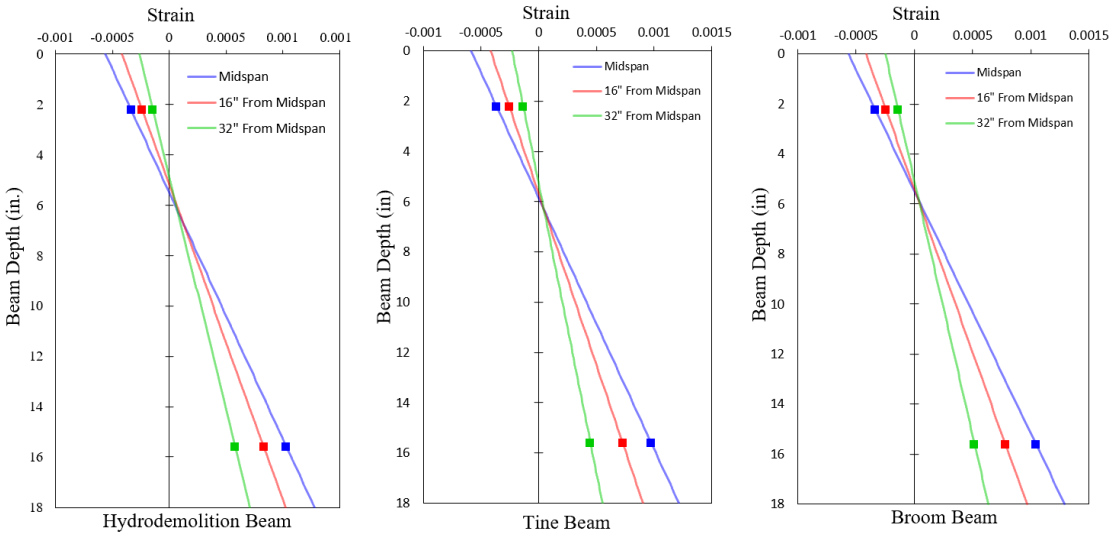

Figure 6-20: Strain profiles from Method A: linear strain along entire depth using strain gauge data.

Table 6-6: Tension and compressive forces using linear strain profile along beam depth.

		Broom	Tine	Hydrodemolition
Midspan	Compressive Force (kip)	163	180	168
	Tension Force (kip)	192	179	190
16" from Midspan	Compressive Force (kip)	116	122	115
	Tension Force (kip)	144	134	153
32" from Midspan	Compressive Force (kip)	64	61	67
	Tension Force (kip)	95	82	107

Method B: Linear strain profile for compression region only and enforcing equilibrium

In this method, strain profiles are derived based on strain gauge data from tension and compression steel, by assuming a linear strain distribution for the compressive region only, and by enforcing equilibrium. This method does not enforce linear strain distribution in the tension region since steel strain presents high variability in the vicinity of a crack. Equilibrium is enforced by calculating the tension force from known tension strains in the reinforcement and setting this equal to the compressive force. The neutral axis and slope of the compressive strain distribution is then determined to match the compressive force resultant and the strain at the level of compression reinforcement.

The strain profiles for the broom, tine, and hydrodemolition beams obtained from Method B are shown in Figure 6-21.

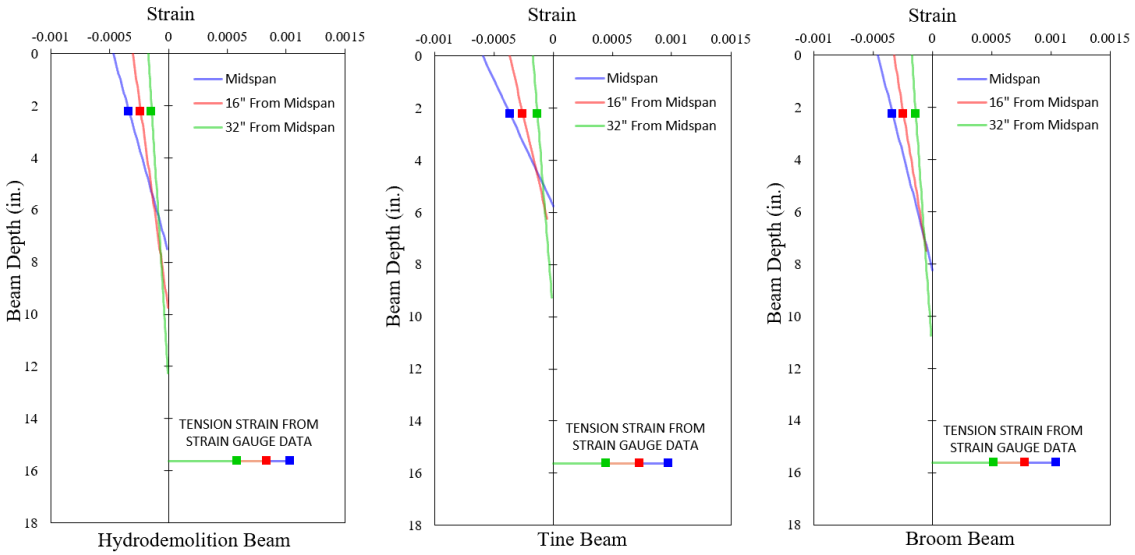

Figure 6-21: Strain profiles from Method B: linear distribution for compressive region but not for tension region. Equilibrium enforced.

Method C: Strain profile from applied moment and moment-curvature analysis

In this method, the strain and stress distributions are determined based on a moment-curvature analysis and the applied moment at failure. The moment-curvature analyses are conducted assuming plane sections remain plane along the entire depth and using the concrete and steel models previously described. The analytical strain profiles at failure for the hydrodemolition, tine, and broom beam are shown in Figure 6-22. The strain values from this analysis are compared to the test data in Table 6-7. While this method enforces equilibrium (compression force is equal to tension force), the analytical strain

distributions differ from strain gauge data ranging from 2% to 18% for tension strains and 29% to 56% for compression strains.

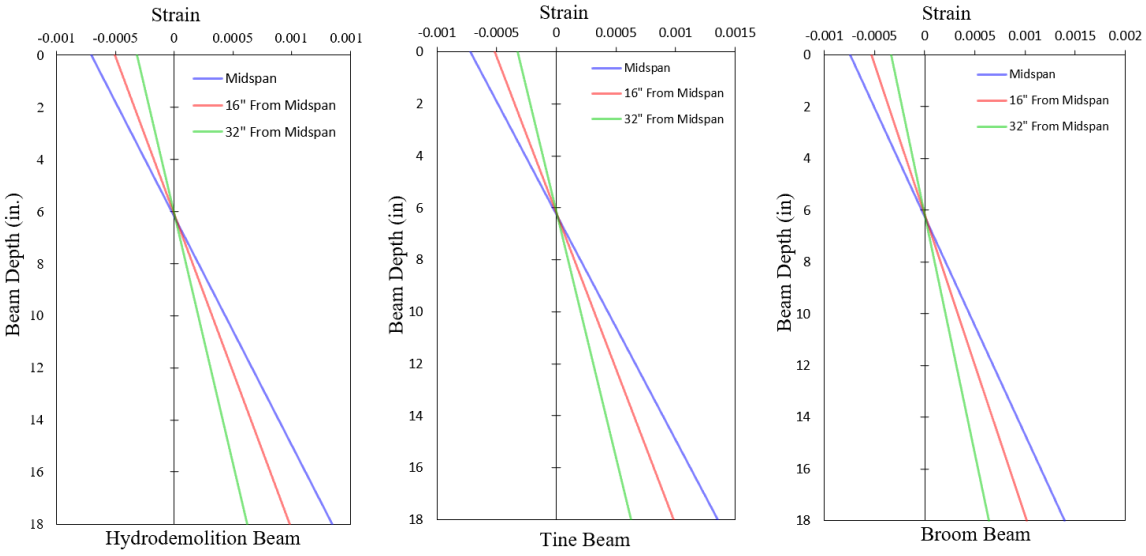

Figure 6-22: Strain distributions from strain compatibility analysis

Table 6-7: Comparison of strains for test data and strains from strain compatibility analysis.

		Tension Strain		**Compression Strain**	
		Test Data	**Strain Compatibility Analysis**	**Test Data**	**Strain Compatibility Analysis**
		-	**Method C**	-	**Method C**
Hydrodemolition	Midspan	0.00104	0.0011	0.00033	0.00045
	16" from Midspan	0.00084	0.0008	0.00023	0.00032
	32" from Midspan	0.00058	0.0005	0.00014	0.00020
Tine	Midspan	0.00098	0.0011	0.00036	0.00046
	16" from Midspan	0.00073	0.0008	0.00025	0.00033
	32" from Midspan	0.00045	0.0005	0.00013	0.00021
Broom	Midspan	0.00105	0.0011	0.00033	0.00048
	16" from Midspan	0.00078	0.0008	0.00024	0.00034
	32" from Midspan	0.00052	0.0005	0.00014	0.00021

Comparing Strain Profile Methods

The three strain profile methods use different assumptions to estimate the sectional response prior to interface failure. Using statics, the moment at each cross section is known at any given load as explained graphically in Figure 6-23. The moments resulting from each strain distribution are calculated as $M = C_1 * jd + C_2 * (d - d')$ where C_1 is the compression resultant from concrete compressive forces, jd is the distance between the compression and tension pair, C_2 is the compression force from compression steel, and d and d' are the distances to tension steel and compression steel, respectively. The methods obtained from sectional analysis are compared to the moment from test data ($\frac{P*L}{4}$) in Table 6-8.

The moments from Method B are larger than moments from Method A, with the exception of the tine-midspan cross section. Moments from Method A ranged from 5% to 43% smaller than those from test data, and moments from Method B ranged from 1% to 18% different than those from test data. In general, the higher compression force resulting from Method B (enforcing equilibrium) created a larger moment that are more consistent with the moments calculated from load data during the test.

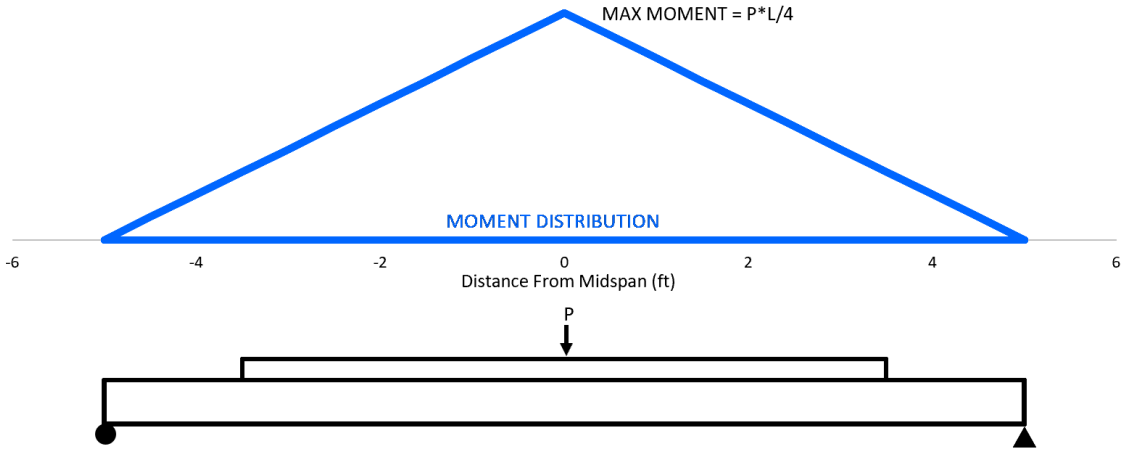

Figure 6-23: Moment distribution along beam length.

Table 6-8: Moments at each cross section for different strain profiles.

		Linear Strain Distribution Along Entire Depth	**Linear Strain Distribution for Compression Region Only**	**Using Test Data (P*L/4)**
		Method A	**Method B**	**Method C**
		(kip-ft)	(kip-ft)	(kip-ft)
Hydrodemolition	Midspan	193	207	217
	16" from Midspan	132	158	159
	32" from Midspan	78	102	101
Tine	Midspan	205	205	217
	16" from Midspan	140	147	158
	32" from Midspan	71	85	101
Broom	Midspan	187	206	224
	16" from Midspan	134	152	164
	32" from Midspan	74	94	104

Horizontal Shear Stress Demands

The horizontal shear stress along the interface is calculated considering the three strain profile methods described in the previous section. By obtaining resultant compression forces in the topping, the average shear stress is estimated by the difference in compression forces divided by the bonded width (b_v) and the distance between compression forces considered (l). This method is shown as Equation 6-1. The compression at the end of topping is taken as zero.

$$v_h = {(C_1 - C_2)}/{(b_v * l)}$$

Equation 6-1

This method was used for the following segments all of which have an 8” width:

- Midspan to 16” from midspan (16” length)

- 16” from midspan to 32” from midspan (16” length)
- 32” from midspan to end of topping (10” length)
- Midspan to end of topping (42” length)

The horizontal shear results for each segment are presented in Table 6-9 and Figure 6-24. As shown, the average horizontal shear stress toward the end of the topping slab (32” to 42” away from midspan) is consistently larger than the other two segments for all three beams regardless of the method used. This stress concentration is explained by the abrupt ending of the topping while the cross section is still subject to bending moment. The compression force measured 32” from midspan must be resolved over 10” where the topping ends.

The maximum horizontal shear stress for all beams is in the segment from 32” to 42” from midspan. Using the three analytical methods discussed, the three different types of interfaces (hydrodemolition, tine, broom) presented a similar range of approximately 750 to 1100 psi for the maximum horizontal shear stress at the topping end. For Method B, which enforces strain compatibility and equilibrium at the sectional level and shows a relatively small error in terms of moment, hydrodemolition presents a slightly higher shear stress (892 psi) than broom (849 psi) and tine (801 psi).

Regarding the average shear stress along the entire interface at failure, the three analytical methods provide a similar range of values of approximately 480 to 570 psi for the three composite beams. For Method B, broom presents a slightly higher average shear stress (548 psi) than hydrodemolition (529 psi) and tine (528 psi).

Table 6-9: Summary of horizontal shear stress at interface failure.

		Linear Strain Distribution along Entire Depth	Linear Strain Distribution for Compression Region Only	Moment Curvature Analysis
		Method A	**Method B**	**Method C**
		(psi)	(psi)	(psi)
Hydrodemolition	Midspan to 16" from Midspan	411	401	382
	16" from Midspan to 32" from Midspan	372	379	390
	32" from Midspan to End of Topping	837	892	1075
	Midspan to End of Topping	497	529	484
Tine	Midspan to 16" from Midspan	442	422	389
	16" from Midspan to 32" from Midspan	469	464	373
	32" from Midspan to End of Topping	765	801	1083
	Midspan to End of Topping	510	528	498
Broom	Midspan to 16" from Midspan	366	370	400
	16" from Midspan to 32" from Midspan	403	407	398
	32" from Midspan to End of Topping	802	849	1103
	Midspan to End of Topping	550	548	567

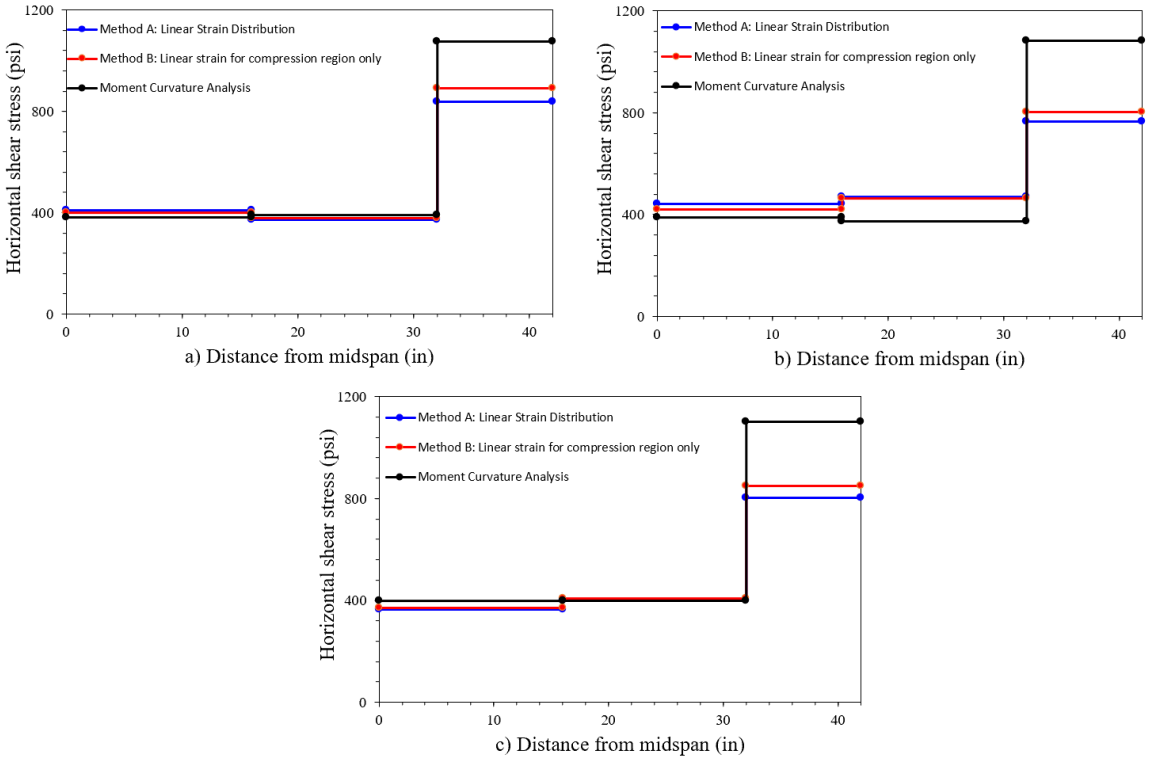

Figure 6-24: Horizontal shear stress versus distance from midspan on the beam failure end: (a) hydrodemolition beam, (b) tine beam, and c) broom beam.

6.4 DIRECT TENSILE AND SHEAR TESTS - PHASE 2

Results of Phase 2 direct tensile pull-off and shear test results conducted on the companion composite slabs are presented in Table 6-10 and Table 6-11. Note that all pull-off tension tests were performed with 3-inch diameter disks as described previously.

Hydrodemolition, broom, and tine had direct shear strengths of 1078 psi, 808 psi, and 471 psi, respectively. Not only did the tine samples have the lowest shear strength, but also had a coefficient of variance (CoV) of 48%. This CoV is much larger than the 19% and 21% CoV from hydrodemolition and broom, respectively.

The same trend is seen for the direct tensile pull-off test results. The hydrodemolition, broom, and tine had average direct tensile strengths of 345 psi, 269 psi,

and 238 psi, respectively. The tine CoV for pull-off testing was 46%, which again was significantly higher than the hydrodemolition and broom results that had CoVs of 13% and 18%, respectively. Given the variability of the tine results and the variability of the tine slab MTD compared to the tine beam MTD, the direct shear and direct tensile strengths may not be comparable to the results from the tine beam horizontal shear behavior.

Table 6-10: Phase 2 direct shear (guillotine) results.

Slab Category	Substrate Roughening Technique	Topping Workability Level	Topping Consolidation Technique	Direct Shear Strength			
				Average (psi)	Std. Dev. (psi)	CoV	Sample Size
Repair	Hydro-demolition	Moderate	V	1078	201	19%	4
Precast	Broom	Moderate	V	808	172	21%	4
Precast	Tine	Moderate	V	417	201	48%	4

Std. Dev.: Sample standard deviation
CoV: Coefficient of variation
V: Vibrated

Table 6-11: Phase 2 direct tensile pull-off results.

Slab Category	Substrate Roughening Technique	Topping Workability Level	Topping Consolidation Technique	Direct Tensile Pull-off Strength			
				Average (psi)	Std. Dev. (psi)	CoV	Sample Size
Repair	Hydro-demolition	Moderate	V	345	44	13%	6
Precast	Broom	Moderate	V	269	47	18%	6
Precast	Tine	Moderate	V	238	109	46%	6

Std. Dev.: Sample standard deviation
CoV: Coefficient of variation
V: Vibrated +

6.5 PHASE 2-DISCUSSION

6.5.1 Comparison of interface roughness and bond strength results from Phase 1 versus Phase 2

The tine specimen had high variability for both direct shear and direct tensile tests. The MTD from the slab was 0.75 mm and the MTD from the beam was 1.3 mm. The tines made in the beam must have been deeper and possibly pulled more paste and/or aggregates up creating a higher amplitude and rougher surface. The tine surface in general has a large area of flat surface with tine ridges spaced roughly 1" apart. This technique is less uniform than the broom, which makes it very dependent on the depth of the tines themselves.

The hydrodemolition average direct shear strength from Phase 1 and Phase 2 were 1006 psi and 1078 psi, respectively. The direct shear strength was 345 psi which is 22% lower than the average direct shear strength of 422 psi from Phase 1. The MTD of the hydrodemolition specimens were consistent from Phase 1 to Phase 2 (and beam from Phase 2). It should be noted the hydrodemolition slab from Phase 1 had a hand consolidated topping while the slab in Phase 2 was vibrated. The sample size for Phase 1 and Phase 2 are also different.

The broom average direct shear strength from Phase 2 was 808 psi which is just 4% lower than the broom (vibrated topping with moderate slump) direct shear average from Phase 1 being 840 psi. The average direct tensile results from Phase 1 and Phase 2 differed by 34% with Phase 1 and Phase 2 being 360 psi and 260 psi, respectively. For comparison the MTD from the Phase 1 and Phase 2 broom-slab specimens with vibrated toppings and moderate slumps were 1.14 mm and 0.6 mm, respectively. These results indicate MTD (or roughness) may have a greater influence on interface tensile strength than interface shear strength.

The MTD results from Phase 1 and Phase 2 are compared in Figure 6-25. The hydrodemolition and sandblast are done by uniformly removing the substrate surface. This practice is constant showing low coefficient of variance between MTD scans from each specimen and even when comparing specimens from Phase 1 to those in Phase 2. These techniques also remove the top layer of the substrate which could be weak due to improper substrate finishing or curing. Tine and broom roughening are done when the concrete is placed and can vary depending on the technician, tools, degree of concrete set-up, and substrate curing technique.

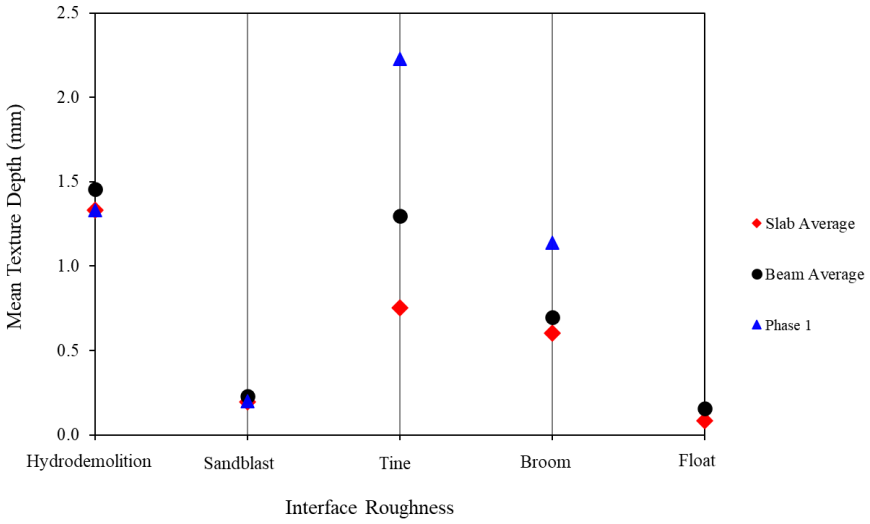

Figure 6-25: MTD results from Phase 1 and Phase 2.

Repair specimens

The repair specimens represent various roughness techniques that remove the top layer of concrete and while increasing the surface roughness. Repair techniques require equipment for each specific type of surface preparation and is commonly done by experienced technicians. For this project, there was a good amount of control of how rough

the repair surfaces were. The technician was able to use the high-pressure water, sandblaster, or bush hammer at increments until the desired roughness was achieved. After each increment, the surface was compared to a surface profile comparator (CSP) to determine is more concrete removal was necessary. This control was verified with MTD data. The sandblast and hydrodemolition were used in a total of four specimens: 2 slabs from Phase 1 and a slab and beam from Phase 2. All four specimens for sandblast and hydrodemolition have no statistically significant difference in means according to a Student's t-test. This shows that different types of specimens (beam/slab), different laboratories, different substrate concrete, and almost a year in time difference (from Phase 1 to Phase 2) did not affect the consistency of the roughening technique.

The surface roughness (MTD) from Phase 1 and Phase 2 repair specimens are statistically the same, but the direct shear and direct tensile results vary, and in the case of the sandblast specimens the bond behavior differs immensely. The sandblast results from Phase 1 for direct shear and direct tensile pull-off were 815 psi and 280 psi, respectively.

Precast specimens

The variation in MTD for both broom and tine specimens from Phase 1 slabs, to Phase 2 slabs, to Phase 2 beams suggests roughening of fresh concrete (representative of new construction) is not as consistent as roughening with repair techniques. The MTD of broomed and tined surfaces may depend on the timing/ how much the concrete has setup, the tool used, the amount of force used while pulling the boom or tining rake, the aggregate size in the substrate (in aggregates get pulled up), and the technician doing the roughening. While we tried to keep the roughening as consistent as possible, there was still large

variability in the MTD results. It is possible the practices at a precasting plant are more consistent as they are done by professions and have more experience.

6.5.2 Direct shear and direct tensile pull-off results from Phase 2 versus beam test results

A summary of Phase 2 results is presented in Table 6-12 and a plot comparing maximum horizontal shear stress from the beam tests, results from direct shear tests, and results from direct tensile pull-off tests is presented in Figure 6-26. Horizontal shear stresses near the topping end of the beam were calculated using strain profile Method B since this method uses strains from test data, enforces sectional equilibrium, and was most consistent with moments acting at the section based on the applied load. The table shows results from hydrodemolition, broom, and tine, but as discussed previously the tine slab results had high variability for direct shear and direct tensile pull-off results. The MTD values are also presented for comparison. As shown, the tine slab MTD was also 72% smaller than the tine beam MTD which makes the relationship of the strength data questionable.

The horizontal shear capacity from beam test to direct shear strength ratio is 1.2 and 0.95 for hydrodemolition and broom, respectively. Hence, the horizontal shear strength of the hydrodemolition beam is slightly smaller than that obtained in guillotine tests and for the broom beam is practically the same. For the tine beam, the horizontal shear strength practically doubles that obtained in the guillotine tests, which can be attributed to difference in the roughness of beam and slab specimens. The horizontal shear capacity from beam tests to direct tensile pull-off tests is 2.6, 3.2 and 3.4 for hydrodemolition, broom and tine, respectively.

Table 6-12: Phase 2 results summary.

Surface Roughness	Horizontal Shear Stress from Beam Tests (psi)	Direct Tensile Pull-off Test Average (psi)	Guillotine Shear Test Average (psi)	MTD Slab (mm)	MTD Beam (mm)
Hydrodemolition	892	345	1078	1.33	1.46
Tine	801	238	417	0.75	1.3
Broom	849	269	808	0.6	0.7

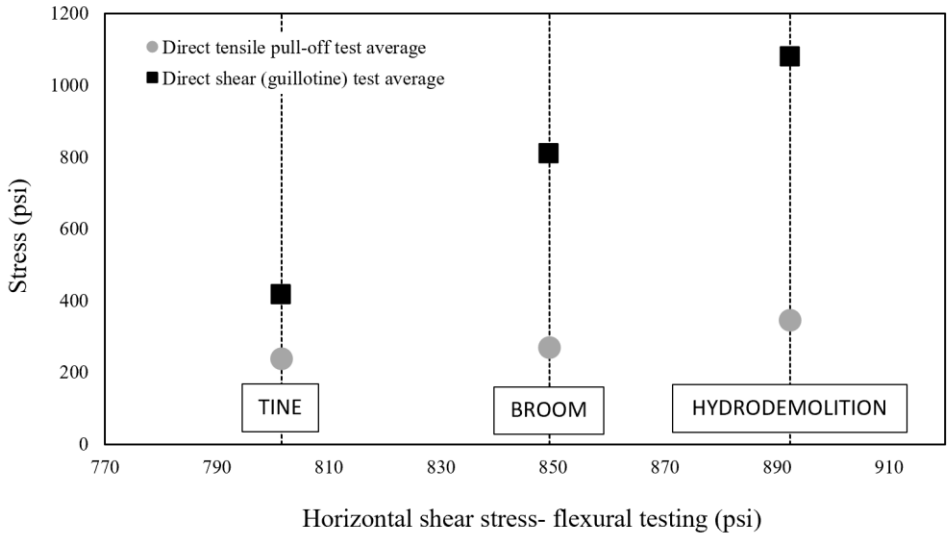

Pull-off test sample size: 6
Direct shear test sample size: 4

Figure 6-26: Direct shear and direct tensile strengths (y-axis) versus beam horizontal shear stress results (x-axis).

6.5.3 Mean texture depth versus beam test results

The beam mean texture depth versus horizontal shear stress from the beams tests is presented in Figure 6-27. While they presented different MTD values, the failure load for all three beams was very similar, and in turn the horizontal shear stress at failure was

similar. Hence, mean texture depth does not have a correlation to the horizontal shear strength for the beam tests.

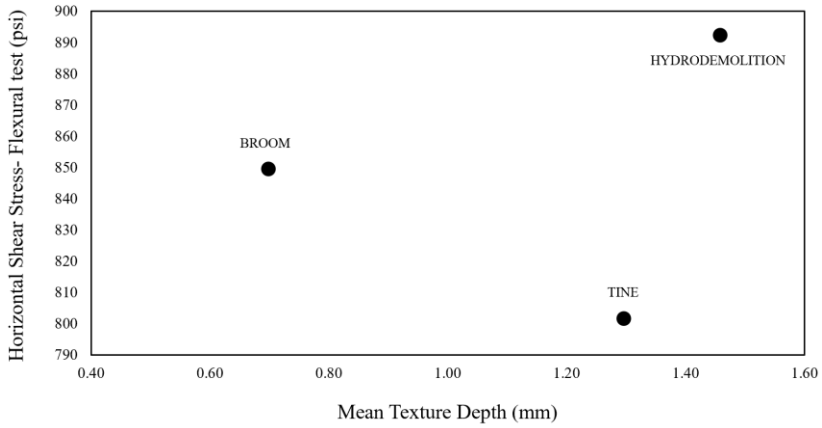

Figure 6-27: Mean texture depth versus horizontal shear stress from beam tests.

6.5.4 Effectiveness of beam test to assess horizontal shear capacity

The broom, tine, and hydrodemolition beams all failed between loads of 86 kip and 89 kip. The maximum horizontal shear strengths for these three beams were estimated at between 800 to 900 psi based on Method B (discussed in section 6.3). The consistency of these failures and small difference between estimated shear strengths is not consistent with the greater distinction between the roughening techniques obtained from local bond assessment data (direct shear and direct tension testing). A number of reasons could explain the similar strength of the beam specimens. One possibility for the consistent failure is concrete material characteristics or placement techniques. If the substrate surface was too dry or too wet (from improper SSD conditions) a weak layer can be created in the topping concrete right at the interface surface from extremely low or high w/c ratio. If a weak layer was present, the failure of the interface may have been governed by the concrete material rather than the roughening technique. Other possibilities are related to

the concentration of tensile stresses at the end of the interface, which could have initiated cracking at a similar load, and/or the weakening of the interface due to differential shrinkage. Further analysis is being done using the DIC vision system results to assess the slip and strains during testing. Samples from the beams and/or slabs will also be examined using petrography analysis to assess the quality of concrete materials at the interface.

6.5.5 ACI 318 horizontal shear code provisions versus beam test results

ACI 318-19 allows for calculation of horizontal shear demand using the segment method and simplified elastic method. The horizontal shear stress for each beam using the segment method for the region with highest shear demand (32" from midspan to end of topping), the segment method using the whole span (midspan to end of topping), and the simplified elastic method is summarized in Table 6-13. For the segment method, the compression forces have been calculated based on strain data from test using Method B presented in section 6.3.

Table 6-13: Summary of horizontal shear stress from beam tests.

	Segment Method		**Simplified Elastic Method**
	$(c_1 - c_2)/(l * b_v)$		$V_u/(b_v * d)$
	Highest*	Average**	-
Surface Roughness	(psi)	(psi)	(psi)
Hydrodemolition	892	529	347
Tine	801	528	347
Broom	849	548	359

* Highest shear stress is calculated using the segment farthest from midsapn (32" from midspan to end of topping).

** Average shear stress is calculated using the segment of the full span (midspan to end of topping).

The three composite beam specimen tests failed at a maximum horizontal shear stress towards the end of the topping (10” segment length) of between 801 psi and 892 psi, as shown in Table 6-13. These stresses are 10 to 11 times the nominal horizontal shear stress limit of 80 psi of ACI 318-19. When considering the entire shear span length (42” segment length), the average shear strength becomes 528 psi to 548 psi, or 6.6 and 6.8 times the nominal horizontal shear stress limit in ACI 318-19. Hence, the strengths obtained from the segment method indicate that the actual horizontal shear resistance of these unreinforced interfaces is much larger than the nominal stress limit in ACI 318. These results also show that the shear stress obtained from the segment method depends significantly on the length of the segment. When the segment is equal to one third of the shear span, the shear strength is approximately 50-65% larger than if the segment was taken as the entire shear span.

The simplified elastic method for calculating horizontal shear stress is permitted by ACI 318-19 in section §16.4.5.1. This method takes no consideration to the bonded interface length or the topping depth (or topping depth to full section depth ratio). The horizontal shear stresses from the segment method using the whole shear span is approximately 50% larger than the horizontal shear stress predicted by the simplified elastic method at the load in which horizontal shear failure occurred. Nevertheless, the values obtained with the simplified elastic method remain significantly larger than the 80 psi limit established in ACI 318.

Chapter 7 : Summary and Conclusions

This chapter presents a summary of the main findings and conclusions of Phase 1 and Phase 2 of this investigation, along with possible practical applications of the research findings.

7.1 PHASE 1

Phase 1 of the experimental program comprised 192 direct shear tests and 84 direct tensile pull-off tests performed on slab specimens with six different interface conditions. The interface conditions were defined in two series; the repair series considered sandblast only, bush hammer + sandblast and hydrodemolition interface preparation techniques, while the precast series considered float, broom and tine (rake) finishes. The interface types were selected to provide a range of surface roughness conditions. The surface texture was quantified using mean texture depth measured using laser line scanning.

The primary objectives of the Phase 1 study were as follows: (a) to collect data on interface shear strength for a range of interface conditions; (b) to study the correlation between direct shear strength from the guillotine shear test method and direct tensile pull-off strength, and (c) to determine whether the ACI nominal interface shear stress limits for unreinforced interfaces in repair and new construction should be redefined. The primary findings of this study are summarized below.

7.1.1 Effect of Interface preparation - Repair Series

- The substrate interface prepared by hydrodemolition had the highest direct shear and tensile pull-off strengths in the repair series specimens from Phase 1. Hydrodemolition produces a surface profile with a high degree of surface roughness with a low risk for microcracking or bruising.

- The bush hammer + sandblast interface had the lowest shear and tensile bond strengths in the repair series. The results suggest that microfractures in the cement paste and loosening of the coarse aggregate occurred at the substrate surface, creating a weakened or bruised layer that was not removed by subsequent sandblasting. This surface preparation type had the highest ratio of shear-to-tensile bond strength of all interfaces investigated, suggesting that the microcracking had a more significant effect on the tensile pull-off strength than on the direct shear strength.
- The sandblast only interface achieved higher direct shear and tensile pull-off strengths than the bush hammer + sandblast interface and had comparable strength results to the broom and tine interfaces in the precast series. These results illustrate the benefits of limited "intentional roughening" that removes laitance and minor surface defects while opening the paste pore structure at the repair interface.

7.1.2 Effect of Interface Preparation - Precast Series

- The broom interface developed an average direct shear strength approximately 20% higher than the tine interface in Phase 1. The average tensile pull-off strength was similar for the two interfaces. The broom interface shear strength results were slightly less variable than the results for the tine surface, although the opposite trend was noted for the tensile pull-off strength results.
- While it is generally assumed that a tine or rake finish will provide more surface roughness than a broom finish and thus improve interface bond strength, the results of this study do not indicate a consistent improvement in bond strength for the tine finish. This finding suggests that bond strength is less influenced by surface

roughness than interface strength due to friction. The uniform roughness provided by the broom finish appears to be as, or more, effective as the deep, widely spaced grooves created by the rake tines in terms of interface shear bond strength.

- The loading direction relative to the broom or tine orientation (parallel or perpendicular) did not provide a statistically significant effect on interface shear strength results.

7.1.3 Effect of Consolidation Method

- Consolidation of moderate slump topping in the precast series by hand consolidation or vibration did not have a statistically significant effect on interface direct shear strength results.

7.1.4 Effect of Interface Surface Roughness on Shear and Tensile Bond Strength

- The shear and tensile bond strengths of the unreinforced interfaces considered in Phase 1 do not appear to be influenced by the degree of surface macrotexture roughness quantified by mean texture depth (MTD).
- The results suggest that the interface bond strength in shear may be less dependent on degree or magnitude of surface roughness, and more dependent on having a uniformly roughened surface that is sound (i.e., no laitance or surface defects) and having well consolidated repair or topping concrete.

Correlation Between Direct Shear Strength and Tensile Pull-off Strength

- The ratio of direct shear strength to tensile pull-off strength ranged from 2.2 to 3.6 for the interfaces considered in Phase 1. The data indicate a modest linear

correlation between interface shear and tensile strength with a coefficient of determination (R^2) value of 0.69.

- The test results from the current study and published research indicate that the ratio of interface shear to tensile strength is dependent on several factors, including interface surface preparation and roughness, material properties and test methods used. These findings suggest that if tensile pull-off tests are intended to provide an indication of shear bond strength for quality control purposes the ratio of interface shear strength to tensile pull-off strength should be determined based on test data on a case-by-case basis.
- The ACI 562-19 Clause R7.4.3 (Commentary) statement that "it is generally adequate to assume that the repair to substrate bond will resist an interface shear equal to the direct tensile pull-off test result" appears to provide a conservative lower bound to the relationship between interface shear and tensile bond strength.

Core Size for Tensile Bond Pull-off Test

- The slab specimens used in Phase 1 had a 2.5-inch topping or repair material thickness, which required a 3-inch core (circular cut) depth to prepare the specimens for tensile bond pull-off testing in accordance with ASTM C1583. Highly variable results and premature failures during coring were experienced in this study using the standard 2-inch diameter core and pull-off disk (no usable results were obtained using 2-inch cores/disks) with a 3-inch core depth. Switching to 3-inch diameter cores/disks effectively eliminated the debonding failures during coring and significantly reduced variability of the test results.

- The results of the current study suggest that larger diameter cores/disks may be required as topping or repair material thickness is increased. This does not appear to be addressed by ASTM C1583, or by ICRI 210.3R-13. Further research into the effect of topping thickness and required core diameter is required.

Interface Shear Bond Strength for Design

- All interface conditions (repair and precast) investigated in Phase 1 with a moderate slump, well consolidated topping achieved average direct shear strengths approximately 8 to 12 times larger than the nominal horizontal shear strength limit of 80 psi specified in ACI 318-19 and ACI 562-19.
- Characteristic design strengths estimated based on the test data using the Tolerance Factor Method (10% fractile at 95% confidence) ranged from 2.5 to more than 7 times higher than the ACI nominal shear strength of 80 psi.

Guillotine Shear Test Method

- The guillotine direct shear test is a practical method to assess interface bond shear strength using cores from laboratory specimens, new construction and existing structures. The core is subjected to direct (single) shear which allows assessment of the bond strength without a normal force acting on the interface. The test can be readily performed in a concrete compression testing frame or universal testing frame using a simple guillotine shear jig.

7.2 PHASE 2

Phase 2 of the experimental program comprised 6 beams: five composite with different interface roughness conditions and one monolithic. The experimental program

also included direct shear tests and direct tensile pull-off tests on cores obtained from companion composite slabs. The interface conditions used for the beams were all previously considered in Phase 1, but not all interface roughnesses from Phase 1 were explored in Phase 2. The interface conditions considered were broom, tine, sandblast, hydrodemolition, float, and monolithic. The surface texture was quantified using mean texture depth measured using laser line scanning. The topping or repair concrete for all specimens was placed with a moderate slump (5.75 inches) and was vibrated for consolidation. At the time of this report only 4 beams (monolithic, broom, tine, and hydrodemolition) had been tested. The monolithic beam developed its full flexural capacity while the three composite beams failed due to horizontal shear at their unreinforced interface.

The primary objectives of the Phase 2 study were as follows: (a) to test the behavior of an unreinforced interface when subject to high horizontal shear stresses well above the ACI nominal interface shear stress limit, (b) to study the correlation between direct shear strength from the guillotine shear test method, direct tensile pull-off strength, and horizontal shear strength determined from flexural tests, and (c) to determine whether the ACI nominal interface shear stress limits for unreinforced interfaces in repair and new construction should be redefined. The primary findings of this study are summarized below.

7.2.1 Effect of Interface Conditions on Beam Interface Bond Capacity

- The three tests completed on the broom, tine, and hydrodemolition beams presented very consistent response and practically identical failure loads. Interface

failures occurred at an estimated maximum interface shear stress of between 800 and 900 psi near the topping end.

- The two beam specimens that were not tested (sandblast and float) presented signs of cracking and debonding along the interface. Debonding in these specimens can be attributed to the insufficient roughness of these interfaces to restrain differential shrinkage between the substrate and topping.
- Of the specimens that did not see pre-testing interface cracks, the interface horizontal shear capacity of the beams does not appear to be influenced by the quantification method of roughness used in this study (mean texture depth).
- A combination of factors including a low surface roughness influence the tendency of topping delamination.

7.2.2 Correlation of Horizontal Shear Capacity from Beam Strengths to Direct Shear Strengths and Direct Tensile Pull-off Strengths

- The ratio of maximum horizontal shear strengths from beam test to direct shear strengths were 1.2 and 0.95 for hydrodemolition and broom, respectively. This ratio was practically 2 for tine, but the companion slab used for the core tests presented a much lower mean texture depth value than the beam specimen.
- The ratio of horizontal shear strengths from beam test to direct tensile pull-off strengths were 2.6, 3.2 and 3.4 for hydrodemolition, broom and tine, respectively.
- Like in Phase 1, the ACI 562-19 Clause R7.4.3 (Commentary) statement that “it is generally adequate to assume that the repair to substrate bond will resist an interface shear equal to the direct tensile pull-off test result” is shown to provide a conservative lower bound to the relationship between interface shear and tensile bond strength.

7.2.3 Effectiveness of the Beam Test to Study Interface Shear

- The beam tests were an effective way to subject an unreinforced concrete-to-concrete interface to high levels of horizontal shear stress caused by bending. Nevertheless, test results need to be further investigated to determine if there were any significant forces normal to the interface in either tension (near topping ends) or compression (near midspan) that would influence their horizontal shear capacity.
- The interpretation of the beam test results has revealed the uncertainties associated to the analytical estimation of the forces acting on the topping and resulting horizontal shear demand. Future analysis of data obtained from digital image correlation will contribute to refine the analytical determination of forces acting on the topping.

7.2.4 Methods of Calculating Horizontal Shear Demand Permitted by ACI 318-19

- The stress values calculated from the horizontal shear demand methods permitted in ACI 318-19 (segment and simplified elastic) can vary significantly depending on the member geometry, moment distribution, and span length.
- The segment method may provide more realistic measure of the actual horizontal shear demand, but careful consideration must be taken when choosing the length of the segment.

7.2.5 Horizontal Shear Capacity from Beam Tests Compared to Limit in ACI 318-19 and ACI 562-19 Code

- The horizontal shear strength capacity of the beam specimens was calculated using the segment method, in which compression forces were estimated based on strain

gage data. Depending on the assumed segment length the maximum horizontal shear stress on the beams were between 6.6 to 11 times higher than the 80 psi nominal horizontal shear stress limit in ACI 318-19 and ACI 562-19.

- When using the simplified elastic method, the maximum horizontal shear stress on the beams were 4.4 times higher than the 80 psi nominal horizontal shear stress limit in ACI 318-19 and ACI 562-19.

7.3 APPLICATION OF RESEARCH FINDINGS

The research results indicate that a sound (i.e., not bruised or microcracked by concrete removal), laitance and defect free interface with uniform surface texture in combination with good consolidation of the repair or topping materials are keys to good shear and tensile bond strengths. The results show that interfaces with these characteristics can achieve interface shear strengths significantly higher than the ACI nominal shear strength of 80 psi.

The research suggests that a performance-based methodology could be considered to establish a design (i.e., nominal or characteristic) interface shear bond strength based on direct shear tests performed using project-specific material, interface and construction parameters. The design shear strength should be established based on a reliability analysis considering the random variability of test results and uncertainty associated to their representation of actual interface conditions. However, in light of differences observed between beam tests and bond strength tests in Phase 2 of this investigation, further research is needed to develop sufficient data to quantify this type of uncertainty and to

characterize the effects on shear strength of differential shrinkage and normal forces acting on the interface.

References

ACI-ASCE Committee 333, (1960). "Tentative Recommendations for Design of Composite Beams and Girders, for Buildings." *ACI Journal, 57(6), 609 – 628.*

ACI 214.4R-10, (2010), "Guide for Obtaining Cores and Interpreting Compressive Strength Results." *American Concrete Institute*. Farmington Hills, MI.

ACI 228.1R-19, (2019), "In-Place Methods to Estimate Concrete Strength." *American Concrete Institute*. Farmington Hills, MI.

ACI 318-63, (1963). "Building Code Requirements for Structural Concrete and Commentary." *American Concrete Institute.* Farmington Hills, MI.

ACI 318-71, (1971). "Building Code Requirements for Structural Concrete and Commentary." *American Concrete Institute*. Farmington Hills, MI.

ACI 318-19, (2019). "Building Code Requirements for Structural Concrete and Commentary." *American Concrete Institute*. Farmington Hills, MI.

ACI 562-19, (2019). "Code Requirements for Assessment, Repair, and Rehabilitation of Existing Concrete Structures and Commentary." *American Concrete Institute*. Farmington Hills, MI.

ACI 355.4R-19, (2019). "Qualification of Post-Installed Adhesive Anchors in Concrete." *American Concrete Institute*. Farmington Hills, MI.

ASTM Standard C39/ C39M, (2020). "Standard Test Method for Compressive Strength of Cylindrical Concrete Specimens.". *ASTM International*. West Conshohocken, PA.

ASTM C143-15, (2015). "Standard Test Method for Slump of Hydraulic-Cement Concrete." *ASTM International*. West Conshohocken, PA.

ASTM C1583, (2013). "Standard Test Method for Tensile Strength of Concrete Surfaces and the Bond Strength or Tensile Strength of Concrete Repair and Overlay Materials by Direct Tension (Pull-off Method)." *ASTM International*. West Conshohocken, PA.

ASTM C496/ C496M-17, (2017). "Standard Test Method for Splitting Tensile Strength of Cylindrical Concrete Specimens." *ASTM International*. West Conshohocken, PA.

ASTM E965-15, (2015). "Standard Test Method for Measuring Pavement Macrotexture Depth Using a Volumetric Technique." *ASTM International*. West Conshohocken, PA.

El Hachem, Y., & Prozzi. J. A., (2019). "The UTexas Seal Coat Design Method Using 3D Laser Technology / by Yorguo El Hachem". *University of Texas.* Austin, Texas.

Fib Model Code 2010, (2013). "fib Model Code for Concrete Structures 2010." *International Federation for Structural Concrete (fib).* Berlin, Germany.

Hanson, N. W., 1960, "Precast-Prestressed Concrete Bridges: Horizontal Shear Connections," *Bulletin, PCA Research and Development Laboratories, V. 2, No. 2, May, pp. 38-58. doi: 10.14359/16708*

ICRI 310.2R-2013, (2013). "Selecting and Specifying Concrete Surface Preparation for Sealers, Coatings, Polymer Overlays, and Concrete Repair," International Concrete Repair Institute.

ICRI 210.3R-2013, (2013). "Guide for Using In-Situ Tensile Pull-off Tests to Evaluate Bond of Concrete Surface Materials," International Concrete Repair Institute.

Kaar, P. H., Kriz, L. B., and Hognestad, E., (1960). "Precast Prestressed Concrete Bridges: (1) Pilot Tests of Continuous Girders," PCA Research and Development Laboratories Bulletin, V. 2, No. 2, May, pp. 21-37. doi: 10.14359/51685340

Kovach, J. D. & Naito, C., (2008). "Horizontal Shear Capacity of Composite Concrete Beams without Interface Ties" *Advanced Technology for Large Structural Systems (ATLSS) Report No. 08-05.* Bethlehem, PA.

Loov, R. E., & Patnaik, A. K., (1994). "Horizontal Shear Strength of Composite Concrete Beams with a Rough Interface". *PCI Journal, 39(1), 48 - 69.*

Momayez, A., Ehsani, M. R., Ramezanianpour, A. A., Rajaiem H., (2005). "Comparison of Methods for Evaluating Bond Strength Between Concrete Substrate and Repair Materials." *Cement and Concrete Research 35 (2005) 748-757.*

Mones, R. M., & Brena, S. F., (2013). "Hollow-core Slabs with Cast-in-place Concrete Toppings: A Study of Interfacial Shear Strength." *PCI Journal 58(3):124-141.*

Ozell, A. M., & Cochran, J. W., (1956). "Behavior of Composite Lintel Beams in Bending." *PCI Journal, 1(1), 38-48.*

Revesz, S., (1953). "Behavior of Composite T-Beams with Prestressed and Unprestressed Reinforcement". *ACI Journal, 24(6), 585 – 592.*

Rosen, C., (2016). "Shear Strength at the Interface of Bonded Concrete Overlays" *M.S. Thesis submitted to the University of Colorado.* The University of Colorado. Denver, Colorado

Saemann, J. C., & Washa, G. W., (1964). "Horizontal Shear Connections between Precast Beams and Cast-inPlace Slabs," *ACI Journal Proceedings, V. 61, No. 11, Nov., pp. 1383-1409. doi: 10.14359/7832.*

Santos, P., "Assessment of the Shear Strength between Concrete Layers." *Thesis for Doctor of Philosophy in Civil Engineering, University of Coimbra*. Coimbra, Portugal.

Seible, F., & Latham, C., (1990). "Horizontal Load Transfer in Structural Concrete Bridge Deck Overlays." *Journal of Structural Engineering ASCE, 116(10), 2691-2709.*

Silfwerbrand, J., (2003). "Shear Bond Strength in Repaired Concrete structures". *Materials & Structures, Vol. 36, July 2003, pp. 419-424.*

Sprinkel, M. (2016) "Bond Strength Between Shotcrete Overlay and Reinforced Concrete Base." *Concrete Repair Bulletin, January/February 2016.*

Swan, A. (2016). "Alternate Methods for Testing Shear Strength at a Bonded Concrete Interface." *M.S. Thesis submitted to the University of Colorado.* Denver, Colorado.